POLITECNICO DI TORINO

Department of Structural and Geotechnical Engineering

Master Degree in Civil Engineering

Master Degree Thesis

Seismic reliability of bridges isolated by single concave sliding bearings

Supervisor
Prof. Eng. Paolo Castaldo

Candidate
Stefano Potì
219881

March 2018

Alla mia famiglia.

Acknowledgement

I would like to thank my mother and my father for giving me the opportunity to undertake this path and for all the sacrifices made during the university years, to make me reach this goal. This success is yours too.

Thank to my sister Francesca, to all my cousins and my uncles who have always helped and supported me in every situation; to my grandparents to whom I adore, that have always been close to me. A thank, it goes also to my uncle Luigi who, with his passions, has transmit me the interest in technique and engineering and that has encouraged and supported me even in the most difficult moments of my university career.

I would like to thank all the friends and colleagues and the various roommates that I have met during these years of studies in Turin, who have given me pleasant moments that I will not forget so easily. In addition, I thank my friends whom I met in Barão Geraldo, who gave me a whole year of joy and happiness and have meant that my year of study in Brazil remain indelible in my memory.

Thank to you, Iliana, who even if on the other side of the world, you always believed in me, encouraging and giving me the strength that I needed.

Finally, a strong thank goes to my supervisor Prof. Paolo Castaldo, for transmit to me some of his knowledge, for being a point of reference for the realization of this thesis and a friend always available to help me in the moment of need. Thank you for enduring me, with my questions and concerns.

Content index

Index of figures

Index of tables

Introduction

This thesis aims at evaluating the seismic reliability of isolated multi-span bridges, with the intent to providing design criteria and design abacuses, respecting the seismic engineering philosophy based on performance objects.

Bridges are structures of high importance in transport systems. Structural damage due to seismic events and induced to these structures, and the significant cost of their reconstruction, have revealed the need for the assessment of their seismic vulnerability based on performance-based design concepts. This method requires an accurate prediction of the seismic capacity of the bridges and of the seismic demand associated to them.

In the last forty years, earthquakes have caused severe damage to civil infrastructure around the world, with a growing trend. Many important bridges have collapsed, even if designed to resist seismic actions: this is mainly due to their usual structural simplicity, which makes them very vulnerable to seismic events. Seismic damage in bridges occurs mainly in the piers, and then it may cause the collapse of the deck. Although the concepts of Capacity Design have been widely accepted for the seismic design of buildings, they may not be appropriate for bridges, since they usually do not show structural redundancy due to their simply supported static scheme.

Among the design strategies aimed to the limitation of the earthquakes effects, seismic isolation has emerged as the most promising. With this technique, by special bearings, a structural discontinuity is created that allows large relative horizontal displacements between the superstructure and the substructure, so that the mass of the superstructure is separated from the seismic movements of the ground. and the energy transmitted by the earthquake to the superstructure is reduced.

The (FPS) are types of seismic isolators, which allow relative displacements by spherical surfaces. The dissipation of energy is provided by the friction encountered during the movement of the sliding surfaces. Thus, the dynamic response of these devices is closely related to their frictional behavior. Moreover, they provide a restoring force, thanks to the curvature of the surfaces, which also allows the devices to return to their initial position after a seismic event. In this way, the isolation system allows to obtain an extension of the natural period of the structure, towards frequency values lower than those typical of earthquakes, and

allows to dissipate the energy of seismic input, thanks to its frictional behavior. Experimental studies have attested the intrinsic randomness of the dynamic behavior of FPS devices, due to the dependence of the friction coefficient on non-controllable parameters, such as sliding speed, contact pressure and temperature. As a result, the modeling of these devices has been set through a probabilistic approach.

In the structural modeling phase, it was considered a system with multiple degrees of freedom, modeling the bridge, in the MATLAB-Simulink® environment, with a linear behavior and isolators with non-linear behavior characterized by a model dependent on speed. Consequently, extensive parametric analysis was performed, considering different structural models of the bridge, varying the fundamental period of the pier, the fundamental period of the deck, the mass ratio and the dynamic friction coefficient of the devices. The latter was taken as a random variable and the values of this parameter were obtained through a statistical sampling process, of stratified type, using the Latin hypercube method. Finally, the seismic response of the structural system was evaluated considering a set of natural seismic recordings, scaled for different values of a spectral displacement taken as intensity measure.

Through an incremental dynamic analysis (IDA), the relationship between the seismic demand and the capacity of the structure has been obtained and the structural performances are carefully evaluated. Finally, the IDA results allowed to evaluate the seismic vulnerability of the bridges and to develop their fragility curves, which were integrated with the hazard curves of the L'Aquila (Italy) site to evaluate the seismic reliability of the structure, to define a reliability criterion to support the design of the dimensions of the Friction Pendulum in plan.

CHAPTER 1

1. STRUCTURAL AND SEISMIC SAFETY

The structures, during their life, may be subject to the application of seismic actions, which, depending on their intensity, can cause multiple damages to the structural and non-structural elements belonging to the building organism.

Particularly, in recent decades, many earthquakes of varying intensity, registered in Italy, have shown that most of the buildings and bridges, designed according to obsolete regulations and in the absence of specific seismic regulations, are inadequate to resist totally or partially, to actions seismic. Therefore, there has been a growing interest in a performance approach to seismic design, and nowadays it is widely recognized that it must be an essential reference for the drafting of the latest generation technical regulations. From all this, arises the need to study and to protect the existing assets, as to reduce seismic risk and its consequences, both in terms of human lives and in economic terms. For this purpose, therefore, it is necessary to define specific methods to evaluate this risk and possibly intervene.

From this point of view, by now, it has been customary to tackle the structural problem by determining a distinct number of states (called "Limit States"), which allow to quantify the resistant capacity of the structure with respect to the corresponding level of damage. It is, therefore, evident that the assessment of structural reliability under seismic conditions is currently one of the most interesting topics of seismic engineering and is the objective of this work.

1.1 Performance Based Seismic Design (PBSD)

In the paper [1] some important terms typical of the project performance philosophy are specified and are listed below.

- **Performance Based Engineering (PBE)**: a design approach, of performance type, that consists in the identification of design criteria, appropriate structural systems, dimensional and constructive choices for a construction. Therefore, consist in the indication of control and maintenance procedures, in such a way that it is not damaged beyond certain pre-set Limit States and if subject to specific levels of the actions that are deemed to be effective during its useful life. It is a design process that "follows" the construction from its first conception and throughout its life.

- **Performance Based Seismic Engineering (PBSE)**: it is the application of the PBE in case of the seismic action. It, therefore, deals with the design, construction, control and maintenance of a building to ensure that it resists the effects of earthquakes of different intensities without exceeding pre-set Limit States.

- **Performance Based Seismic Design (PBSD)**: it is the PBSE step focused only on the design phase, concerning the seismic risk identification, the selection of performance levels and project performance objectives, the verification of suitability of the construction site, the structural concept, the general and definitive structural verifications, as well as the definition of control and monitoring specifications to be carried out during the life of the building.

The basic concept of Performance Based Design is, in essence, the definition of a multiplicity of Performance Objective (PO) obtained from the coupling of (structural and non-structural) performance requirements with prefixed levels of actions intensity: we can then define the performance objectives, that a structure in the seismic field must meet, as the achievement of certain Performance Levels in correspondence of expected levels of seismic intensity, defined in terms of frequency of exceeding (Seismic Hazard Level). The (*Figure 1.1*), from the Vision2000 technical document [2], illustrates this design philosophy significantly: on one side, four reference seismic inputs are defined conventionally based on

the Return Period (Frequent 43 years, Occasional 72 years, Rare 475 years, Very Rare 975 years), on the other side, four Performance Level are identified:

- *Fully Operational:* damage to non-structural components and systems must be avoided in the case of minor seismic events, with a high probability of occurrence, during the useful life of the structure;
- *Operational:* damage limited to non-structural components is allowed, whereas they must be completely avoided in structural ones in the case of medium-low intensity earthquakes that can occur less frequently;
- *Life Safe:* damage to persons must be avoided and the structure must be repairable after the earthquake if the intensity of the seismic event is medium-high;
- *Near Collapse:* structural collapse is avoided even in case of severe earthquakes with a low probability of occurrence.

		Earthquake Performance Level			
		Fully Operational	Operational	Life Safe	Near Collapse
Earthquake Design Level	Frequent (43 years)	Basic Objective	Unacceptable	Unacceptable	Unacceptable
	Occasional (72 years)	Essential/Hazardous Objective	Basic Objective	Unacceptable	Unacceptable
	Rare (475 years)	Safety Critical Objective	Essential/Hazardous Objective	Basic Objective	Unacceptable
	Very Rare (975 years)	Not Feasible	Safety Critical Objective	Essential/Hazardous Objective	Basic Objective

Figure 1.1: Performance Objectives in the Performance Based Design.

In the performances listed above, it is easy to recognize the performance levels required in the Limit States introduced by the “Norme Tecniche per le Costruzioni”, D.M. 14/01/2008 [3], in particular: the "Fully Operational" level is associated with the operating limit state (SLO), the "Operational" level is associated with the state limit of damage (SLD), the levels of “Life Safe” and “Near Collapse” are associated with the homonymous limit states (SLV and SLC). The POs are appropriately matched with the seismic actions of reference and, therefore, the performance objectives are defined, generally different depending on the importance of the work ("Basic Objective" for the structures of ordinary importance, "Essential Objective" and "Safety Critical Objective" for the increasingly important structures

such as schools, hospitals, barracks, power stations, etc.). However, while the definition of acceptable levels for the structural response and the service limit status damage is an exclusively engineering task, the conventional definition of the Performance Level Exceedance Probabilities goes beyond the strictly engineering-structural field, necessarily requiring also the involvement of financial, social and urban aspects. The design process must therefore place greater emphasis on the prediction of structural performance; this, however, given the numerous intrinsic uncertainties in the seismic analysis, can be carried out only in a probabilistic sense [1].

POs can also be represented with a curve within the "Performance Space". An example of Performance Space for fixed-base structures is represented in (*Figure 1.2*), where the exceedance probability (for a useful life of 50 years), in logarithmic scale, is represented on the vertical axis and on the horizontal axis is instead reported the measure of the structural response, that for buildings corresponds to the Interstory Drift Index (IDI).

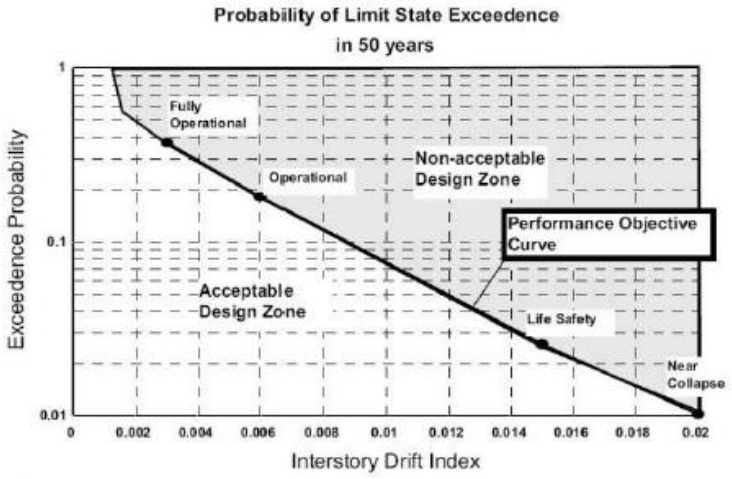

Figure 1.2: Performance space for fixed-based structures [1].

The definition of the performance limit states, from which the evaluation of structural reliability is followed, is a complex problem and must be resolved through the identification of suitable variables to describe the state of the structural system, that is, the damage parameter. In buildings seismic design, one of the most relevant parameters, often used in seismic design, corresponds to the maximum displacement of inter-storey (d_r), divided by inter-storey height (h_i). This parameter, corresponds to the previously mentioned “Inter-story Drift Index” (IDI). In (*Table 1.1*) are represented the values of IDI, for the four Limit States

used in the seismic evaluation and in the design of fixed-base structures, recommended by different authors [1], [4], [5] just like the national regulations.

Table 1.1: Inter-story Drift Index of fixed-base structures for the four Performance Level.

Limit State	Inter-story Drift Index
Fully Operational	IDI = 0,3%
Operational	IDI = 0,6%
Life Safety	IDI = 1,5%
Near collapse	IDI = 2,0%

In bridges seismic design, instead, one of the most important parameters is the ratio between the maximum pier displacement and the pier height, also known as "Pier Drift Index", (PDI) (*Table 1.2*). This parameter strictly depends on the structural typology and may be inferred from both experimental surveys and inspections on earthquake-damaged structures.

Table 1.2: Pier Drift Index for no isolated bridges, for the four Limit States.

Limit State	Pier Drift Index
Fully Operational	PDI=0,7%
Operational	PDI=1,5%
Life Safety	PDI=2,5%
Near collapse	PDI=5%

1.2 Evaluation Elements of Seismic Risk

After a seismic event, the seismic risk is defined in economic terms as the possible loss of functionality of structures. In other words, the risk is defined as the probability that in a certain time interval a predetermined loss level is reached. The variable that characterizes the level of loss is represented by an index that indicates all the possible levels of loss, that go from full functionality to collapse. Loss is usually identified in the cost to be incurred, to bring back the damaged system to the conditions it had before to the seismic event. From a

quantitative point of view, the risk can be expressed with a relationship that correlates seismic hazard, vulnerability and exposure:

Seismic Risk = Seismic Hazard x Vulnerability x Exposure

Where:

- *Seismic Hazard* of an area is defined as the probability, that in a certain period, an earthquake will occur with a given intensity; or even as: the expected number of events that in a unit of time exceeds a certain intensity threshold.
- *Vulnerability*, is defined as the tendency for people or goods to suffer damage or modification due to a given earthquake with a given intensity measure. Such damages can lead to the momentary loss of functionality or even to total irrecoverability.
- *Exposure* indicates the quality and quantity of the goods exposed to the seismic hazard, the number of people involved and their ability to react.

Another definition of *Seismic Risk* can be considered going to neglect the issues related to *Exposure*, related to urban and infrastructural risk that are the responsibility of urban planning matters. In fact, if we consider the *Exposure* unitary and if with the loss levels we indicate the aspects related to the structural damage, and therefore to the limit states that can be reached following a seismic event, then the seismic risk can be defined as the probability of collapse in a time interval (e.g. the useful life of the structure), whose limit state function Z is not positive if the corresponding limit condition is reached or exceeded.

From a seismic and structural point of view, the function of state Z can be expressed by comparing the seismic demand (D), which represents the required performance to the structure by the seismic action, and the capacity (C) of the structure itself, which in general can be represented in terms of displacement or resistance. According to these definitions, by indicating the probability function of failure with P_f, the risk can be expressed by the following formulation:

$$P_f = P[Z \leq 0] = P[C \leq D] \tag{1.1}$$

The way to evaluate this probability consists in separating the estimate of the structural answer from the probabilistic one of the question [7]:

$$P_f = P[Z \leq 0] = P[C \leq D] = \sum_{im} P[C \leq D | IM = im] \cdot P[IM = im] \tag{1.2}$$

The first term of the (1.2) indicates the *Fragility (Vulnerability)* that represents the probability of failure conditioned at a given *IM* seismic intensity, while the second term indicates the *Seismic Hazard* at the site of interest, which represents the probability of occurrence of an earthquake of intensity *IM* equal to *im*, and that *IM* is a synthetic parameter wherewith the intensity of the earthquake is measured. In common engineering practice, generic parameters of peak are used to evaluate the intensity, such as the PGA and the response spectrum. Integral parameters such as duration are used but play a secondary role in structural performance. The equation (1.2), whose graphical interpretation is shown in (*Figure 1.3*), can ultimately be read as follows: "The Seismic Risk is the Vulnerability to each level of intensity weighed for the Seismic hazard".

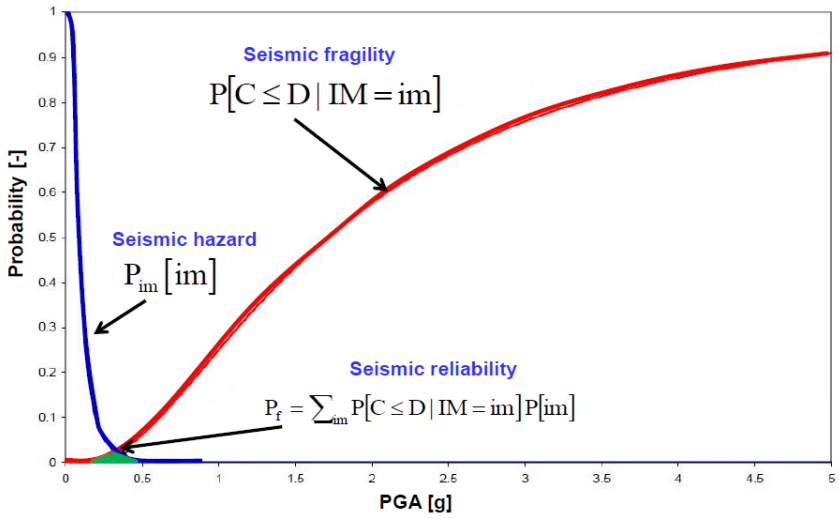

Figure 1.3: Graphical interpretation of the probability function of failure.

Assigned a site of interest, subjected to n genetic sources, the average number of events that cause the collapse of the structure, usually indicated with λ_f, is calculated as the sum of the occurrence rates of the earthquakes on each source, multiplied by the probability that the seismic demand D is greater than the structural capacity C. By applying the *Total Probability Theorem*, we can write the following equation, which is a mathematically more correct expression with respect to (1.2):

$$\lambda_f = \sum_i \lambda_i \cdot \int_{IM} P[C < D|IM = im] \cdot f_{IM_i} \cdot d(im) \qquad (1.3)$$

where:

- λ_i is the rate of occurrence of earthquakes on the i-th source;
- IM_i is the Intensity Measure of ground motion relative to the i-th source;
- f_{IM_i} is the probability distribution function (PDF) of IM relative to the i-th source.

The term f_{IM_i} is calculated by means of hazard studies that consider seismic parameters such as magnitude M and the seismic-site source distance of interest R. This, can be written in symbols through the following mathematical formula:

$$f_{IM_i} = \int_{R_{min}}^{R_{max}} \int_{M_{min}}^{M_{max}} f_{IM|M,R}(im|m,r) f_R(r) f_M(m)\, dr\, dm \tag{1.4}$$

Where $f_{IM|M,R}$ represents the distribution of the IM intensity given the magnitude M and the distance R.

Making the product between the occurrence rate of the earthquakes at the i-th source, λ_i, and the distribution f_{IM_i}, is equivalent to calculating the Integral of Hazard; then we obtain the curve that, when the IM changes, shows how the rate of occurrence of IM at the site of interest varies.

Known the rate of events λ_f causing structural collapse, the probability of collapse in any time interval [t, t+Δt] is then calculated using the following formula:

$$P_f[t, t+\Delta t] = 1 - e^{-\lambda_f \Delta t} \tag{1.5}$$

which allows to evaluate the seismic reliability as the probability that in the time interval [t, t+Δt] it may take at least one seismic event that causes the collapse of the structure under examination; since *at least one event that causes collapse* is the complementary of 1 of *zero events that cause collapse*, remembering that the earthquake occurrence process is modelled as a Stationary Stochastic Process of Poisson with random selection [8] of the type:

$$P\left[N_f(t, t+\Delta t) = n\right] = \frac{(\lambda_f \Delta t)^n}{n!} e^{-\lambda_f \Delta t} \tag{1.6}$$

where N_f is the number of seismic events that cause the collapse and it is simple to derive the expression (1.5).

1.3 Evaluation Elements of Seismic Hazard

The seismic hazard represents a measure of the destructive potential of the earthquake. A more correct definition can be given in probabilistic terms by defining the hazard as the probability of overcoming a prefixed spectral order (or PGA) for a fixed period in a reference time frame. From this point of view, the study of the seismic hazard leads to the construction of the hazard curves that for a given period, or peak acceleration at the ground, correlate the acceleration spectral ordinate with a certain probability of exceedance that is generally given in a time frame of 50 years.

The evaluation of the hazard curves is carried out through statistical studies based on the databases of past earthquakes and is the subject of geophysics studies. Currently in Italy, accessing the site of the INGV (National Institute of Geophysics and Volcanology) exists the ability to view the interactive maps of seismic hazard of the entire national territory [9] (*Figure 1.4*). This site also provides, as a function of longitude and latitude, the 9 annual exceeding frequencies, defined as the inverse of the return period, T_R, of the same values of the spectral acceleration (as a function of the structural periods) and of the PGA, referring to a probability of exceedance in 50 years. In any case, obtain the hazard curves and set a probability of exceedance, the acceleration spectrum, and subsequently the displacement spectrum, can be calculated.

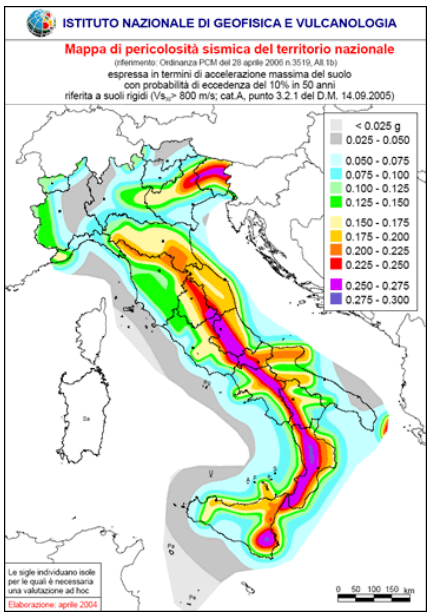

Figure 1.4: Map of seismic hazard of the Italian territory.

1.4 Evaluation Elements of Seismic Vulnerability

The seismic vulnerability represents the propensity of people, goods or activities to suffer damage following the occurrence of the seismic event. It consists of three components, that are:

- Direct vulnerability: defines the propensity of a single (or complex) physical element to be damaged by an earthquake;
- Induced vulnerability: it is defined according to the crisis that is induced by the collapse of a single physical element or complex of goods;
- Deferred vulnerability: defines the effects that occur after the seismic event and the first emergency.

In this thesis, we want to study the seismic vulnerability applied to the bridges and we will refer to the direct vulnerability only. The seismic vulnerability of a bridge is therefore considered as a measure of the greater or lesser propensity of the bridge itself to suffer damages due to an earthquake of assigned characteristics. The vulnerability therefore relates the seismic action on the one hand, and on the other hand the damage caused on the physical system.

Regarding the measurement of the seismic IM, different parameters can be chosen to identify it, including peak ground acceleration (PGA), the spectral pseudo-acceleration evaluated at the fundamental vibration period of the structure and so on; in fact, it is important that any IM is chosen, it is possible with it to describe the capacity of an earthquake to damage a structure.

For the choice of the damage parameter, a possible aspect may be correlating the damage to the economic costs to be incurred for restore the structure that has been invested by the seismic action. In a structural analysis the damage can be linked to certain limit states defined through the achievement of specific levels of displacement or resistance of the structures. However, at the end of the vulnerability assessment process it is possible to construct a fragility curve (vulnerability curve) that correlates the damage of a structure or a class of structures with the IM intensity chosen to represent the seismic action.

In particular, the fragility (vulnerability), in probabilistic terms, represent the probability of exceeding a predetermined limit state for a fixed seismic IM; another definition that can be given is that the fragility curves represent the probability of exceeding a predetermined level

of damage, caused in correspondence with an appropriate control parameter. Using such curves, it is therefore possible, to determine in probabilistic terms the intensity of the seismic action necessary to bring a structure to a determined level of seismic or damage response.

For each structure, or for each class of structures, it is possible to construct multiple fragility curves, each corresponding to a predetermined level of damage. An example of fragility curves constructed as a function of peak ground acceleration (PGA) is shown in (*Figure 1.5*):

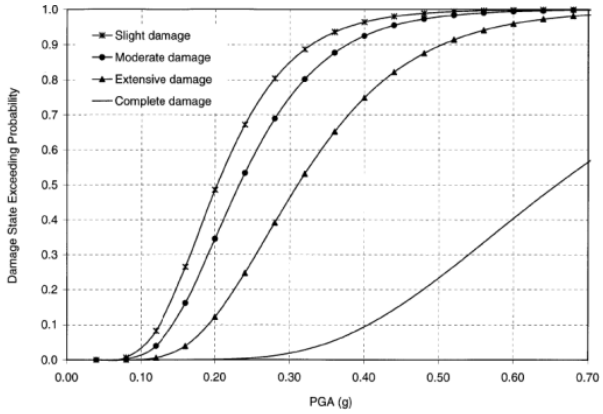

Figure 1.5: Fragility curves for prefixed levels of damage.

For the construction of seismic fragility curves, currently there are different approaches; these approaches can be grouped into three categories:

- Methods based on expert judgment;
- Empirical methods;
- Analytical methods.

A detailed description of the three approaches is reported.

Methods based on expert judgment

These methods are based on the attribution to each structure of a vulnerability index (v), determined through some rules based on indicators not interpreted with typological meaning but based on their suitability to withstand earthquakes (for example efficiency of connections, resistance of materials, morphological regularity); in a second time, a vulnerability curve or a

damage probability matrix is associated with each value of the vulnerability index. Normally the vulnerability index is calculated based on partial indices corresponding to each indicator and attributable following qualitative examinations of the structure. This type of method, semi-quantitative, or even diagnostic-type, implements qualitative or quantitative assessments of the factors that govern the seismic response and the related knowledge-based elaborations, while retaining the characteristics of rapidity of use and economy, allow to introduce information on regularity, ductility, resistances, geometry, etc., obtaining the evaluation of a vulnerability index. The problem with these methods is that they are not mechanical-analytical and therefore consider the behavior of typologies of structures based on experience and knowledge.

Surely, among all the methods based on the judgment experts, the most widespread and that currently used in Italy is that based on the first and second level vulnerability maps prepared by the National Group for the Defence of Earthquakes (GNDT) of the INGV [10].

Empirical methods

This type of approach, which is certainly the most widespread, is based on the statistical analysis of the damage caused by earthquakes [11]. However, the accuracy of the method may not always be appropriate due to the lack of a sufficiently large database. These (typological) methods evaluate the vulnerability of each class of structures. These classes are characterized by typological or functional indicators [12], [13]. For example, in the definition of a class, factors such as construction type, plant morphology, height, year of construction etc., are involved. To each class is associated a matrix of probability of damage or a curve of vulnerability. The verification of the hypotheses formulated during the construction of vulnerability curves or damage matrices is entrusted to the statistical processing of damage caused by past earthquakes, to structures. Assigning a certain class to a structure means assigning the vulnerability curve, or the damage probability matrix, that belongs to the class.

Analytical methods

The damage is evaluated totally in mechanical and analytical way. We then proceed to an analysis of the structure usually of the non-linear type. The damage is associated with the achievement of a limit state that can be identified by the setting of a limit rotation or a

collapse mechanism of the structure, while the action is generally expressed in terms of spectral quantities, such as the $S_a(T)$ or $S_d(T)$. For the analytical mechanical generation of seismic fragility curves, structural analyzes can be implemented with different levels of sophistication: linear, non-linear, pseudo-static or dynamic. The most commonly used analytical approaches, in fragility studies, are nonlinear dynamic step analysis or, otherwise, nonlinear static analysis.

1.5 Structural reliability

Structural reliability, or probability of success, can be defined as the probability that the structure will continue to perform the functions for which it was conceived, designed and constructed during a pre-established period ("useful life"), and below pre-established loading conditions. The uncertainties in the prediction of the loads and the characteristics of the materials make that one can never be certain (in a "deterministic" way) that a structure is safe.

It is necessary to compare the stresses "S", linked to the loads applied to the structure, with the "R" resistances, linked to the characteristics of the materials used. Therefore, a construction can be considered reliable if the probability of success, P_s, that continues to perform its functions throughout its useful life, will be greater than a pre-set P^* acceptability value.

1.5.1 Methods for evaluating structural reliability

The evaluation of the structural (or seismic) reliability of a structural system in the seismic area, has had considerable changes over time, passing from a deterministic approach (in which attention was focused solely on resistances) to a modern probabilistic approach (as described in the NTC08 and EC2 Regulations). Considering, in fact, the probabilistic nature of the phenomena involved in the design, which in this case is constituted by the randomness of the seismic actions, it is necessary to consider that the level of protection in respect of performance limit states can only be expressed in probabilistic terms, i.e. through the probability that each predefined limit state is exceeded, at least once, during the useful life of

the structure. The evaluation of the level of protection, with respect to a given limit state, can be carried out by checking that the relationship is satisfied:

$$P_{fail} \leq P_{fail}^{*} \tag{1.7}$$

where P_{fail}^{*} is a limit value of the probability of collapse, representative of the risk accepted in relation to the consequences deriving from the achievement of the limit state taken into consideration.

To the structures are required to have a high degree of security, and this translates into a relatively low probability of collapse. To minimize the value P_{fail}^{*}, means to design more important and therefore more expensive structures, so that the costs could be incompatible with the function of the structure, as well as with the economic and development conditions of the country. The determination of an acceptable value of the probability of collapse, therefore, involves political and socio-economic as well as structural competences, and for this reason it is not so simple.

The different methodologies for the evaluation of structural reliability can be grouped into the following categories:

- Allowable stress design method (ASD) (Zero Level Method);
- Semi-probabilistic method to limit states (First-level probabilistic method);
- Simplified probabilistic approach (Second-level probabilistic method)
- "Exact" probabilistic approach (Third-level probabilistic method).

In this thesis, however, we will consider only the "Exact probabilistic approach", as required by the Regulations.

Third level probabilistic method

This method involves the modeling of random variables, such as material resistances and permanent and variable actions, acting on the structure, which intervene in the definition of safety through the respective probability density functions. The probability of failure is represented by the following numerical formulation:

$$P_{fail} = P[X \in U] \tag{1.8}$$

where X is the vector of the variables that define the system and U is the failure domain, defined as the subspace of the variables X, in which the condition that the stresses S are not higher than the resistances R (S ≤ R) is not verified. Using the JPDF (joint probability density function) of the X vector representing the random variables characterizing the problem under examination, the probability of collapse is expressed as:

$$P_{fail} = \int_U f_x(X)\, dx \tag{1.9}$$

while the probability of success is expressed as:

$$P_S = \int_S f_x(X)\, dx \tag{1.10}$$

where S is the complementary subspace of U with respect to the space of the variables X for which the condition that the stresses are less than or equal to the resistances S ≤ R is verified.

Furthermore, given the vector of the project variables X = (X_1, X_2, …., X_n) (loads, geometry, etc.) a function G=G(X) can be defined such that:

- G > 0 if the limit state is not exceeded;
- G = 0 if the limit state is reached;
- G < 0 if the limit state is exceeded.

this function is called performance function and its simplest form is G (R, S) =R-S. Once the function G has been introduced, the probability of collapse can be rewritten in the following form:

$$P_{fail} = \int_{G(X)\leq 0} f_x(X)\, dx \tag{1.11}$$

The problem of structural reliability is apparently reduced to the solution of this multidimensional integral. Solving this integral analytically in a closed form, is possible, however, only when the two functions (performance and joint probability density JPDF) are expressed in a very simple way, under very restrictive assumptions; in all other cases the integral is solved only by numerical means, thanks to the simulations performed with the Monte Carlo method. However, if we assume a two-dimensional nature of the problem of structural reliability, with independent variables, then for example a space resistance (R) - stress (S), in which we assume the functions of probability density PDF of the two variables, $f_R(r)$ and $f_S(s)$, the probability of collapse can be formulated as follows:

$$P_{fail} = \int_{G(X)\leq 0} f_x(X)\, dx = \iint_{[R-S<0]} f_{R,S}(r,s)\, drds \tag{1.12}$$

and having made the hypothesis of independent variables, we can write:

$$f_{R,S}(r,s) = f_R(r) f_S(s) \tag{1.13}$$

and replacing them in the previous integral we have:

$$\iint_{[R-S<0]} f_{R,S}(r,s)\, drds = \int_0^\infty f_S(s)\left[\int_0^\infty f_R(r)dr\right]ds = \int_0^\infty f_S(s) F_R(s)\, ds \tag{1.14}$$

therefore, P_{fail} is given by the convolution integral of two functions of s, whose geometrical interpretation is represented in (*Figure 1.6*), where $f_S(s)$ is the JPDF of S and $F_R(s)$ = P[R<S] is the CDF (Cumulative Distribution Function) of R.

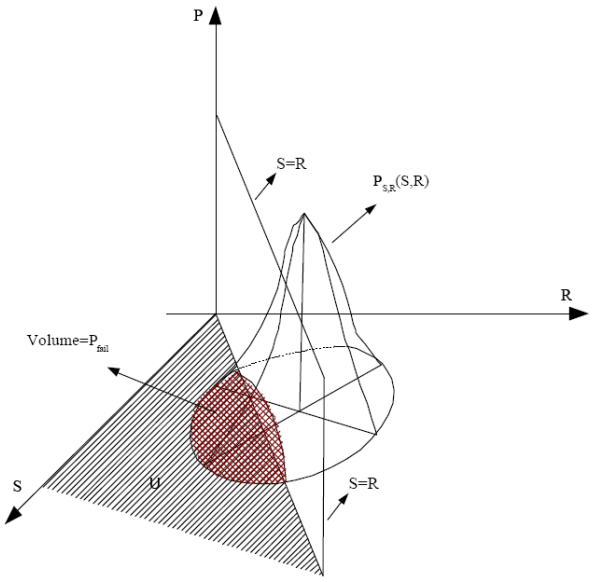

Figure 1.6: Geometric meaning of $P_{fail.}$

This procedure quickly becomes impracticable as the number of random variables increases. To overcome this problem, very effective simulation methods have been developed over the years, such as "Monte Carlo" simulations, methods based on import sampling, stratified methods, etc.

1.5.2 Monte Carlo Method

With the term "Monte Carlo method" or "MC method", are called all those techniques that use random variables for solving mathematical problems. Their main characteristic is to evaluate a certain quantity through parameters such as mean, variance and correlation of a certain probability distribution known (or that can be hypothesized) to obtain an estimate, by randomly generating a sample from the corresponding population. Certainly, this is not a very efficient way to find a solution problem, because the simulated sampling procedure leads to a result that is always affected by the statistical error. In practice, we are often faced with situations where it is too difficult, or impossible, to use traditional numerical or analytical procedures and in all these cases the Monte Carlo method becomes the only alternative available. The application of this method is not restricted only to problems of a statistical nature, as it may perhaps seem from the use of probability distributions but includes all those cases in which a connection can be found between the problem under examination and the behavior of a prefixed random system: the value of a definite integral is certainly not a random quantity, but it can, for example, also be calculated using random numbers.

This method, therefore, allows to evaluate the probability of failure in the case of explicit and implicit limit state functions. The initial step is to define the problem by considering all the random variables, followed by the quantification of these by the PDF; in this sense, a sufficiently large set of values of the considered standard variables is generated, through statistical sampling techniques, according to the corresponding probability distributions. The process is repeated n times, to obtain n sets of values based on which to obtain the solution sought, based on the number of samples.

In the case of the structural reliability problem, in the limit state function seen in the previous paragraph, G(X) = G (X_1, X_2, ..., X_n), the X_i variables represent the random project variables such as resistances, stresses and displacements. A set of values of X, according to their PDF, is then generated numerically through a generator of random numbers. This set is replaced in the limit state G function and its value is verified, positive (no collapse) or negative (collapse). Repeating the process n times (with n very high), it is possible to simulate the PDF of G. The probability of collapse can therefore be estimated through the following formulation:

$$P_{fail} = P[G(X) \leq 0] = \lim_{N \to \infty} \frac{n_f}{N} \tag{1.15}$$

where N is the total number of simulations and n_f represents the number of times when collapse occurs (G (X) < 0). The probability so obtained, however, has an intrinsic uncertainty, depending on the value of N used. In fact, the variance of the ratio n_f /N, and therefore the uncertainty of the evaluation of the probability, decreases with the growth of N. The above procedure demonstrates how the evaluation of P_{fail} is approximated by means of the integral above, then through an approach based on the frequency of probability.

Sampling method

In the Monte Carlo probabilistic simulations, the statistical sample generation method is of particular importance. The sampling method used, directly affects the goodness of the results obtained and especially the computational efficiency of the whole process. In fact, the sampling method requires to produce a statistically representative sample of the statistical population examined and to optimize the computational efficiency of the probabilistic simulation, to maintain a good representation of the sample as its size decreases. The simplest and most intuitive sampling method, commonly called “Brute force sampling”, is based on purely random or more properly pseudo-random generation of the elements of the sample itself. Unfortunately, it is also the least efficient as to maintain an adequate statistical representativeness requires a high sample size and is, therefore, so inefficient from the computational point of view that it is inapplicable to the study of complex problems in which several random variables are involved. To improve the efficiency of the MC method, thus making it applicable to the study of complex problems, it is necessary to use a more refined sampling method that generates the individuals which constitute the statistical sample, following appropriate criteria that ensure their representativeness even for small dimensions.

Generation of continuous random variables

The basic method for all MC simulations is to use the cumulative or cumulative probability density CDF of a random variable x. It is necessary to define immediately what is meant by uniform probability density. A continuous variable x, which assumes values in the

finite interval [a, b], is said to be uniform in [a, b] when it has a constant probability density, called uniform or flat, shown in (*Figure 1.7*), given by:

$$u(x) = \begin{cases} \frac{1}{b-a}, & a \leq x \leq 0 \\ 0, & x < a \; o \; x > b \end{cases} \tag{1.16}$$

The normalization condition is satisfied by:

$$P[a \leq x \leq b] = \int_a^b u(x)dx = 1 \tag{1.17}$$

while, mean and variance are given by:

$$\mu = \frac{1}{b-a}\int_a^b x \, dx = \frac{b+a}{2} \tag{1.18}$$

$$\sigma^2 = \frac{1}{b-a}\int_a^b (x - \frac{b+a}{2})^2 \, dx = \frac{(b-a)^2}{12} \tag{1.19}$$

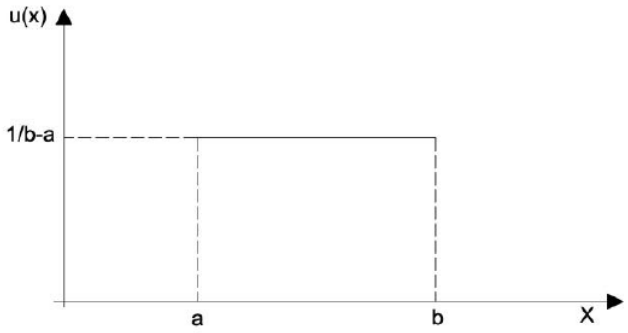

Figure 1.7: Uniform probability density function of a random variable that assumes values included in [a, b].

For a random variable ($a \leq x \leq b$) with uniform density, the probability of localization in (x_1, x_2) is proportional to the amplitude of the interval:

$$P[x_1 \leq x \leq x_2] = \int_{x_1}^{x_2} p(x)dx = \frac{(x_2 - x_1)}{(b-a)} \tag{1.20}$$

On the other hand, if a continuous random variable satisfies the previous one, it is distributed uniformly. It is also shown that, if x is a random variable having a continuous density p(x), the cumulative random variable C:

$$C(X) = \int_{-\infty}^{x} p(x)dx \tag{1.21}$$

is uniform in [0,1]. In fact, the probability that a value x is included within [x_1, x_2] is identical for construction to the probability that the cumulative variable C is included within the values [$c_1 \equiv c(x_1)$, $c_2 \equiv c(x_2)$]. Then, we have:

$$P[c_1 \leq C \leq c_2] = P[x_1 \leq x \leq x_2] = \int_{x_1}^{x_2} p(x)dx = \int_{-\infty}^{x_2} p(x)dx - \int_{-\infty}^{x_1} p(x)dx = c_2 - c_1 \tag{1.22}$$

from which it is seen that C is uniform in [0,1], satisfying Equation (1.19) for (b – a) = 1. The conceptual and practical importance of what we have just seen should not escape: the variable cumulative is always uniform, regardless of the origin distribution.

If the integral $C(x) = \int_{-\infty}^{x} p(x)dx$ is known analytically, then the values of the cumulative variable C can be expressed as a known function C=F(x). If this function is invertible, then the variable:

$$x = F^{-1}(C) \tag{1.23}$$

has density p(x). Having a generator of uniform variables in [0,1], variables with probability density can be generated using the equation:

$$x = F^{-1}(random) \tag{1.24}$$

This procedure is identified as the “Inverse Transformation Algorithm”.

The previous report has a convincing graphic interpretation, shown in (*Figure 1.8*). Considering the probabilities p [$x_1 \leq x \leq x_2$] and p [$x_3 \leq x \leq x_4$] defined within the values [x_1, x_2] and [x_3, x_4]: they are represented by the areas subtended by the density function p(x).

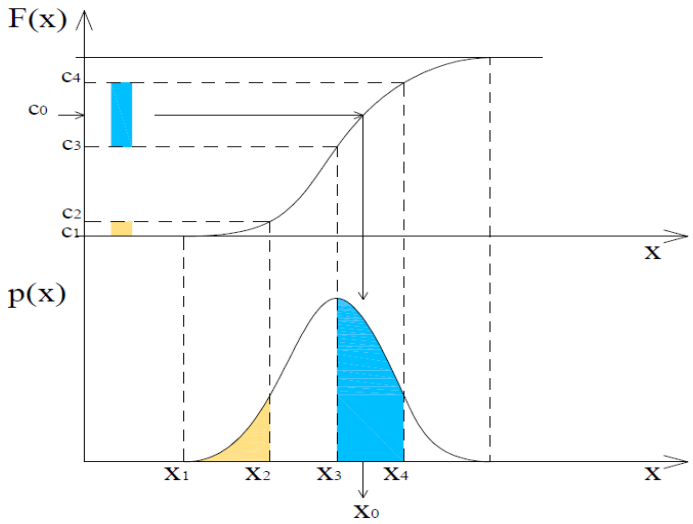

Figure 1.8: Graphic interpretation of the properties of the cumulative. The functions p(x) and F(x) are, respectively, a generic probability density and its corresponding cumulative.

The area related to the least probable values included in $[x_1, x_2]$ is less than that relating to the most probable values included in $[x_3, x_4]$. The value of these two areas is identical to the length of the intervals $[c_1, c_2]$ and $[c_3, c_4]$, obtained from the cumulative F(x). A variable C comprised in [0, 1], will fall more frequently in $[c_3, c_4]$ than in $[c_1, c_2]$ with probabilities given exactly by the amplitude of these intervals. Therefore, at a value c_0 assumed by uniform variable C, we obtain the corresponding value x_0; repeating the procedure several times we obtain a sample of values of the random variable x of density p(x).

Based on the "Inverse Transformation Algorithm", it would seem possible to solve all random generation problems. This situation, is not so simple, because the function p(x) to be integrated can only be known numerically, or the integral (1.21) it may not be solvable or result in an analytically non-invertible function.

Generation of Gaussian variables

The Gaussian density is the most important distribution of the probability calculation. For the Central Limit Theorem, we have seen that it represents the limit density of the linear combination of several random variables. The cumulative probability distribution of a Gaussian is given by the following function:

$$F(x) = \frac{1}{\sqrt{2\pi}\sigma} \int_0^x e^{\left[\frac{-1}{2}\left(\frac{x-\mu}{\sigma}\right)^2\right]} dx \tag{1.25}$$

This integral is usually evaluated with numerical methods, by developing in series the exponential, and numerically calculating the limit of the integrated series; this is done because the primitive of F(x) is not known analytically. This complication is solved by using a standard Gaussian, which is obtained by defining the standard variable:

$$t = \frac{x-\mu}{\sigma} \tag{1.26}$$

which measures the deviation of a value x from its average in units of standard deviation. By operating a change of variable in the previous integral, we obtain:

$$\Phi(x) = \frac{1}{\sqrt{2\pi}} \int_0^x e^{\left(\frac{-t}{2}\right)^2} dt \tag{1.27}$$

this primitive, being independent of μ and σ, can be calculated once and for all by developing the exponential in series, it is found tabulated in all the statistical texts and is available in many scientific software.

The standard Gaussian density is then governed by the following equation:

$$g(x) = \frac{1}{\sqrt{2\pi}} e^{-x^2/2} dx \tag{1.28}$$

characterized by mean zero and unitary standard deviation. By operating the previous change of variables, an ordinary Gaussian, it can always be traced back to the standard one.

Wanting to generate a random variable from a Gaussian distribution, we encounter, as we have seen, a difficulty linked to the fact that the cumulative function is not invertible. In these cases, we resort to the appropriate algorithms, that among the most used, the simplest is that based on the Central Limit Theorem.

Suppose that we generate N numbers (ξ_1, ξ_2, ..., ξ_n) uniformly distributed in the interval [0,1]; from the Central Limit Theorem, for N quite high, the mean:

$$M = \frac{1}{N} \sum_{i=1}^{n} \xi_i \tag{1.29}$$

it is a Gaussian variable of average 1/2. The variance of M is given by the variance of the uniform distribution for the number of events generated:

$$Var[M] = \frac{1}{12N} \tag{1.30}$$

Introducing the standard variable of M, we have:

$$t = \frac{M-1/2}{\sigma[M]} = \frac{\sqrt{12}}{\sqrt{N}} \cdot \sum_{i=1}^{N} \xi_i - \frac{\sqrt{12N}}{2} \tag{1.31}$$

Generally placing N = 12, we already get a distribution close to the Gaussian one; the variable x searched will therefore be the following:

$$x = (\sum_{i=1}^{n} \xi_i - 6)\sigma + \mu \tag{1.32}$$

1.5.3 Latin Hypercube Sampling Method

The high N number of simulated events, required by the Monte Carlo method, depends essentially from the sampling technique. In its basic definition, the method MC uses for the choice of input values the “Simple Random Sampling”, and to better estimate the function of distribution of the probability of the output, it would be necessary to carry out a considerable number of analyses. It is certainly the most intuitive, but also the least efficient in case it is necessary to reduce the number of analyses to be performed. In fact, there is a risk of obtaining a false sampling, which does not cover the entire range of variation of the random variable.

In this regard, if the computational burden in terms of time for each "launching" of the calculator is limited, then it is reasonable to increase the sample size to reduce the error related to sampling: if, instead, the time for each analysis begins to be high, we must necessarily reduce the size of the sample, trying to reduce the resulting percentage of error by intervening on the sampling method, using for example, methods of stratified sampling, more or less sophisticated.

Stratified Sampling

This is an evolution of the Simple Random Sampling, since it is proposed to avoid the possibility of having an unallocated sampling over the whole range of the random variable. Specifically, the sampling space is subdivided ("stratified") into n intervals not overlapped each other, from each of which a value of the relative random variable is randomly extracted.

Latin Hypercube Sampling

Was developed by Mckay et al. [14], represents a further evolution of the basic Stratified Sampling, always aimed at increasing statistical efficiency with a reduced computational burden. It is part of those so-called "smart" methods, which basically allow to "drive" the simulations to reach the collapse faster. The input range, consisting of the cumulative probability function, is appropriately divided into n disjoint intervals having the same probability equal to 1/n (equal intervals). For each interval, a value is randomly extracted between 0 and 1 which, depending on the interval considered, leads to a precise value of the cumulative probability, which reverses, produces the value of the random variable (*Figure 1.9*).

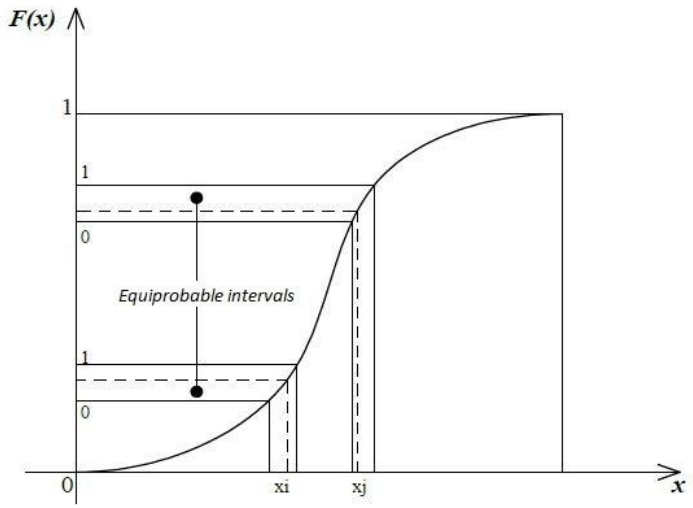

Figure 1.9: Generation of two random variables using LHS sampling.

The cumulative probability for each of the n intervals can then be calculated through a linear transformation expressed by the law:

$$P_m = \frac{1}{n} U_m + \frac{m-1}{n} \tag{1.33}$$

where, m is a number between 1 and n; U_m is the value generated randomly between [0, l] and P_m is, as mentioned above, the value of the cumulative probability valid for the m-th interval. The equation also shows how one, and only one, of the generated values falls within each of the n intervals:

$$\frac{m-1}{n} < P_m < \frac{m}{n} \tag{1.34}$$

where $(\frac{m-1}{n})$ and $(\frac{m}{n})$ are respectively the lower extreme and the upper extreme of the m-th interval.

Finally, after having obtained the values for each interval and notes the analytical expression of the accumulated interest, we obtain the values of the random variable searched for by the following expression:

$$X_{k,m} = F_x^{-1}(P_m) \tag{1.35}$$

In this relation, $X_{k,m}$ is the m-th value generated for the k-th variable aleatory and F_x^{-1} is the inverse of the cumulative probability distribution representative of the random variable k-th; the values generated for each variable can then be coupled to each other, through a still random permutation.

CHAPTER 2

2. SEISMIC DAMAGE IN BRIDGES AND SEISMIC ISOLATION

In the latest forty years, earthquakes caused severe damages to civil infrastructures all over the world, with an increasing trend. Lots of important bridges collapsed, even if designed to resist seismic actions: this was mainly due to their usual structural simplicity, which makes them be very vulnerable to seismic damaging. For these structures, evaluating their damage is fundamental, to assess that of road and highway systems: the related risk is actually calculated with specific reference to the direct damage of bridges and to the delay on travelling time due to bridges' closure.

2.1 Frequent seismic damages in the bridges

The damage due to earthquakes can affect all the structural components of a bridge: in particular, damage to the bridge, which usually does not have a primarily anti-seismic function, are linked to errors in the kinematic concept, which lead to different mechanisms of collapse (dissociation, pounding); on the other hand, the various types of damage observed on the piers are generally caused by flexural ductility and shear resistance defects.

2.1.1 Deck collapse

Deck collapse caused by relative displacement of spans in longitudinal direction was very recurrent, especially in simply supported multispan bridges: in most cases seats and corbels resulted in a scanty length, so that spans became unseated and collapsed.

The following (*Figure 2.1*) show some examples of this type of failure: it is worth noting how the deck remained perfectly intact, as the seismic action does not specifically harm this structural component of the bridge. Conversely, seats would need to be oversized: in (*Figure 2.2*) is depicted the hinge of a new arc bridge, that was cleanly cut due to horizontal seismic actions. In this case there were inadequate seismic restrainers, consisting of bolts connecting the arch end plates to the transverse beam of the collapsed span.

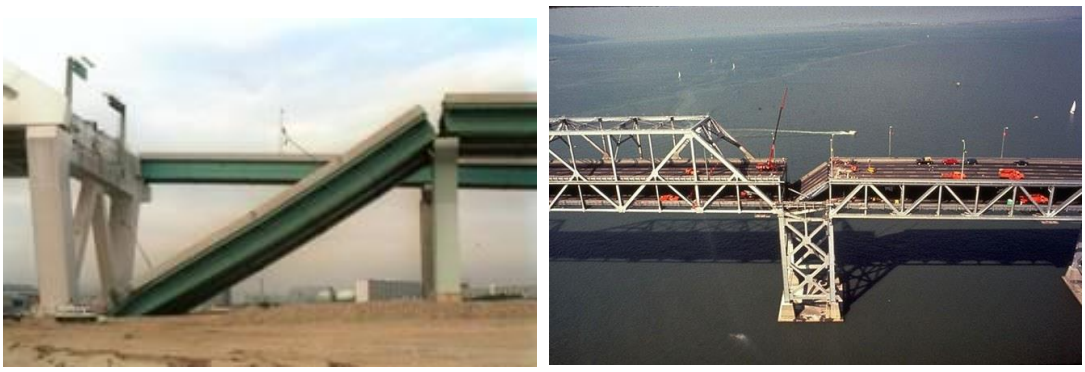

Figure 2.1: Kobe earthquake, Japan, 1995: Unseating, Nishinomiya-ko Bridge a); Loma Prieta earthquake, California, USA, 1989: Viaduct approaching the East Bay Bridge b).

Figure 2.2: Kobe earthquake, Japan, 1995, Bearing failure, Higashi-Kobe Bridge.

When bridges are built on soft or liquefiable soils, their vulnerability exponentially increases. This because, soft soils generally yield the structural response amplification, so that the loss of support becomes more probable (*Figure 2.3*). In the case of saturated sandy silt or silty sand soils, liquefaction may occur, and the induced soil movements may push the foundations out of place; if the bridge foundation system is made of piles, their carrying capacity may cease.

Figure 2.3: Loma Prieta earthquake, California, USA, 1989. West Grand Viaduct: Soil liquefaction effects.

When adjacent structural components have different stiffness and the distance among them is not enough to allow their differential displacements, damage may occur due to cyclic pounding (*Figure 2.4*). Moreover, as the fundamental frequencies may result in out of phase, shear forces and consequent pounding are amplified.

Figure 2.4: Pounding damage: a) Kobe earthquake, Japan, 1995, Near Nishinomiya Port; b) Sichuan earthquake, China, 2008, Miao Zi Ping Bridge.

2.1.2 Piers collapse

The piers of the bridges often failed after a progressive flexural yielding followed by a cyclic deterioration of the cross section due to insufficient confinement and, consequently, by a decrease of the shear resistance. This collapse mechanism reveals a flexural ductility depletion (*Figure 2.5*), usually combined with exceeding the shear resistance.

Figure 2.5: Northridge earthquake, California, USA, 1994, Gothic Avenue Viaduct: Plastic hinge collapse.

These failures lead to high residual deformations and so, especially if the deck is very broad and supported by a single line of piers, a complete collapse caused by the loss of equilibrium may occur, also due to the high moment of inertia generated by the deck rotation (*Figure 2.6*).

Figure 2.6: Kobe earthquake, Japan, 1995, Hanshin Viaduct: collapse due to loss of equilibrium.

A further vulnerable element in framed piers is represented by the inadequate dimensioning of the beam-pier joints, which are very sensitive to shear failure (*Figure 2.7*).

Figure 2.7: Kobe earthquake, Japan, 1995, Shinkansen Viaduct.

2.2 Vibration control system

Today, the approaches currently used for structure protection are all oriented towards a common line of thought, which could be defined as "Vibration control". This approach is based on a philosophy that consists mainly in regulating "dynamically" the vibrations induced by the wind or by the earthquake, through devices that are not properly structural. The control systems can be classified in topological terms into two distinct categories [16]:

- Systems with open loop control laws: this is a system in which the control action is independent of the output, as shown in (*Figure 2.8*). As can be seen, the control law consists in filtering the input signal in the primary system. Therefore, in the base isolated systems, a type of "open loop passive control" is realized, in fact, the excitation is filtered by the level of isolation, that assumes the role of controller as it regulates the transmittance of the excitation to the superstructure. For a fixed base system instead, the excitation is transmitted directly to the structure.

Figure 2.8: Open loop control system.

- Systems with closed loop control laws: this is a system in which the control action depends in some way on the output and is therefore said to be feedback because it arises from a closed sequence of return between effect and cause as shown in (*Figure 2.9*).

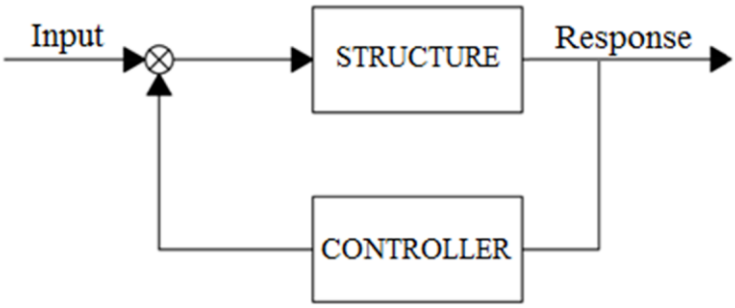

Figure 2.9: Close loop control system.

From the application point of view, it is possible to distinguish the following control methods:

- Passive control of the dynamic of the structure, which acts through forces that are developed in response to the motion of the structure and, therefore, does not require energy input from the outside. Seismic isolation, Supplementary Energy Dissipation and Mass Damping are the fundamental passive systems;
- Active control of the vibrations, however, includes the whole of those systems endowed with the ability to intervene in the dynamic process through the contribution of external energies, according to the dynamic state in which, moment by moment, the building is found following the seismic actions, to precisely adjust the structural response in a more favourable way;
- Hybrid Control, is the application of an active control system to a system already equipped with passive control. With this methodology, there is the advantage that, with the same performance, the regulation forces and energies are less than those necessary for the regulation of a system without passive control.

Focusing attention on the technique of passive control of a structure, it can be achieved using two systems:

- passive energy dissipation system (dissipators), which absorb part of the transmitted energy and limit the excursion in the elastic field of the structure;
- base isolation system (isolators), which achieve a decoupling of the motions of the superstructure and the ground, to reduce the energy transmitted by the earthquake to the construction and consequently the magnitude of the stresses and structural deformations.

This thesis focuses mainly on the base isolation system, in which the operating principles and the main devices used for its practical realization will be seen below.

2.3 Seismic base isolation in the structures

The technique of seismic base isolation of a structure [15] consists in interposing between the ground (S), on which the foundations are placed, and the structure in elevation (B) a series of elements (I) of low horizontal, high rigidity vertical stiffness, and high dissipative capacities, which greatly reduce the acceleration perceived by the structure. In this way a dynamic decoupling of the horizontal motion of the structure and of the ground is thus created, which drastically reduces the energy transmitted by the earthquake to the superstructure. Considering now a Z system composed of the three sub-systems (S) - (I) - (B) arranged in series, it is easy to understand how the seismic waves coming from the bed-rock are first "filtered" during their propagation by the layers of ground crossed, with a consequent change in the amplitude and frequency characteristics of their harmonic components; at the interface (S) - (I), the incident seismic waves are partly transmitted to the superstructure and partly reflected due to the fact that the crossed vehicles have different mechanical characteristics.

Since the seismic excitations generally have a high energetic content in correspondence with the harmonics with a frequency close to that which characterizes the dynamics of medium-low constructions (Frequencies 1-10Htz), the main function of the seismic isolation is to filter this type of frequencies. A correct use of the isolation devices will have to consider the dynamic characteristics of the superstructure and of the foundation to avoid unwanted and dangerous resonance phenomena.

The general philosophy of the seismic isolation strategy, however, remains to increase the fundamental period of construction, to take it from the typical range of fixed base structures (0.3-1.5s) to values above 2s and even up to 4s, entering therefore in the field of the response spectrum characterized by lower accelerations and, therefore, by lower base shear forces (*Figure 2.10a*). On the contrary, the displacement spectra present small displacements in the field of the low periods, but they grow rapidly as the periods grow; the greater demand in terms of displacement will therefore have to be absorbed by the isolators, which will have to present as mentioned above a high horizontal deformability such as to allow it the wide excursions required (*Figure 2.10b*).

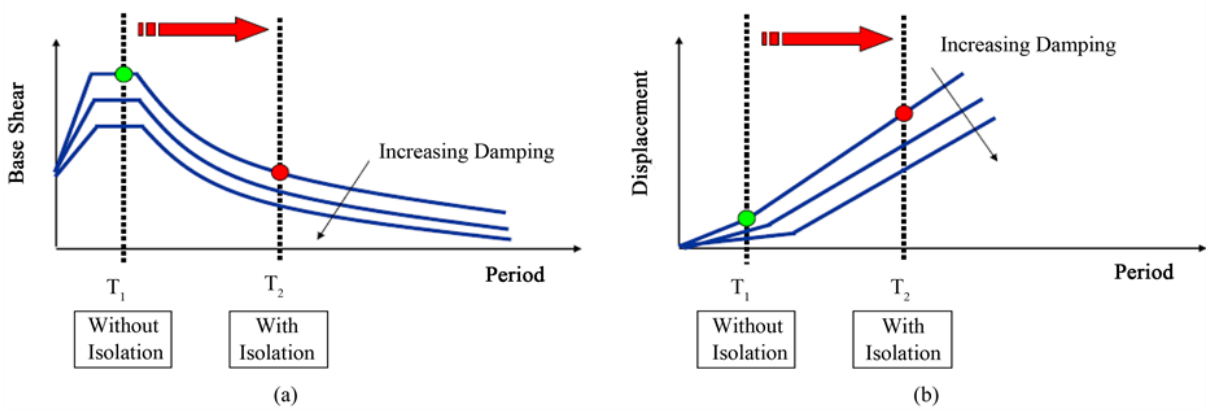

Figure 2.10: Effect of the seismic isolation on the base shear forces (a) and on the displacements (b) when the damping varies.

The isolation performance can then be improved through the dissipation by the system of an aliquot of mechanical energy transmitted from the ground to the structure.

From the seismic isolation derive two important benefits for the structure: there is a significant reduction of the accelerations transmitted to the superstructure (also to the last floors in case of very high constructions) and a significant reduction of inter-floor deformations. The isolators, in fact, accumulate most of the deformations and the superstructure behaves like a rigid block under the seismic action. From this, there are some constructive advantages that can be summarized as follows:

- the structure remains substantially in the elastic field, thus avoiding any damage of a structural nature that could compromise a loss of load-bearing capacity for vertical loads;

- damage to non-structural elements, such as infill walls, is avoided;
- you have complete functionality of the building in the post-seismic period: the greatly reduced accelerations cause little damage even to everything that is contained inside the building (for example: falling paintings, overturning of furniture, damage to electronic equipment);
- there is greater psychological safety of the occupants, whose perception of the seismic event, given the poor accelerations transmitted to the superstructure, is truly acceptable and not the harbinger of panic, anxiety and fear in the unfortunates.

To get a visual idea of the behavior difference between a fixed base structure and an isolated structure at the base, the deformation of a building in the two respective cases is shown below (*Figure 2.11*).

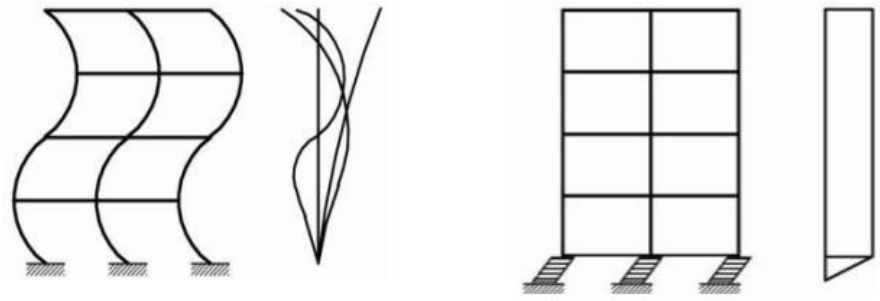

Figure 2.11: Difference of behavior, in terms of deformation, of a conventional building with a fixed base and one isolated at the base under seismic excitation.

The objective of the project of an isolated structure at the base is to obtain a behavior of the isolated system governed by a single modal component, with a frequency close to that of the isolated system, considered rigid with respect to the isolation plane: the first vibration mode, to which almost the whole mass is associated, is configured in a slow translation. From this derives, a concentration of displacements in correspondence with the isolated plane, and these must be absorbed by the isolators located at the base of the system.

The effectiveness of the isolation at the base is obtained from the ratio between the fundamental frequency of the superstructure ω_s and that of the overall system rigidly oscillating on the isolators ω_{is}, and this ratio is defined "Degree of Seismic Isolation" [15]:

$$I_d = \frac{\omega_s}{\omega_{is}} = \frac{T_{is}}{T_s} \tag{2.1}$$

moreover, the reduction of the seismic response of the superstructure increases with the increase in the degree of seismic isolation; at the same time the movements of the base plane tend to grow considerably more markedly at the low values of this parameter.

2.3.1 Seismic base isolation in the bridges

Now we want to go on to a more detailed analysis for what concerns the seismic isolation in bridges, always taking into consideration the basic principles of seismic isolation in structures, seen in the previous paragraph.

The superstructure of a bridge generally consists of a continuous multispan deck, supported by the isolation system. The bridge substructure consists in piers and abutments. The first are structures, generally made of reinforced concrete, with a prevalent vertical development that support the girder in intermediate points, while the second are structures that support the deck at its ends and which constitute a transition element between the bridge and the sections of adjacent road. By inserting a seismic isolator between the elements of the substructure and the deck, the horizontal damping and flexibility characteristics are exploited, so that only a portion of the seismic force impinging on the bridge is transmitted. In this way, a part of the incoming energy is substantially dissipated, and the displacement of the deck is thus reduced.

Having said that, we can therefore make some important hypotheses in the study of bridge isolation:

- The bridge superstructure (deck) and the bridge substructure (piers and abutments) must remain in the elastic field during the earthquake, in this way the basic isolation reduces the seismic response;
- The deck remains straight and is supported along its longitudinal axis through transverse diaphragms;
- The contributions of stiffness of non-structural elements (such as parapet walls, coat, sheaths) are neglected, but to be in favour of safety, inertial forces are considered;
- The force - deformation behavior is considered linear.

2.4 Types of seismic isolation devices

The anti-seismic isolators are classified according to the way the high deformability is obtained in a horizontal direction at the foot of the structure, and two main categories can be considered: Elastomeric isolators and Sliding isolators. Furthermore, for each category there are different types of devices, which are reported and described below.

2.4.1 Elastomeric isolators

Armed elastomeric isolators are currently the most diffused devices. They base their behavior on the deformation of the rubber used and then realize the dissipation of energy at the expense of large plastic deformations, through large cycles of hysteresis. They are characterized by the alternation of layers of elastomer (thickness of 5 ÷ 20mm) and steel sheets (thickness of 2 ÷ 3mm) solidarized by hot vulcanization processes. The presence of the laminations is fundamental, as it allows to confine the elastomer limiting its vertical deformability to a few millimeters (1-3mm) and generally they are shorter than the rubber layers, to be completely incorporated into the latter and be protected from corrosion. The performance of this type of device also depends on the characteristics of the rubber used and we can highlight two sub-categories:

- natural rubber elastomeric isolators;
- synthetic rubber elastomeric isolators.

The rubber is a hydrocarbon and is described by the chemical formula $(C5H8)_{n.}$ C4H8 is called isoprene and natural rubber consists of regular isoprene sequences arranged in such a way as to configure a chain that gives high elasticity to the material. In the natural rubber there are few links between the chains and when there is the action of an external force such chains stretch out to break the connections. Macroscopically, the material is subjected to deformations such as to be able to withstand large displacements, at least until the above links are broken. With specific treatments, further connections can be created. The synthetic rubber elastomeric isolators are based on the use of neoprene instead of isoprene. Neoprene has some advantages over natural rubber: it has greater fire-retardant capacity, gas impermeability and is less prone to aging.

Regardless of the type of rubber used, we can have elastomeric isolators with low or high damping rubber. In fact, rubber, whether natural or synthetic, has non-high damping capacities that must therefore be increased. The main elastomeric isolators are shown below.

Low Damping Rubber Bearings (LDRB)

This type of devices can be made either with natural rubber or with neoprene. Both types of rubber have very stable properties and do not exhibit creep for long-lasting loads. The behavior exhibited is substantially elastic as deformation increases (*Figure 2.12*).

The advantages associated with these devices are: simple production, low production costs, mechanical properties independent of temperature and aging. On the other hand, they have the disadvantage of having a low damping value (order of 2-4%) and not small displacements for horizontal operating loads (such as wind), which is why it is advisable to add auxiliary systems.

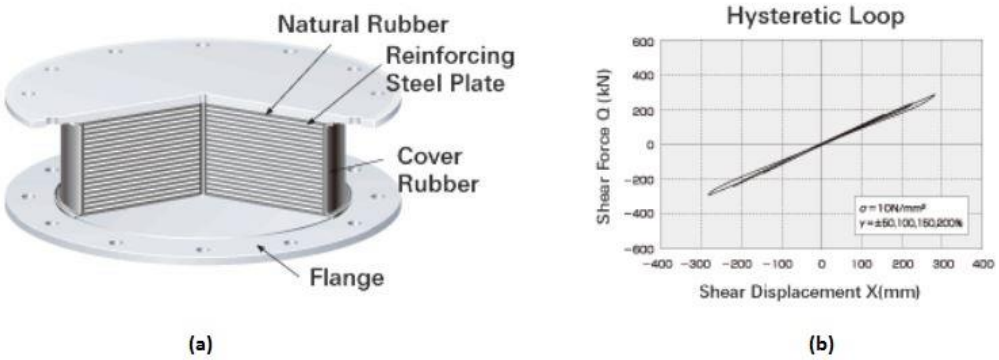

Figure 2.12: LDRB elastomeric isolator (a) with its relative hysteretic loop (b) (Bridgestone catalog).

Lead Rubber Bearings (LRB)

LRB devices are like LDRBs but contain one or more lead inserts in a hole in the centre of the isolator. The function of the insert is to dissipate energy by yielding. The constitutive force-displacement bond is of the bilinear type and their behavior is a combination of the linear elastic behavior typical of the elastomeric bearings and of the elastic-plastic behavior due to the lead core (*Figure 2.13*).

The deformation regime to which the insert is subjected, is of the cutting type, thanks to the confinement due to the steel plates. The equivalent viscous damping associated with the hysteresis cycles of the device is between 15% and 35%. The comparison between the hysteresis cycles recorded for LRB and LDRB isolators shows how the dissipated energy is greater for the first, which also shows greater stiffness.

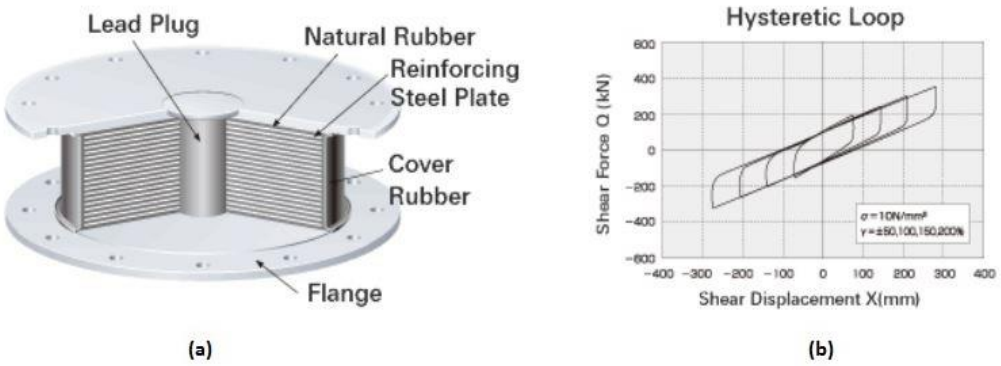

Figure 2.13: LRB elastomeric isolator (a) with its relative hysteretic loop (b) (Bridgestone catalog).

High Damping Rubber Bearings (HDRB)

These devices were developed in 1985 by Prof. Kelly at the University of California at Berkeley. They allow to have sufficient damping to eliminate the need for auxiliary devices and therefore constitute a complete system. The addition of special additive charges to the rubber, such as carbon black and silicon, allows to achieve a high damping, variable between 10% and 20% in correspondence of a 100% deformation. This damping reduces environmental vibrations; the isolators, in fact, act as a filter for high-frequency vibrations due to traffic.

Observing a force-displacement diagram, we notice a greater initial stiffness, which allows to resist the operating loads (like the wind), a lower and constant rigidity for a certain stretch and a consequent increase of the same for high loads (to avoid excessive deformations). Generally, therefore, non-linear behavior is exhibited with high initial stiffness and damping due to shearing deformations of less than 20%. In the 20-120% shear deformation range, the module is kept low and constant. For high deformations the module grows thanks to the

process of crystallization of the rubber, which is accompanied by energy dissipation (*Figure 2.14*).

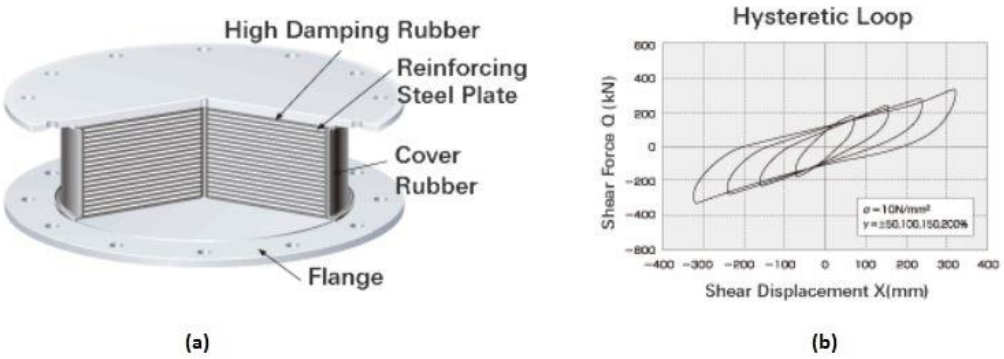

Figure 2.14: HDRB elastomeric isolator (a) with its relative hysteretic loop (b) (Bridgestone catalog).

2.4.2 Sliding isolators

The sliding isolators can be of two types:

- unidirectional (generally used for bridges);
- multi directional (generally used for buildings).

Flat surface sliding device (SD)

They are multi-directional support devices and in their simplest form the SD are made up of two different diameter discs that slide one on the other (*Figure 2.15*). The materials used are generally stainless steel and PTFE (Teflon), since they are materials capable of developing low friction resistance. The dynamic friction coefficient is generally between 5% and 20%, but also reduces to 1-2% in case of lubrication. Because of the variability of the coefficient and the uncertainties on the environmental conditions (temperature, humidity, cleaning), it is generally decided to neglect the dissipation of energy by friction and then resorted to lubricated devices, thus zeroing the dynamic friction coefficient and renouncing explicit action. In practice, the movements are left free. For the reasons outlined above, the SDs are never used alone, unless they present elements capable of increasing initial stiffness, providing dissipative capacity and providing capacity for re-centering.

Moreover, about the dynamic friction coefficient, it is a function of the contact pressure, the sliding speed, the temperature of the environment in which the device is inserted and the number of cycles. It can be said, therefore, that it:

- shows a very variable trend with respect to the speed, which for very low speeds is rapidly decreasing and subsequently, for higher speeds, increases until it becomes practically constant in the speed range that is typically reached in seismic conditions (200-800 mm/s);
- reduces almost linearly as the temperature increases;
- decreases as the temperature increases;
- is strongly influenced by the lubrication status of the contact surfaces.

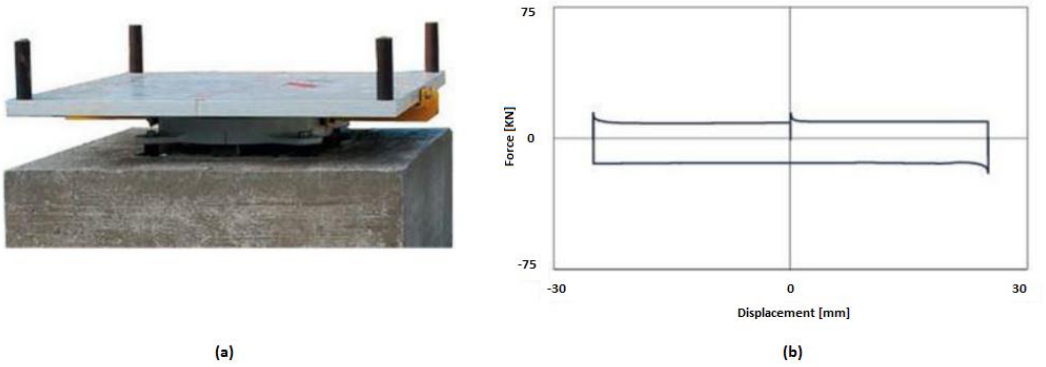

Figure 2.15: SD isolator (a) with its relative hysteretic loop (b) (Fip Industriale catalog).

Friction Pendulum System (FPS)

FPS are devices with curved sliding surfaces, that allow relative displacement between the superstructure and the substructure and are the only (sliding) isolators that incorporate the recentring and dissipative function (*Figure 2.16*). Their operation is based on the friction pendulum.

During the earthquake, the articulated steel and Teflon shell moves along the spherical concave surface, thus causing the supported mass of the superstructure to rise. The centering function is obviously given by the curved surface, which allows the device to return to position when the external action ceases. The vertical load, in fact, gives rise to a component in the tangential direction to the spherical surface allowing the device to re-center. The

elevation achieved by the pendulum converts kinetic energy into potential energy and the latter recalls the oscillating mass in its initial position of stable equilibrium. The dissipative function, on the other hand, is due to an unlubricated surface, and therefore to non-zero friction.

In the following chapter we will go into more detail on all the characteristics of this type of isolators, and insert below only the essential characteristics of these devices:

- The radius of curvature of the spherical surface determines the proper period of vibration of the structure;
- The proper period is practically independent of the mass of the structure;
- The friction of the equivalent surface determines the equivalent viscous damping.

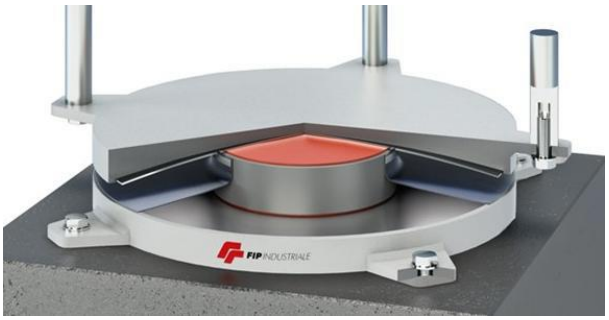

Figure 2.16: Single curved sliding isolator (FPS) (Fip Industriale catalog).

CHAPTER 3

3. THEORY AND MODELING OF ISOLATED SYSTEMS WITH FPS

The following chapter will deal with the theory of seismic isolation through the FPS devices, explaining at the beginning the bases that outline it, then we will continue with the study of dynamic behavior and experimental investigations on isolators. All this will be expressed not directly considering the application to bridges, as this modeling is a consequence of the theory developed for the buildings. In the following chapters, therefore, we will pass, to the development of the application to the bridges.

3.1 Theory of base isolation

The linear theory of seismic isolation is provided in detail by James M. Kelly in [17] which will be referred to below.

Similarly, to what happens for the fixed base structures, where the study of the dynamic behavior starts from the study of the simple oscillator, the characteristic aspects of the dynamic behavior of the isolated structures at the base can be derived from the analysis of a simplified model, at just two degrees of freedom (DOF), which represent the isolation system and the superstructure.

The study of the simple two-degree freedom system (2 DOF) (*Figure 3.1*), with linear springs and viscous linear damping, is developed with the modal analysis technique, which allows to identify the changes to the dynamic characteristics, vibration frequencies and modal forms determined by the isolation system on the superstructure. Let's remember, before going into more detail the dynamic study of the isolated systems, that, since many of the isolation systems are intrinsically non-linear, a linear analysis of these structures, as Kelly himself points out, will be considered only an approximation of the real dynamic behavior of the

structure, and the actual parameters of stiffness and damping must be estimated with the different linearization techniques proposed in the literature.

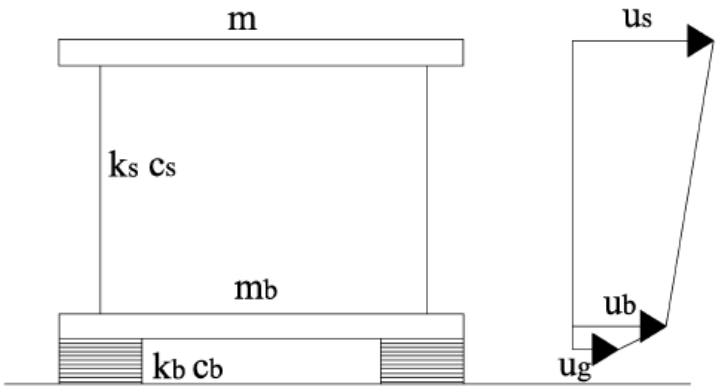

Figure 3.1: 2DOF model of a building isolated with FPS [17].

The mechanical and kinematic parameters that characterize the absolute motion of a two-degree freedom system are:

- m_s - mass of the superstructure;
- k_s, c_s - stiffness and damping of the superstructure;
- m_b - mass of the deck above the isolation system;
- k_b, c_b - stiffness and damping of the isolation system;
- u_g - displacement to the ground;
- u_s - absolute displacement of the superstructure;
- u_b - absolute displacement of the isolation system.

We then consider the equations of motion, written using the D'Alembert's Principle, which assert that any problem of dynamic equilibrium can be tackled as a problem of static equilibrium, provided that in writing the equations of balance between all the forces involved also consider the forces of inertia; the equilibrium conditions between the forces acting on the 2 DOF system in terms of absolute displacements are as follows (respectively for the superstructure and the isolation level):

$$m_s\ddot{u}_s = -c_s(\dot{u}_s - \dot{u}_b) - k_s(u_s - u_b) \tag{3.1}$$

$$m_s\ddot{u}_s + m_b\ddot{u}_b = -c_b(\dot{u}_b - \dot{u}_g) - k_b(u_b - u_g) \tag{3.2}$$

The displacement parameters with which it is more convenient to work are relative displacements, that is the relative displacement of the mass of the superstructure with respect to the isolation level and the relative displacement of the isolation level with respect to the motion of the ground:

$$v_s = (u_s - u_b) \tag{3.3}$$

$$v_b = (u_b - u_g) \tag{3.4}$$

Operating, therefore, with these new lagrangian coordinates the equations of motion become:

$$m_s(\ddot{v}_b + \ddot{v}_s + \ddot{u}_g) + c_s \dot{v}_s + k_s v_s = 0 \tag{3.5}$$

$$m_b(\ddot{v}_b + \ddot{u}_g) + m(\ddot{v}_b + \ddot{v}_s + \ddot{u}_g) + c_b \dot{v}_b + k_b v_b = 0 \tag{3.6}$$

By observing the two equations, the quantities related to ground acceleration can be highlighted, obtaining:

$$m_s \ddot{v}_b + m_s \ddot{v}_s + c_s \dot{v}_s + k_s v_s = -m_s \ddot{u}_g \tag{3.7}$$

$$(m_b + m_s)\ddot{v}_b + m_s \ddot{v}_s + c_b \dot{v}_b + k_b v_b = -(m_b + m_s)\ddot{u}_g \tag{3.8}$$

It is easy to notice that if within the second equation the term, which represents the relative motion of the superstructure relative to the isolation level, was suppressed, the second equation returns the classical equation of equilibrium valid for one-degree system of freedom; same reasoning can be repeated if within the first equation the term v_b was substituted.

At this point the presented equations system of motion can be solved by direct integration or by exploiting the principles of modal analysis, which allows to determine the modes of vibration, the participation factors and the modal frequencies of the described system.

We then rewrite the equation system using a matrix notation:

$$\begin{bmatrix} M & m_s \\ m_s & m_s \end{bmatrix} \begin{Bmatrix} \ddot{v}_b \\ \ddot{v}_s \end{Bmatrix} + \begin{bmatrix} c_b & 0 \\ 0 & c_s \end{bmatrix} \begin{Bmatrix} \dot{v}_b \\ \dot{v}_s \end{Bmatrix} + \begin{bmatrix} k_b & 0 \\ 0 & k_s \end{bmatrix} \begin{Bmatrix} v_b \\ v_s \end{Bmatrix} = -\begin{bmatrix} M & m_s \\ m_s & m_s \end{bmatrix} \begin{Bmatrix} 1 \\ 0 \end{Bmatrix} \ddot{u}_g \tag{3.9}$$

or even, in a more compact form:

$$[M]\underline{\ddot{v}} + [C]\underline{\dot{v}} + [K]\underline{v} = -[M]\underline{r}\ddot{u}_g \tag{3.10}$$

where [M] indicates the mass matrix of the system, [C] is the damping matrix of the system and [K] is the stiffness matrix of the system, while $\underline{v}$ indicates the vector of the relative displacements. Defining now:

- $\omega_s = \sqrt{\frac{k_s}{m}}$ frequency of the fixed base structure; (3.11)
- $\omega_b = \sqrt{\frac{k_b}{M}}$ frequency of the isolation system of stiffness k_b; (3.12)
- $\xi_s = \frac{c_s}{2\, m\, \omega_s}$ damping of the structure in elevation; (3.13)
- $\xi_b = \frac{c_b}{2\, M\, \omega_b}$ damping of the isolation level. (3.14)

Where the mass M is equal to the total mass of the isolation system plus the mass of the superstructure.

Assuming $\omega_s \gg \omega_b$, if we indicate with $\varepsilon = \left(\frac{\omega_b}{\omega_s}\right)^2$ the ratio between the two newly defined pulsations, it becomes clear that if the isolated system is well designed, it will have dimensions of the order of 10^{-2}. Also, defining the mass ratio γ:

$$\gamma = \frac{m_s}{m_s+m_b} = \frac{m_s}{M} < 1 \tag{3.15}$$

because it is implicitly assumed that $m_b < m_s$, we can rewrite the system of equations of motion in a dimensionless way, dividing the first equation for m_s, and the second for $(m_s + m_b) = M$:

$$\frac{m_s}{m_s}\ddot{v}_b + \frac{m_s}{m_s}\ddot{v}_s + \frac{c}{m_s}\dot{v}_s + \frac{k}{m_s}v_s = -\frac{m_s}{m_s}\ddot{u}_g \tag{3.16}$$

$$\frac{(m_b+m_s)}{M}\ddot{v}_b + \frac{m_s}{M}\ddot{v}_s + \frac{c_b}{M}\dot{v}_b + \frac{k_b}{M}v_b = -\frac{(m_b+m_s)}{M}\ddot{u}_g \tag{3.17}$$

Obtaining:

$$\ddot{v}_b + \ddot{v}_s + 2\,\xi_s\,\omega_s\,\dot{v}_s + {\omega_s}^2 v_s = -\ddot{u}_g \tag{3.18}$$

$$\ddot{v}_b + \gamma\,\ddot{v}_s + 2\,\xi_b\,\omega_b\,\dot{v}_s + {\omega_b}^2 v_s = -\ddot{u}_g \tag{3.19}$$

Inverting the two equations described above and using the matrix notation:

$$\begin{bmatrix} 1 & \gamma \\ 1 & 1 \end{bmatrix} \begin{Bmatrix} \ddot{v}_b \\ \ddot{v}_s \end{Bmatrix} + \begin{bmatrix} 2\,\xi_b\,\omega_b & 0 \\ 0 & 2\,\xi_s\,\omega_s \end{bmatrix} \begin{Bmatrix} \dot{v}_b \\ \dot{v}_s \end{Bmatrix} + \begin{bmatrix} {\omega_b}^2 & 0 \\ 0 & {\omega_s}^2 \end{bmatrix} \begin{Bmatrix} v_b \\ v_s \end{Bmatrix} = -\begin{Bmatrix} 1 \\ 1 \end{Bmatrix} \ddot{u}_g \qquad (3.20)$$

A system of differential equations of the second order is obtained coupled which represents the starting point for development of the modal analysis. Before continuing, however, it is instructive to point out that the variables ω_b, T_b, ξ_b and ω_s, T_s, ξ_s are the pulsation, the period and the damping ratio of two elementary oscillators, respectively, the first consisting of the whole mass constrained by the system of isolation, the other by the single superstructure assumed fixed at the base. Next to the pulsation ratio, can be introduced the ratio (or degree) of isolation, equal to the ratio between the periods T_b / T_s, and therefore equal to the square root of the inverse of ε:

$$\frac{T_b}{T_s} = \Omega = \sqrt{\frac{1}{\varepsilon}} \qquad (3.21)$$

If we assume $\varepsilon << 1$, that is equivalent to hypothesizing a much stiffer superstructure of the isolators (situation found in many ordinary cases), the problem of modal analysis is greatly simplified; let's start then from defining the main ways of the system:

$$\underline{\phi}^n = (\phi_b^n, \phi_s^n)^T \quad con\ n = 1{,}2 \qquad (3.22)$$

of pulsations equal respectively to ω_1 and ω_2, calculated through the following equation characteristic:

$$(1 - \gamma)\omega_n^4 - (\omega_b^2 + \omega_s^2)\omega_n^2 + \omega_b^2\omega_s^2 = 0 \qquad (3.23)$$

The smallest value of the roots of this equation, which will be indicated with ω_b^*, represents the pulsation of the isolation system, while the bigger value of the roots, indicated with ω_s^*, represents the pulsation of the superstructure, modified by the presence of the isolation.

It could be demonstrated, based on the assumptions made on ε, and therefore considering $\omega_b \ll \omega_s$, that the values of $\omega_1^2 \equiv {\omega_b^*}^2$ and $\omega_2^2 \equiv {\omega_s^*}^2$ coincide with the following expressions:

$$\omega_1^2 \equiv {\omega_b^*}^2 = \omega_b^2(1 - \gamma\varepsilon) \qquad (3.24)$$

$$\omega_2^2 \equiv {\omega_s^*}^2 = \frac{\omega_s^2}{(1-\gamma)}(1 + \gamma\varepsilon) \qquad (3.25)$$

In many cases it is sufficiently accurate to consider for ω_b^{*2} and ω_s^{*2} the following approximations:

$$\omega_b^* = \omega_b \tag{3.26}$$

$$\omega_s^* = \frac{\omega_s}{\sqrt{1-\gamma}} \tag{3.27}$$

The expressions just found make it possible to observe that the frequency of the isolation system (ω_b) is only slightly modified (the variation is of the order of magnitude of ε) from the deformability of the structure, while the frequency of the structure in elevation (ω_s) is significantly increased by the presence of the mass at the base. The initial difference between the frequency of the fixed base structure and the frequency of the isolation can be increased by suitably combining the 2 elements.

The pulsations thus found represent the eigenvalues of the problem, while the eigenvectors coincide with the modal forms, which if we ignore orders of magnitude greater than those present the following simple mathematical expressions:

$$\underline{\phi}_1^T = \{1, \varepsilon\} \tag{3.28}$$

$$\underline{\phi}_2^T = \left\{1, -\frac{(1-(1-\gamma))\varepsilon}{\gamma}\right\} \tag{3.29}$$

As shown in (*Figure 3.2*), the first vibration mode of the 2 DOF system, φ_1, is roughly a rigid motion of the superstructure relative to the isolation system, unless a displacement at the top of the superstructure of the order of magnitude of ε. Unlike the 1st mode, the 2nd vibration mode, φ_2, causes deformations both in the isolation system and in the superstructure.

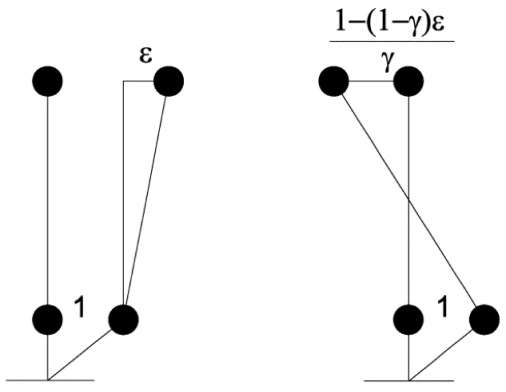

Figure 3.2: Modal forms of the 2 DOF system [17].

The pulsation of the 1st mode, as expressed by equation (3.24), can be considered as the variation, due to the elasticity of the superstructure, of the pulsation of the isolated system at the base with an infinitely rigid superstructure; however, the order of magnitude of this variation remains extremely low if one considers that the superstructure has a certainly greater stiffness than the isolation system.

The 2nd mode of vibrating, on the other hand, is very similar to the motion of two masses, m and m_b, which oscillate independently in the space around the center of mass of the overall 2 DOF system. The pulsation of the first mode, indicated above with (3.24), undergoes variations due to the stiffness of the isolation system.

Having passed to the space of the modal coordinates, we can now return to the space of the geometric coordinates indicated above with v_b and v_s, through the following equations:

$$v_b = q_1\phi_b^1 + q_2\phi_b^2 \tag{3.30}$$

$$v_s = q_1\phi_s^1 + q_2\phi_s^2 \tag{3.31}$$

Therefore, through a linear combination of the modal forms with a coordinate q_i, with i = 1,2, known as the i-th principal or normal coordinate, function of the time t and thanks to the introduction of vibration modes, we can write equation (3.10) in the following way:

$$\ddot{q}_1 + 2\omega_b^*\xi_b^*\dot{q}_1 + {\omega_b^*}^2 q_1 = -L_1\ddot{u}_g \tag{3.32}$$

$$\ddot{q}_2 + 2\omega_s^*\xi_s^*\dot{q}_2 + {\omega_s^*}^2 q_2 = -L_2\ddot{u}_g \tag{3.33}$$

that representing the equations of the motion of 2 simple oscillators, of angular frequency and relative damping respectively equal to ω_b^*, ξ_b^* and ω_s^*, ξ_s^*, subject to an earthquake $\ddot{u}_g$ reduced once by the participation coefficient L_1, and once from L_2. The hypotheses made on ε are assumed to be valid once again, and therefore:

$$L_1 = 1 - \gamma\varepsilon \tag{3.34}$$

$$L_2 = \gamma\varepsilon \tag{3.35}$$

this shows how L_2, or the way that induces deformations in the superstructure, being the order of magnitude of ε, is very small if the vibration frequencies ω_b and ω_s assume sufficiently different values between them.

The dissipation of energy by the isolation system is certainly an aspect of primary importance. Up to now, in the model described, the energy absorption has been considered

through the introduction of the damping force, proportional to the damping constants c_b and c_s through the velocities $\dot{v}_b$, $\dot{v}_s$. Now let's see how to evaluate the relative damping factors ξ_b^*, ξ_s^* associated this time with the modal analysis here described: if they are considered the equations (3.24) and (3.25), then we will indicate the damping on the first and second modal forms respectively with ξ_b^*, ξ_s^* and we will assume them equal to:

$$\xi_b^* = \xi_b \left(1 - \frac{3}{2}\gamma\varepsilon\right) \tag{3.36}$$

$$\xi_s^* = \frac{\xi_s}{\sqrt{1-\gamma}} + \frac{\gamma\xi_{sb}\sqrt{\varepsilon}}{\sqrt{1-\gamma}} \tag{3.37}$$

As can be seen, the structural damping is increased by the presence of the damping in the isolator of the order of $\varepsilon^{1/2}$. The product between ξ_b and $\varepsilon^{1/2}$ could result in a significant increase in structural damping, which assumes greater importance if it does not reach very high values. Remember in this regard that the structural damping is usually in the order of 2-3%, while the damping provided by the isolation system stands at values of 10-30%.

A linear analysis of the isolated structures at the base, as mentioned at the beginning of the chapter, is independent of a real modeling of isolation devices, many of which have a markedly non-linear behavior, and therefore, if we do not want to give up to a solution in the closed form of the problem, it remains to choose one of the different linearization techniques proposed in the literature.

The FPS (Friction Pendulum System), of which the present work aims to study the physical and dynamic characteristics, are among those devices, so-called attritives, which have numerous sources of non-linearity linked, as will be better shown below, to a close correlation between the dynamic coefficient of friction and quantities such as velocity, pressure acting on isolators and temperature. The dynamics of a structure isolated at the base with FPS will be addressed based on the considerations made by [17], and therefore opportunely modifying, due to the specific characteristics of the isolators, the equations of motion of the 2 DOF system presented above, however resolved given the non-linearity of these devices, through a dynamic integration to the step.

3.2 Friction Pendulum Devices

In the last thirty years, seismic engineering has made considerable progress, developing modern seismic protection strategies, such as seismic isolation.

The seismic isolation between the base and the superstructure in the case of buildings, or between the piers and the deck in the case of bridges, represents a seismic protection technique with which it is possible to guarantee, through the concentration of deformations in the devices, an adequate limitation of structural damage, governing the proper period of oscillation of the superstructure. The use of an isolation system, thanks to the abatement of the seismic force transmitted to the superstructure, compared to what happens for a traditional non-isolated structure, shows increasing technical and economic efficiency with the increase of the maximum acceleration level expected on the ground for the site of construction. Furthermore, it foresees that the almost elastic behavior of the superstructure is assured also for a seismic event in the last conditions; this involves a limited request for structural ductility in the face of a displacement demand concentration at the isolators, with a consequent very low post-earthquake expected damage picture for the structures.

Among the modern isolation devices there are the sliding pendulum isolators, so called because they exploit the physical law of the pendulum motion to lengthen the natural period of the isolated structure [19], [20], [23]. From a technological point of view, as shown in (*Figure 3.3*), with reference to simple curvature devices, the decoupling between the horizontal motion of the superstructure and that of the substructure, takes place thanks to the possibility of sliding between a spherical concave dish, made of steel and integral with one of the two parts of the isolated structure and a articulated slider, bound to the opposite portion.

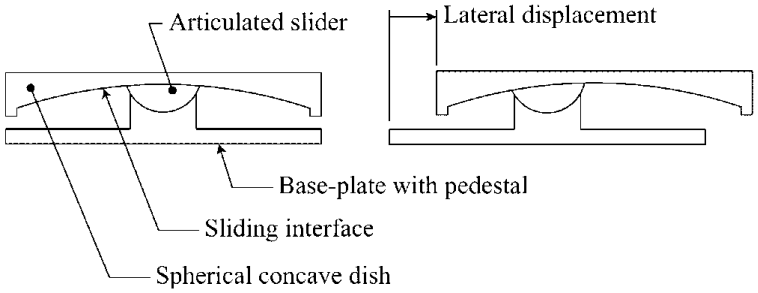

Figure 3.3: Motion decoupling through the sliding mechanism, in single curved FPS.

There is also the possibility of adopting two equal hemispherical surfaces, united respectively with the superstructure and substructure, with the interposition of an articulation; in this case we speak of devices with a double sliding surface (*Figure 3.4*), where the displacement capacity is twice compared to traditional friction pendulum system [21]. For devices with a double sliding interface, the adoption of a radius of curvature of the spherical surface equal to half the radius of a hypothetical single-curved isolator, leads to an equivalence in the geometry of the oscillatory motion of the two systems.

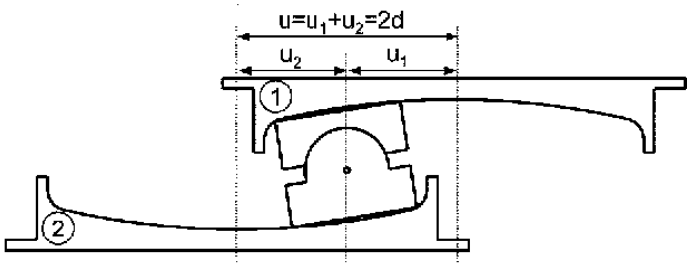

Figure 3.4: Motion decoupling through the sliding mechanism, in double curved FPS.

The behavior of the sliding pendulum isolator is governed by the characteristics of the interface between the spherical concave dish and the articulated slider (Radius of curvature, static and dynamic friction), from which flow the fundamental properties of the sliding devices: the ability to dissipating energy through friction, which is generated by the motion induced by seismic attack and which determines the birth of a side action that opposes the forces of solicitation; the possibility of generating the return force for the re-centering of the structure through the action of gravity and the curved geometry (Bending Radius), which allows precisely the device to return to position when the external action ceases. Specifically, with reference to the dissipation properties of energy through the attracting phenomenon, in the case of sliding isolators there are: a friction of first detachment or initial, which determines the resistance to be overcome to start the movement, and the dynamic friction, which instead determines the mechanism by which the energy introduced by the seismic event is dissipated, and in this respect it should be as high as possible, even if this could increase the horizontal stiffness and hinder the device's recentering movement. It is clear then how energy dissipation and recentering, are two functions of the isolator which have diametrically opposed coefficients of friction and their relative importance depends on the specific case being examined.

At the state of the art, the sliding surfaces in the pendulum isolators are made by coupling a metal surface, in stainless steel or chromium and a plastic material, mainly unlubricated Polytetrafluoroethylene (PFTE or Teflon®) or its composites, giving rise to a coefficient of friction between 0.03 and 0.12; the friction that develops as a result of the PFTE-steel coupling has been the subject of numerous studies over the years (Constantinou et al 1987), (Mokha et al.1990a-b, 1993), which showed that it is incorrect to consider the latter as obedient to the Coulomb law (constant friction during the oscillator movement), since the macroscopic behavior at the interfaces is strongly influenced by quantities such as the sliding velocity, the pressure between the surfaces and the temperature. The dynamic friction coefficient is also influenced by the number of cycles performed by the contact surfaces in the relative sliding, due to the deterioration of the surfaces themselves (Hwang et al, 1990).

In the following, we will speak more specifically of the non-linear character of the coefficient of friction associated with the above parameters, but in general it can be assumed that it increases more than linearly with the increase of the sliding velocity, while decreasing with the increase of apparent pressure.

3.2.1 Dynamic behavior

The constitutive relation of the FPS-type isolation devices in motion conditions, and with reference to the horizontal plane response, is usually idealized as bi-linear, based on three parameters K_1, K_2 and Q, according to the scheme reported in (*Figure 3.5*), and defined by the following formula:

$$F = Mg\mu + \left(\frac{Mg}{R}\right) d \tag{3.38}$$

where (Mg) represents the vertical action N, resulting from the product of mass M and the acceleration of gravity g, R is the curvature radius of the spherical surface, μ is the bearing friction coefficient, and d is the displacement of the spherical joint on the sliding surface.

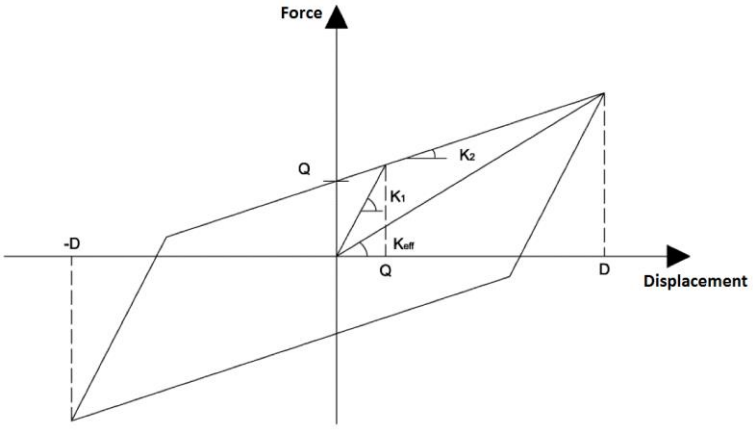

Figure 3.5: Bilinear cyclic behavior of the FPS.

With reference to the equation written above, the second term, $\left(\frac{Mg}{R}\right)d$, represents the recentering force due to the mass raising during the motion, which therefore offers a horizontal stiffness equal to:

$$K_2 = \frac{W}{R} \tag{3.39}$$

It is shown that for the isolated structure the period T is equal to:

$$T = 2\pi\sqrt{\frac{R}{g}} \tag{3.40}$$

that result, therefore, independent of the mass carried.

The stiffness K_2 is often defined as secondary stiffness, to distinguish it from the initial stiffness or K_1, that the device has before developing the motion and can be estimated both by the hysteresis cycles and empirically, as a multiple of the K_2 stiffness. Kelly [18] suggested for example $K_1 = 51K_2$; the isolators present in fact a theoretically infinite rigidity until the breaking of the friction bonds, or at the beginning of the sliding and this is why, many times, the first part of the hysteresis cycle is assumed pseudo-vertical, just to recall the idea of K_1 stiffness tending to infinity before the start of the motion. Until the condition of detachment then, the superstructure and the substructure are rigidly linked to one another and the behavior is identical to that of a not isolated structure. Upon the exceeding of the separation friction threshold, the pendular motion is triggered and the stiffness is expressed by equation (3.39).

In (*Figure 3.6*) a typical hysteresis diagram is shown for a sliding isolation system, where the total force developed by the isolator is shown on the ordinate axis, (which as already explained above, if the isolator is in conditions of motion is equal to $F = f_p + f_h$, where there is a superposition of two different actions, one resulting from the pendulum effect associated with the recentering action produced by the weight W, f_p, and the other resulting from the frictional force that develops at the interface, f_h), and on the abscissas axis the displacements induced on the isolation system; the image shows in particular the typical parallelogram shape determined by a first phase, called "sticking", in which the behavior of the system is similar to a body rigidly connected to the ground. After this phase of high stiffness, in which the motion evolves on an almost vertical straight line and exceeded the maximum frictional force available, the pendulum movement is triggered, characterized by a lower stiffness (the straight line is inclined); when the motion is reversed, there is an instantaneous zeroing of the friction coefficient, and therefore of the force associated with it, the pendulum in this phase, in order to resume the motion in the opposite direction, must recover the friction that had already passed in the phase initial and consequently, in the hysteresis cycle before traveling the inclined section in the opposite direction to the initial one, a vertical stretch equal to twice the maximum available frictional force is considered, which is usually indicated in the literature as a characteristic force Q.

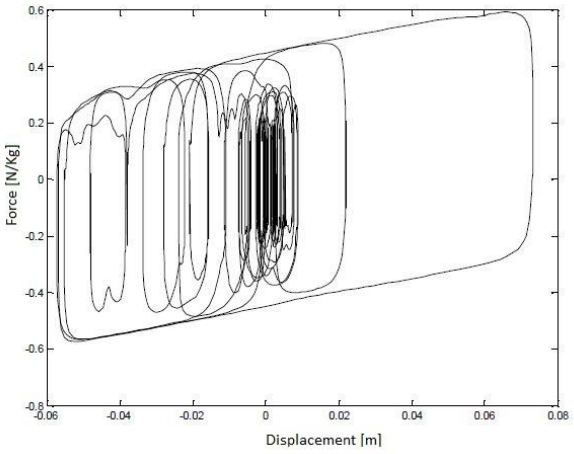

Figure 3.6: Hysteresis diagram of an FPS isolator.

The operating scheme in motion regime of the isolator, through which it is possible to derive the secondary horizontal stiffness K_2 and the period associated with it T, is presented in (*Figure 3.7*), as originally described in [22].

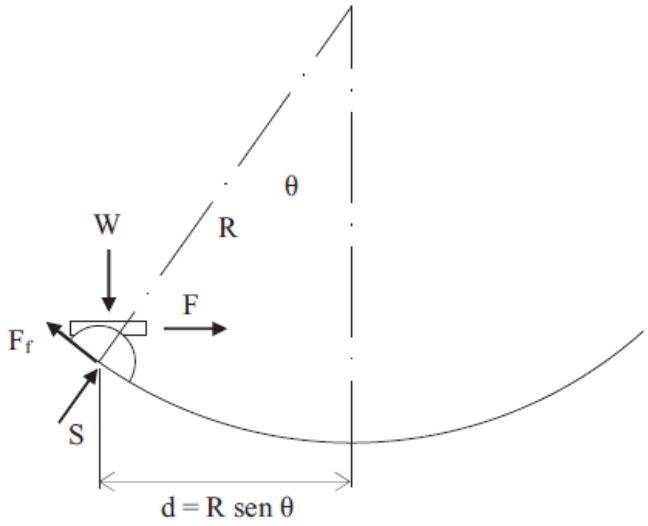

Figure 3.7: Theoretical sliding concave behavior and equilibrium of the forces involved during the motion.

In this configuration, the forces acting on the slider are:

- The vertical load, W, which weighs on the isolator;
- The lateral force, F, acting on the cursor;
- The friction force, $F_f = \mu W$, acting along the sliding surface;
- The contact force, S, normally acting at the sliding interface due to the mass of the superstructure;
- The tensile forces acting along the surface of the cursor t_1, whose effect is part of the frictional force F_f and, therefore, not appear explicitly in the equilibrium equations.

From the presented scheme we can obtain the equations of vertical and horizontal equilibrium, and we obtain:

$$W - S\cos\vartheta + F_f \sin\vartheta = 0 \tag{3.41}$$

$$F + S\sin\vartheta - F_f \cos\vartheta = 0 \tag{3.42}$$

and, through geometrical considerations, the displacement of the spherical joint on the sliding surface is:

$$d = R\sin\vartheta \tag{3.43}$$

with R representing the effective radius of curvature, evaluated as distance of the center of the spherical surface of the cap, from the point of articulation of the cursor. By combining equations (3.41), (3.42) and (3.43), the horizontal recall force is obtained:

$$F = W\ tg\vartheta + \frac{F_f}{cos\ \vartheta} = \frac{W}{R\ cos\ \vartheta} d + \frac{F_f}{cos\ \vartheta} \tag{3.44}$$

For the hypothesis of small oscillations, we can put: $cos\ \vartheta \cong 1$, $sin\ \vartheta \cong \vartheta \cong\ tg\ \vartheta\ \cong {}^{1}/_{R}$. Thus, the two components of the vertical force W, become $W\ cos\ \vartheta \cong W$, and $W\ sin\ \vartheta \cong {}^{W}/_{R}$, and (3.44) it is simplified as follows:

$$F = \frac{W}{R} d + F_f \tag{3.45}$$

where, the friction force, F_f, acts along the tangent to the sliding surface with a sign corresponding to the tangential component of the vertical force, W, and is a function of the coefficient of friction, μ, and of the component of W orthogonal to the sliding surface. Therefore, we can write:

$$F_f = \mu\, W cos\vartheta \tag{3.46}$$

which, as already mentioned at the beginning of the paragraph, is not constant but varies with the variation of different quantities, among which the most significant are certainly the sliding velocity and the contact pressure. By replacing the attractive law in (3.45) we can write:

$$F = \frac{W}{R} d + \mu\, W sgn(\dot{d}) \tag{3.47}$$

Where, W is the weight that weighs on the isolator, R is the radius of curvature, d is the horizontal displacement, μ is the coefficient of friction, $sgn(\dot{d})$ denotes the signum function of the sliding velocity $\dot{d}$.

The expression of the displacement along the sliding surface can also be obtained as a function of the coefficient of friction:

$$d = -\frac{F_f}{W} R = \mu\, R \tag{3.48}$$

From this formula, we also obtain the admissible domain in which a stable equilibrium is achieved:

$$F_f \geq F_e \rightarrow d \leq \mu\, R \tag{3.49}$$

that is, for shifts below μR the system will not be able to re-center itself, being in a stable equilibrium configuration, while it will re-center for higher displacements. This concept is the reason why we use low friction coefficients such as Teflon to make re-centering more likely.

Following this introduction on the dynamic behavior of sliding isolators, we must analyse in more detail the aspects that govern the phenomenon of friction. The following paragraphs will examine the dependence of friction and the numerous experimental investigations [19], [20] conducted on devices with a Teflon stainless steel-PTFE interface that have shown a strict dependence on the same coefficient of friction from the velocity flow and apparent pressure.

3.2.2 Basic Principles of the Friction

The use of seismic sliding isolation devices, in seismic applications, inevitably requires a collection of experimental data on the friction coefficient properties present at the interface between the sliding surfaces, and this both under low velocity of motion conditions (service conditions) and in high-velocity conditions.

Friction is a dissipative force that opposes the relative motion between two bodies in contact; in cases of engineering interest we will talk about solid bodies in contact and is due to the tangential forces exchanged between the contact surfaces. In all the most important theories of friction, the importance of superficial topography is emphasized because no surface, in practice, is flat and smooth at the microscopic level. However, attention will be focused on the interpretation of the phenomenon at the macroscopic level, which is the most interesting in relation to frictional seismic isolation devices, and in general in engineering applications.

The value of the frictional force, F_f, at the sliding interface, is given by the following relation:

$$F_f = \mu N \tag{3.50}$$

where μ is the friction coefficient and N is the normal action at the interface. The frictional force that occurs between surfaces in a quiet position is called static friction, whereas between surfaces in relative motion it is called dynamic friction (or sliding). The classical law of

friction used in many cases of engineering interest is certainly Coulomb's law (constant friction during sliding), which, however, is inapplicable in the case of sliding isolators, whose friction coefficient value is strongly dependent on the parameters: flow velocity and apparent pressure [21].

Basic Mechanisms

It is interesting to understand what are the phenomena that govern the friction relative to the scale of interest, i.e. the macroscopic one. The following phenomena are based on the studies by [21]:

Adhesion

When two solid bodies come into contact one with the other, they form atomic bonds through the contact interfaces. These contact regions are called junctions, and the sum of their areas constitutes the real contact area: "effective area", which is significantly smaller than the "apparent area", (*Figure 3.8*). The junctions are characterized by interface forces, that represent the adhesion, due to the creation of interfacial bonds steel-carbon, which are established between the clean metal surfaces and the Teflon. Therefore, the friction force is given by the product of the effective area, A_r, for the shear strength of the junctions, s:

$$F_a = s\,A_r \tag{3.51}$$

The mechanism of adhesion is dominant for interfaces that flow on top of each other characterized by clean surfaces.

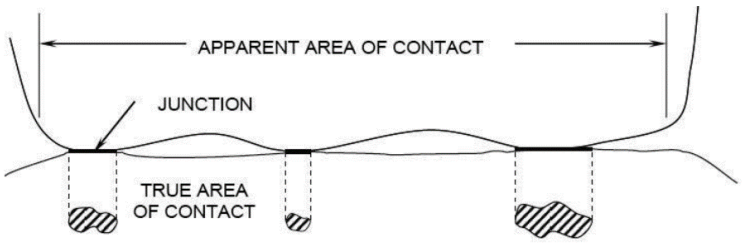

Figure 3.8: Schematic illustration of an interface, showing the apparent and real areas of contact.

Plowing

All surfaces are characterized by roughness which, when in contact, undergo elastic or plastic deformations. The plowing component of friction is due to the dissipation of energy that occurs during the plastic deformations of the bumps. This phenomenon can be more easily understood considering a hard and spherical roughness over a soft and flat surface. If an axial action is applied to the bumps, these attach themselves to the underlying surface and at the same time contact areas are created, the "junctions". Then inducing a tangential action, the bumps move horizontally, dragging with it part of the softer material below and creating a sort of groove along the trajectory traveled. The plowing component of friction results from the drag effect caused by the roughness of the underlying soft material.

Viscoelastic Effects

Polymers, like PTFE, exhibit a viscoelastic behavior: this is because if a harder material tends to flow on a material with viscoelastic characteristics, additional energy dissipation is achieved by those same characteristics.

The Stick-Slip phenomenon

The stick-slip movement is a succession of blocking and slipping phases, very common in many ordinary situations and responsible for phenomena such as the squeaking of doors, the squeaky chalk, the sound of the violin, etc. It occurs in lubricated mechanisms and is due to two causes (*Figure 3.9*):

- the coefficient of kinetic friction is lower than that of static friction;
- the system can store energy in an elastic form.

In fact, the nature of the phenomenon consists in discharging from time to time in the dynamic phase the elastic energy stored in the static phase due to the forces acting on the system, to establish a cycle of jerky oscillations. It is an oscillatory behavior typical of elastic mechanical systems that contain friction forces and can occur only in the presence of a natural variation of the friction coefficient.

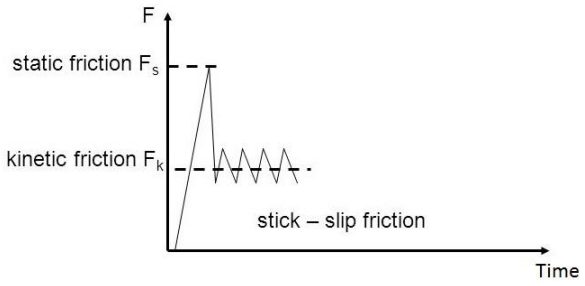

Figure 3.9: Stick-Slip phenomenon.

Studies by Yoshizawa and Israelachvili (1993) have shown the possibility of another interpretation of the stick-slip phenomenon: when a thin film of polymeric fluid is present on an interface, it is possible that the fluid film is affected by a phase transition from liquid to solid, resulting in changes in the flow characteristics of the film itself inducing stick-slip.

3.2.3 Experimental investigations on Friction Pendulum Devices with curved surfaces

For a complete characterization of the seismic behavior of the pendulum devices it is essential to define the properties of the friction phenomenon in correspondence with the different phases of motion. A history to distinguish between coefficients of dynamic friction, achieved during the sliding phases, which indicates the values of the displacements and characteristics characterizing an isolated structure 100-200mm and 0.4-0.5 Hz, are between 160 mm/s - 400 mm/s; value to the detachment μ_s, developed in line of the instant immediately preceding the beginning of the dynamic phase of oscillation; value to the inversion of the μ_{inv} motion, i.e. corresponding to the instants in which the direction along which the sliding occurs, and which intermediate values between the coefficient of friction and the given data in conditions of first detachment.

A wide series of experimental investigations have allowed to formulate a series of analytical expressions, which highlight the dependence of the dynamic friction coefficient on the sliding speed, as well as on other parameters, and that now gives a detailed description.

Dependency on Velocity of Sliding and Normal Load

The (*Figure 3.10*) shows how the coefficient of dynamic friction is characterized by a low value immediately after the beginning of the sliding, f_{min}, and by a progressive increase as the velocity increases. At high velocities, it reaches a constant value, f_{max}. Furthermore, if the normal load increases, there is a reduction in the friction coefficient [19], [20] until a constant value is reached for a load limit value. The reduction rate is practically constant: doubling the contact pressure (from 9.36 to 18.7 MPa) there is a variation of the coefficient of friction from 25% to -10 °C up to 33.4% at 50 °C [21].

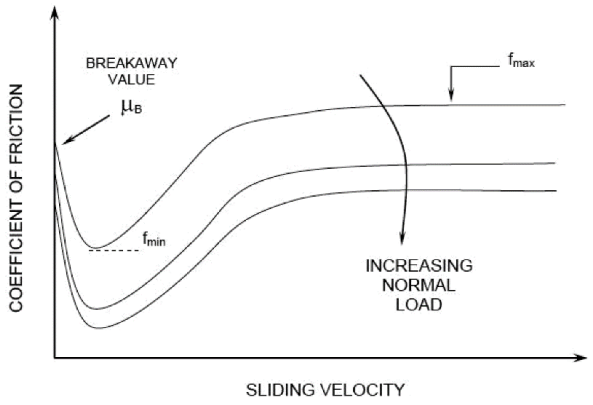

Figure 3.10: Dependency on Sliding Velocity and Normal Load [21].

The high value of the static friction coefficient, μ_B, is instead due to the adhesion phenomenon: two contact bodies form junctions characterized by high interface forces.

At the beginning of the sliding, a thin crystalline and oriented PTFE film (of a few hundred Angstrom thickness), is deposited on the surface of stainless steel and thus reduces the friction value from μ_B to f_{min}, all this is caused by the low shear strength that such material possesses. As the sliding velocity increases, the value of the friction coefficient increases, until reaching a peak threshold equal to f_{max}, with values up to 5-6 times greater than f_{min} (160-400 mm/sec or more). More precisely, the difference between the maximum and the minimum value of the dynamic friction coefficient $\Delta = \mu_{max} - \mu_{min}$ is higher when the contact pressure is low, assuming values close to 12% at 9.36MPa and below 7% at 28.1 MP. The temperature instead has a low influence on the Δ. In general, for a fixed value of the apparent contact pressure, the sliding friction coefficient depends on the velocity, as described by [19], [20], [21] and explained in the following equation:

$$\mu = f_{max} - (f_{max} - f_{min})e^{-\alpha|v|} \tag{3.52}$$

where f_{max} is the friction coefficient attained at high velocities of sliding (200 - 800 mm/s); f_{min} is the friction coefficient attained at very low velocities of sliding; v is the sliding velocity; α is a constant for a given pressure, temperature and condition of FPS interfaces and presents variable values from 20-30 s/m for devices with a Teflon-PTFE stainless steel interface and has the task of controlling the variation of the friction coefficient and therefore the passage from the minimum value to the maximum value at high velocity. The curves shown in (*Figure 3.11*), are based on the (3.52) report, which adequately describes the previously reported experimental results and shows how the parameter α influences the behavior of the adimensionalized friction coefficient with respect to the maximum for two different values of f_{max} / f_{min} = 2.5 and 5. It is noted that a sliding velocity greater than about 150 mm/s is sufficient to obtain the maximum value of the sliding friction coefficient of all the PTFE-based materials at normal temperatures.

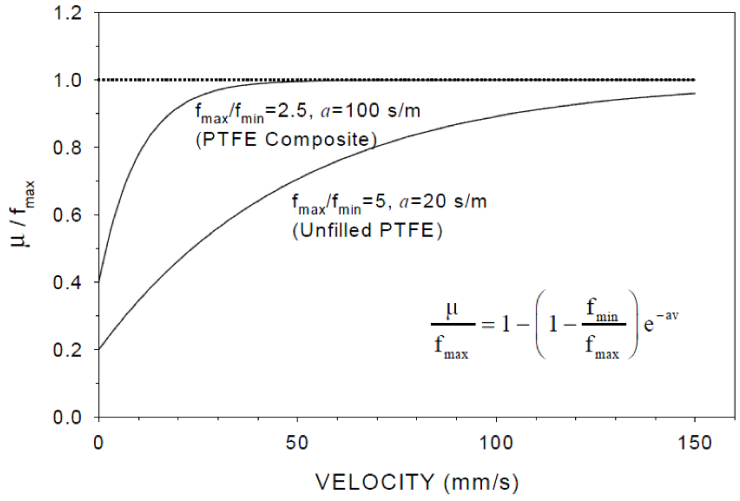

Figure 3.11: Effect of the parameter α in the variation of the coefficient of friction with the velocity [21].

It can ultimately be affirmed that:

- The friction coefficient increases rapidly with velocity until it reaches a value, after which it remains constant. This value is about 150mm/s, regardless of the ambient temperature and the pressure on the device;
- The friction coefficient for devices with a steel-PTFE interface decreases as the load applied to the sliding plane increases. The rate of reduction depends on the sliding

velocity and the air temperature: there is a maximum variation of 30% for a variation of ± 50% in the contact pressure (for t = 20°C, p = 18.7 MPa, v ≥ 150 mm/s), regardless of the lubrication status of the interfaces;

• The difference between the minimum value (f_{min}) and the maximum value (f_{max}), is the greater the lower the agent pressure.

Effect of Temperature

The effects of temperature on friction devices can be very negative, especially regarding the static friction coefficient, μ_B, and dynamic at low flow rates, f_{min}. The (*Figure 3.12*) shows the friction of detachment, the sliding friction at low velocities and at high velocities as a function of temperature. It highlights the substantial effect that the temperature has on the coefficient μ_B and f_{min}, and the rather limited effect on the coefficient of dynamic friction f_{max}. The following conclusions can be drawn:

• the friction of separation is practically the same as the sliding friction at low velocities;

• the effects of temperature in composite PTFE are, in general, lower than in unfilled PTFE;

• the coefficient of friction decreases with increasing external temperature with a higher reduction rate if you switch from low to medium and medium to high temperatures. Furthermore, it depends on the sliding velocity, while it is practically independent of the contact pressure. At the rates of interest for seismic applications, the reduction rate is of the order of 0.15-0.3% /°C.

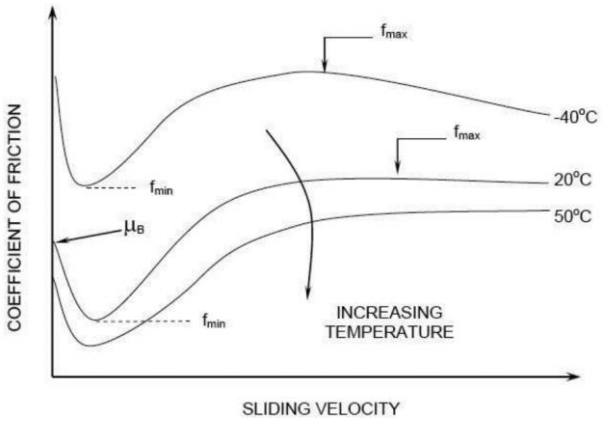

Figure 3.12: Effect of temperature on the variation of the coefficient of friction with the sliding velocity [21].

This latter conclusion is to be linked to the heating effects: the heat flow generated by friction is proportional to the coefficient of friction itself, to the average pressure and to the sliding velocity, also at high velocities (500mm/s), it is many hundreds of times greater than the flow that would be generated at modest velocities (<1 mm/s), therefore, this heat flow tends to offset the effects that the low temperatures have on the viscoelastic properties of PTFE: in this way a temperature variation of 20 °C to -40 °C leads to an increase in the f_{max} coefficient of only 50%. The values reported by Constantinou are in line with those of Campbell et al., (1991).

Effect of the permanence of loads

Since PTFE is a material with viscoelastic properties, it would be expected that the effect of the permanence of the loads on the effective contact area and, therefore, on the friction is greater the longer the time spent under the action of such loads (Bowden and Tabor, 1964). What emerges from experiments conducted [19], [20] is that the value of the static friction coefficient is substantially the same for a load applied for 0.5 hours or 594 days. Many other tests have been conducted, and all have shown that fluctuations in the value of the friction coefficient cannot be traced back to the duration of application of the load. Rather, tests carried out on samples subjected to previous test cycles showed a markedly lower coefficient of static friction coefficient following a first loading cycle, reflecting the existence of a PTFE film which is deposited on the surface in steel after a first cycle.

The experimental data presented in [19], [20], [21] indicate that when considering the natural variability of the friction properties, obtained from different samples or from different tests on the same sample, and the probable measurement errors are considered, the static friction between surfaces in polished-PTFE stainless steel is not influenced by the permanence of the load.

Effect of Cumulative Movement

A review of the literature Campbell and Kong (1987), Kauschke and Baigent (1986), Long (1969, 1974), on the effect of cumulative movement (travel) on the coefficient of friction of PTFE-stainless steel interfaces produced conflicting results.

The results of a test conducted on unfilled PTFE specimens, at apparent pressure of 20.7 MPa [21], (*Figure 3.13*) demonstrate that the coefficient of dynamic friction at high velocities (f_{max}) decreases as the distance traveled increases, from an initial value of 12.5% to 10% already after 40 m of distance traveled; on reaching a threshold of about 300 m, it shows instead a new increase. The dynamic coefficient at low velocities (f_{min}) has fluctuations in the range 0-40 m. The initial value of the high velocity coefficient of sliding friction (f_{max}) is 0.125 but drops to 0.100 after 40 m of travel (this value is also attained after a travel of 510 m), the low velocity coefficient of friction (f_{min}) shows a sharp increase for a travel of less than 15 m.

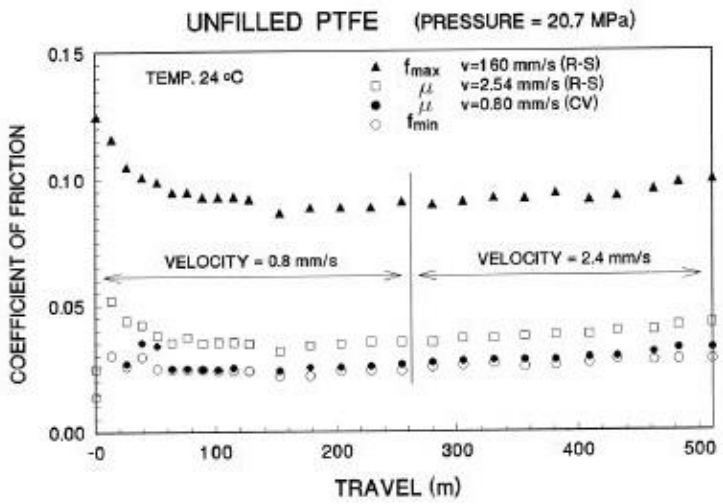

Figure 3.13: Effect of Cumulative Movement (Travel) on the Sliding Coefficient of Friction of Unfilled PTFE in Contact with Polished Stainless Steel [21].

Effects of the variation of the axial action on the seismic behavior of the devices

The FPS isolators, with reference to the behavior towards vertical actions, are born as vertical constraint devices of the single-latero type (compression only) and this must be considered in the design phase, this because the device, if subjected to actions of traction design, it could be damaged at the sliding and/or exit interface of the articulation from its housing seat. The permanence in compression is, among other things, a necessary condition for the use of linear analysis methods.

While the period T depends only on the radius of curvature adopted for the hemispherical cap on which the relative sliding occurs between the two parts, the equivalent period T_{eff} and the horizontal force F developed by the isolation system, are a direct function of the axial load, N, at level of the devices. Equivalent period and shear are both subject to the continuous variations of the N load, following the force system that opposes the overturning moment due to horizontal actions and the simultaneous seismic action in the vertical direction. Variations in the axial action involve irregularities in the force-displacement bonding of the isolators.

3.2.4 Modeling criteria

For a correct evaluation of the isolation properties of the devices, a distinction must be made depending on the stiffness value used. As already pointed out, if we consider the slope of the plastic response branch, corresponding to the oscillating state along the spherical surface, the period T (isolated) is a function of the radius of curvature R of the spherical cap and is in fact equivalent to that of a pendulum:

$$T = 2\pi\sqrt{\frac{M}{K}} = 2\pi\sqrt{\frac{M}{\frac{Mg}{R}}} = 2\pi\sqrt{\frac{R}{g}} \tag{3.53}$$

Assuming instead as a reference the value of secant stiffness K_{eff}, defined as the ratio between the maximum horizontal force at the maximum lateral displacement exhibited by the isolator and the displacement itself, is obtained:

$$K_{eff} = \left(\frac{1}{R} + \frac{\mu}{d}\right) W \tag{3.54}$$

Combining the (3.53) and the (3.54) we reach the individuation of the effective period:

$$T_{eff} = 2\pi\sqrt{\frac{M}{K_{eff}}} = 2\pi\sqrt{\frac{M}{\left(\frac{1}{R}+\frac{\mu}{d}\right)Mg}} = 2\pi\sqrt{\frac{Rd}{(R+\mu d)g}} \tag{3.55}$$

If the system can be represented by an equivalent linear model, the value of the period obtained as a function of secant stiffness at the maximum displacement differs from the corresponding tangent value by no more than 14%; therefore, also the deviation, in terms of dynamic response parameters, between linear and non-linear model is not very significant. In the absence of the necessary requirements for the use of an equivalent linear model, according

to (NTC08) for the evaluation of the dynamic response, it is necessary to resort to non-linear analysis, able to capture the associated phenomena to the transition, from states characterized by different stiffness.

Another important parameter that defines the behavior of the friction isolator is the equivalent viscous damping coefficient. It identifies the dissipation of energy produced by friction, and can be estimated from the formula:

$$\xi_{eff} = \frac{Hysteresis\ cycle\ area}{4\,\pi K_{eff} d^2} \tag{3.56}$$

that is an equivalence between energy dissipated by friction and energy dissipated by a viscous behavior. Considering that the area of the hysteresis cycle is equal to 4μWd, and remembering the first written expression for the K_{eff}, we obtain:

$$\xi_{eff} = \frac{4\mu W d}{4\,\pi\left(\frac{1}{R}+\frac{\mu}{d}\right) W d^2} = \frac{2\mu}{\pi\left(\frac{d}{R}+\mu\right)} \tag{3.57}$$

where, it can be seen how the equivalent damping is a function of the friction coefficient, of the radius of curvature and of the displacement demand: the latter can be understood as the design value of the displacement for the considered limit state. It follows that, the equivalent damping to be adopted in an elastic analysis is a function of the limit state considered and assumes different values in relation to the demand for moving the system. Generally, the value in question refers to the life-saving limit state (SLV), used for the verification of isolated structures.

For the design of the devices, in relation to the fragility of the system with respect to breaking mechanisms linked to exceeding the ultimate capacity, in displacement, reference is made to the application under collapse conditions (i.e. the ultimate limit state SLC), indicated according to (NTC08) with the symbol d_2.

Linear modeling

The idealization of the isolation system as a linear spring, characterized by its own stiffness and its own equivalent viscous damping, is an obvious simplification of the modeling and analysis phases, and as such, based on the provisions of the (NTC08), can only be applied under specific conditions:

- the equivalent stiffness of the isolation system must be at least 50% of the secant value for cycles with a 20% deformation of the reference displacement. For pendulum devices, the above limitation translates into imposing:

  $$\frac{R}{d_{dc}} \leq \frac{1}{3\mu}$$

  where d_{dc} is the displacement of the rigidity center of the considered limit state isolation system, R the radius of curvature and μ the dynamic friction coefficient of the device;

- the equivalent linear damping of the isolation system must be less than 30%;
- the force-displacement characteristics of the isolation system must not be subject to deviations of more than 10% due to variations in the deformation velocity, the vertical action on the devices;
- the increase of the strength in the isolation system for displacements between $0.5d_{dc}$ and d_{dc} must be at least equal to 2.5% of the total weight W of the superstructure. This request involves the use of a radius of curvature limited to 20 times the value of the project shift.

Non-linear modeling

From the critical analysis of the necessary requisites established in the (NTC 08) for the use of an equivalent linear model, it emerges that it is not possible to use an equivalent linear model, if not in presence of a vertical seismic component lower than 0.1g.

In any case, even in the absence of a vertical acceleration component, it must be verified that the variation of the axial load on the devices, which originates in opposition to the overturning induced by the horizontal forces, is less than 10% compared to the value in almost permanent conditions. Otherwise, it is necessary to resort to non-linear analyses, adopting a suitable constitutive law and proceeding with an integration to the step of the equations of motion.

CHAPTER 4

4. DYNAMICS OF ISOLATED BRIDGES WITH FPS

Seismic isolation is today a very widespread anti-seismic protection technique (both in new and existing structures, as a technique for improving seismic performance), particularly in the context of infrastructural works such as bridges and road and rail viaducts, considering the function strategic that generally perform. Although the basic principles of seismic isolation have now been well clarified, attention is now focused on the dynamic behavior of isolated bridges with continuous girder.

In this approach the mass of the superstructure is disconnected from the substructure through the FPS devices. In the absence of an earthquake, these behave like normal supports, but in the event of a strong earthquake, they add flexibility to the bridge, extending its period and dissipating in part the input energy. This allows oscillation of the superstructure at a lower frequency with respect to the piers, and thus large displacements relative to the interface are generated. Such displacements can be controlled by incorporating damping elements in the bearing or by adding dampers.

The aim of this chapter is to study the structural problem through the non-linear modeling of isolation devices, understanding the proposed mathematical model and the related equations of motion. These, in fact, are at the base of subsequent modeling in the professional work environment (MATLAB & Simulink®), that allow to determine the structural response varying different parameters and considering different values of these latter, through integration of the response in the time domain.

4.1 Mathematical modeling of the structural problem

The structure, object of study of this thesis, is a symmetrical and continuous bridge, with respect to the straight line perpendicular to the deck that passes through its midpoint, with three spans. The pier in the bridge model has been considered of uniform circular cross section throughout the height, and the FPS isolators have identical properties and are arranged between the substructure and the superstructure, i.e. on each pier and each abutment (*Figure 4.1*). The structural symmetry permits to analyze the abutment-pier interaction, thus identifying a more simplified model, from the point of view of computational complexity and the system of equations of motion, which goes to study the relative displacements that are generated through the installation of the FPS under the deck.

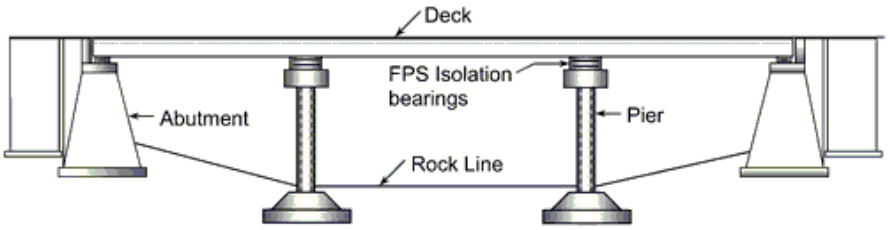

Figure 4.1: Three-span continuous deck bridge seismically isolated by the FPS [24].

The abutment-pier interaction of the bridge, based on the Jangid theory [24], can be modeled with any number of degrees of freedom, model (n+1) DOF (*Figure 4.3*), considering however the stability of the model and the convergence of the analysis, to avoid high computational times.

Furthermore, we consider the following modeling hypotheses:

- the deck is a mass m_d (equal to 771120 Kg) that rests on the abutment and on the pier, but is detached from these through the isolator, and is hypothesized rigid and straight;
- the deck is modeled as a single concentrated mass, and therefore with only one DOF;
- the abutment is modeled as a fixed support above which the FPS is positioned, that supports only half the deck, (m_d/2);

- the pier is modeled with n DOF; in particular, is defined as a lumped mass system divided into n segments, each segment is connected to a node with a horizontal DOF; then the mass of each segment is represented in the form of a mass point overlying the segment. In addition, the last segment is connected to the foundation and therefore represents a fixed support;
- The force-deformation behavior of the FPS was considered to be rigid bilinear. as shown in (*Figure 4.2*).

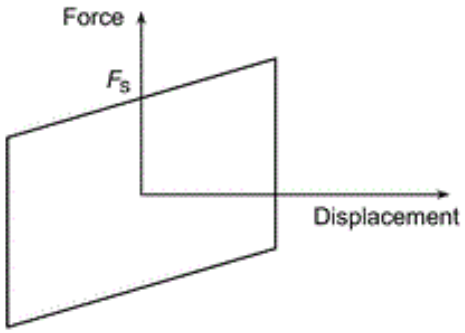

Figure 4.2: Force-deformation of FPS.

The abutment-pier model proposed is shown below:

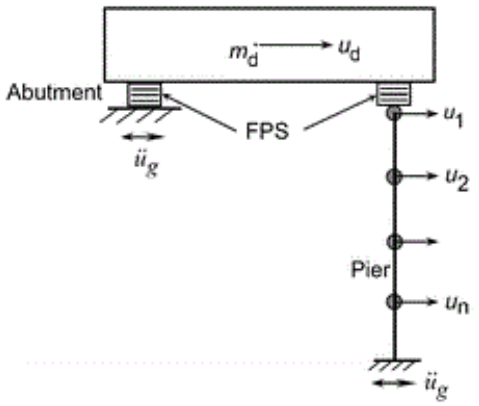

Figure 4.3: Mathematical model of the abutment-pier interaction [24].

The dynamic analysis that will be carried out is non-linear type, thus allowing the evaluation of the seismic response through the direct integration of the equations of motion, applying the appropriately chosen ground motion records to the nodes of the substructure.

This is the most complex, but also the most complete, method of analysis, that allows to know the trend over time of stress and deformation states of the structure components, and therefore to verify the integrity of the structural elements in relation to possible fragile behaviors, as well as to evaluate the dynamic behavior of the structure in the nonlinear field.

Once the mathematical model of the bridge structure has been defined, it is possible to proceed with the writing of the equations of motion that govern the pier, abutment, isolator and deck interaction. In this thesis, however, we consider the isolation of the bridge in the longitudinal direction only, and then we will consider the response of the structure, for many parameters and making to varying the values of these latter, along this direction.

4.1.1 Equations of motion

The equations that govern the motion of the isolated bridge, according to [24], are:

$$m_d \ddot{u}_d + F_a + F_p = -m_d \ddot{u}_g \tag{4.1}$$

$$[m_p]\{\ddot{u}_p\} + [c_p]\{\dot{u}_p\} + [k_p]\{u_p\} - \{\psi\}F_p = [m_p]\{1\}\ddot{u}_g \tag{4.2}$$

where:

- m_d represents the mass of the deck;
- $[m_p]$, $[c_p]$ and $[k_p]$ represent the mass, damping and stiffness pier matrix (with dimension n x n) based on the number of nodes in which it is divided;
- F_a and F_p are the recall forces acting on the FPS respectively at the abutment and at the pier;
- u_d is the displacement of the deck, while $\{u_p\}$ is the displacement vector of the various nodes of the pier;
- $\{\psi\} = \{1, 0, 0, ..., n\}$ is a vector that applies the recall force of the FPS;
- $\{1\}$ is a unit vector (with dimension 1 x n), which represents the coefficient of influence of the seismic acceleration, indicated with $\ddot{u}$.

The equations above are written in terms of absolute displacements, in this way the displacements of each degree of freedom, with respect to the base of the pier and abutment,

are calculated. This can be seen from the fact that, by rewriting the two equations in a single system, we obtain the masses matrix that are diagonal, while the damping and stiffness matrices are symmetrical. However, it is more convenient to work with the damping and stiffness matrices that are diagonal, thus obtaining a decoupled system of equations that is easier from the computational point of view. To achieve this, the system of equations is rewritten in terms of relative displacements, using Kelly's theory [18], and the displacements of each degree of freedom, with respect to the underlying one, will be calculated. Rewriting the two equations in a single system, we can see as the masses matrix is symmetrical, while the damping and stiffness matrices are diagonal.

The relative displacements are then written:

$$\ddot{u}_d = \ddot{v}_d + \ddot{v}_{p_1} + \cdots + \ddot{v}_{p_n} \tag{4.3}$$

$$\ddot{u}_{p_n} = \ddot{v}_{p_1} + \cdots + \ddot{v}_{p_n} \tag{4.4}$$

$$\ddot{u}_{p_1} = \ddot{v}_{p_1} \tag{4.5}$$

and therefore, the equations can be rewritten as follows:

$$m_d(\ddot{v}_d + \ddot{v}_{p_1} + \cdots + \ddot{v}_{p_n}) + F_a + F_p = -m_d\ddot{u}_g \tag{4.6}$$

$$m_{p_n}(\ddot{v}_{p_1} + \cdots + \ddot{v}_{p_n}) - F_a - F_p + c_{p_n}\dot{v}_{p_n} + k_{p_n}v_{p_n} = -m_{p_n}\ddot{u}_g \tag{4.7}$$

$$m_{p_{n-1}}(\ddot{v}_{p_1} + \cdots + \ddot{v}_{p_{n-1}}) + c_{p_{n-1}}\dot{v}_{p_{n-1}} + k_{p_{n-1}}v_{p_{n-1}} - c_{p_n}\dot{v}_{p_n} - k_{p_n}v_{p_n} = -m_{p_{n-1}}\ddot{u}_g \tag{4.8}$$

$$m_{p_1}\ddot{v}_{p_1} + c_{p_1}\dot{v}_{p_1} + k_{p_1}v_{p_1} - c_{p_2}\dot{v}_{p_2} - k_{p_2}v_{p_2} = -m_{p_1}\ddot{u}_g \tag{4.9}$$

The recall forces F_a and F_p are described by the following generic formula, in terms of absolute displacements:

$$F_i = \frac{m_d g}{R}u_d + \mu_{d,i}\, m_d\, g\, sgn(\dot{u}_d) \qquad per\ i = a, p \tag{4.10}$$

that is composed of two terms: the first one elastic, depending on the stiffness of the superstructure k_d (given by the ratio $\frac{m_d g}{R} = \frac{W}{R}$), the second one frictional, dependent on the dynamic friction coefficient inside the FPS. This friction can be defined by the following formula:

$$\mu_d = f_{max} - (f_{max} - f_{min})e^{-\alpha|\dot{u}_d|} \tag{4.11}$$

Where the various terms have all been explained in detail in the third chapter.

Since F_i and F_p are also dependent on displacements and velocities, we must also rewrite the equations according to the quantities in the relative field. It is also necessary to divide, both the elastic term and the frictional term for two, since the weight of the deck is distributed equally between the two structural parts, and therefore half the weight will be carried from the abutment and half from the pier.

$$F_p = \frac{W}{2R} v_d + \mu_{d_p} \frac{W}{2} sgn(\dot{v}_d) \tag{4.12}$$

$$F_a = \frac{W}{2R} (v_d + v_{p_1} + \cdots + v_{p_n}) + \mu_{d_a} \frac{W}{2} sgn(\dot{v}_d + \dot{v}_{p_1} + \cdots + \dot{v}_{p_n}) \tag{4.13}$$

By combining these equations in one system, the following system can be written:

$$\begin{bmatrix} m_d & m_d & \dots & m_d \\ m_d & m_d + m_{p_1} & \dots & m_d + m_{p_1} \\ \vdots & \vdots & \ddots & \vdots \\ m_d & m_d + m_{p_1} & \dots & m_d + \sum m_{p_i} \end{bmatrix} \begin{bmatrix} \ddot{v}_d \\ \ddot{v}_{p_1} \\ \vdots \\ \ddot{v}_{p_n} \end{bmatrix} + \begin{bmatrix} c_d & 0 & \dots & 0 \\ 0 & c_{p_1} & \dots & 0 \\ \vdots & \vdots & \ddots & \vdots \\ 0 & 0 & \dots & c_{p_n} \end{bmatrix} \begin{bmatrix} \dot{v}_d \\ \dot{v}_{p_1} \\ \vdots \\ \dot{v}_{p_n} \end{bmatrix} +$$

$$+ \left(\begin{bmatrix} k_d & 0 & \dots & 0 \\ 0 & k_{p_1} & \dots & 0 \\ \vdots & \vdots & \ddots & \vdots \\ 0 & 0 & \dots & k_{p_n} \end{bmatrix} + \begin{bmatrix} 0 & 1 & \dots & 1 \\ 1 & 1 & \dots & 1 \\ \vdots & \vdots & \ddots & \vdots \\ 1 & 1 & \dots & 1 \end{bmatrix} \left(\frac{W}{2R} \right) \right) \begin{bmatrix} v_d \\ v_{p_1} \\ \vdots \\ v_{p_n} \end{bmatrix} + \begin{bmatrix} W/2R \\ 0 \\ \vdots \\ 0 \end{bmatrix} u_d + \begin{bmatrix} 1 \\ 0 \\ \vdots \\ 0 \end{bmatrix} \mu_{d_p} \frac{W}{2} sgn(\dot{v}_d) +$$

$$+ \begin{bmatrix} W/2R \\ 0 \\ \vdots \\ 0 \end{bmatrix} v_d + \mu_{d_a} \frac{W}{2} sgn \left(\left[\begin{pmatrix} 1 \\ 0 \\ \vdots \\ 0 \end{pmatrix} \dot{v}_d + \begin{pmatrix} 0 \\ 1 \\ \vdots \\ 0 \end{pmatrix} \dot{v}_{d+\cdots+} \begin{pmatrix} 0 \\ 0 \\ \vdots \\ 1 \end{pmatrix} \dot{v}_d \right] \right) =$$

$$= - \begin{bmatrix} m_d & m_d & \dots & m_d \\ m_d & m_d + m_{p_1} & \dots & m_d + m_{p_1} \\ \vdots & \vdots & \ddots & \vdots \\ m_d & m_d + m_{p_1} & \dots & m_d + \sum m_{p_i} \end{bmatrix} \begin{bmatrix} 0 \\ 0 \\ \vdots \\ 1 \end{bmatrix} \ddot{u}_g \tag{4.14}$$

with $\mu_{d_p} \propto (\dot{v}_d)$, while $\mu_{d_a} \propto \left(\left\| \left[\begin{pmatrix} 1 \\ 0 \\ \vdots \\ 0 \end{pmatrix} \dot{v}_d + \begin{pmatrix} 0 \\ 1 \\ \vdots \\ 0 \end{pmatrix} \dot{v}_{d+\cdots+} \begin{pmatrix} 0 \\ 0 \\ \vdots \\ 1 \end{pmatrix} \dot{v}_d \right] \right\| \right)$.

that can be written in compact form as follows:

$$[M]\{\ddot{v}\} + [C]\{\dot{v}\} + ([K] + [K]_1)\{v\} + F_p + F_a = -[M]\{I\}\ddot{u}_g \quad (4.15)$$

By dividing the previous equations for the mass of the deck, the following dimensionless parameters can be identified:

- Mass ratio: $\lambda = \frac{m_p}{m_d}$ (4.16)
- Relative damping of the deck: $\xi_d = \frac{c_d}{2m_d\omega_d}$ (4.17)
- Relative damping of the pier: $\xi_p = \frac{c_p}{2m_p\omega_p}$ (4.18)
- Natural pulsation of the deck: $\omega_d = \sqrt{\frac{k_d}{m_d}}$ (4.19)
- Natural pulsation of the pier: $\omega_p = \sqrt{\frac{k_p}{m_p}}$ (4.20)

4.2 Modeling in MATLAB & Simulink®

The simulation of the dynamic system studied in this thesis was possible thanks to the Simulink software (an internal application of the Matlab calculation program and produced by Mathworks Inc.), which extends the potential of Matlab, adding many specific functions and maintaining its general characteristics. Simulink is used in two phases: the first is the definition of the model to simulate, the second is the analysis of the system itself. So that the model definition is immediate, Simulink uses a windowed environment called “Block diagram windows”, through which models can be created simply by using the mouse. The analysis of the model takes place either by choosing the options from the Simulink menus or by reusing the commands through the Matlab Command Windows. The results of the simulation are available during the simulation phase itself and the result available in the Matlab Workspace.

The (*Figure 4.4*) shows a simple example of a block diagram created in Simulink to solve a second order differential equation, that is the basis to implement the step by step integration of a n DOF system of dynamic equations. We can identify in the diagram the seismic input signal, which represents the history of the induced accelerations to the base of the analysed structure, the integrator blocks (in number equal to the order of the differential equation), which allow to trace the history of the system displacements, represented by the response

block. It is also possible to introduce some "gain" blocks, through which the system's velocity and displacement histories, produced by the various "integrator" blocks, are multiplied by the entity set by the user in the respective dialog box: in the present case such entities are represented by the damping matrix and the stiffness matrix. In this way, the software package performs the step by step integration of the input signal and, at each step, makes that integration pass through its respective gains and cyclically comes back to the add block, returning the looked-for results.

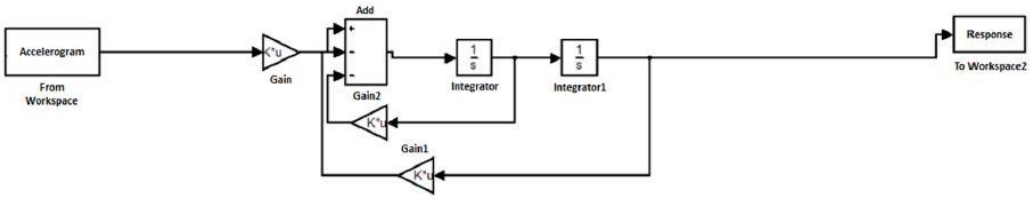

Figure 4.4: Second order differential equation solving within Simulink®.

Taking into consideration the structure model and the relative equilibrium equations, seen in the previous paragraph, we can now describe the modeling of the pier-abutment interaction done within the MATLAB & Simulink® environment. In this work of thesis, the pier was modelled subdividing it into 5 masses (5 DOF), thus obtaining the total system with (5+1) DOF and considering the non-linearity of FPS devices (*Figure 4.5*).

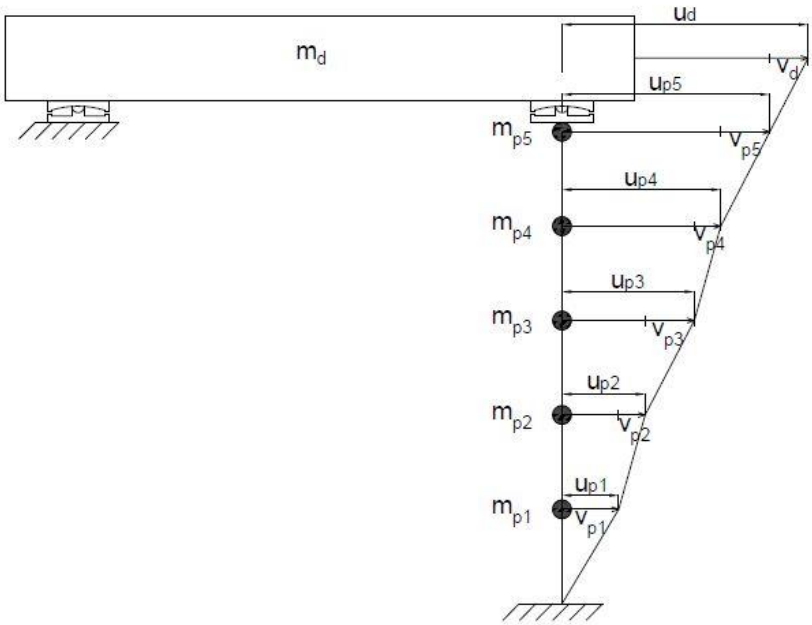

Figure 4.5: Mathematical model of (5+1) DOF pier-abutment interaction, implemented in a MATLAB & Simulink® environment.

The first phase of work consisted in writing a calculation code (script) in Matlab. This script contains the input data of the problem (variables and parameters), the algorithm for the calculation of stiffnesses and, furthermore, the construction and filling of all the matrices necessary for the resolution of the motion equations system takes place. Also, in the script are recalled and loaded files containing the seisms (ground motion records that are scaled within a function called by the script) and the coefficients of friction of the FPS. The second phase involved block modeling in the Simulink environment, where input data arrives, are processed, i.e. the system of non-linear equations is solved through a step by step integration, and finally the results are sent back to the script for final processing and for saving data. The analysis has been implemented with fixed input parameters, considering a fixed-step (ode3, step 0.0005 s) integration.

The block model implemented in Simulink is shown in (*Figure 4.6*) and a brief explanation of its operation will be given.

Starting from the left, there is the first block that represents the input signal, i.e. the accelerations (a_g), to which a "Gain" block is applied that has the function of dividing it by the mass and therefore to make it be dimensionless in relation to it; the result is integrated in each cycle, two times in sequence through a step by step integration, obtaining first the velocity vector and then the displacement vector which is sent to the Matlab Work Space. At this point follow the following steps:

1. The velocities vector dimensionless by the mass is directed to the Gain 2 block, which multiplies it by the damping matrix and directs it back to the starting system ("Add" block), and to the Gain 7, 8, 9, 13, 14, 15, 16 blocks, which multiply the velocity vector for the vector containing a single unit term (in the position corresponding to each DOF) and all the other nulls. These Gains blocks send the vectors to the set of blocks that reproduce the mechanics of the frictional behavior of the FPS isolator [25], with velocity dependent components. Respectively, the Gain 7 sends it to the first set of blocks for determining the frictional force of the pier side FPS, the Gain from 8 to 16 send it to the second set of blocks for determining the FPS abutment side. Finally, the results come back into the cycle, adding to the initial Add block.
2. The displacements vector dimensionless by the mass enters within the Gain 1 block which multiplies it by the total stiffness matrix and makes it re-enter within the cycle, and in the Gain 5 and 11 blocks which multiply them by the elastic terms of the forces

of the FPS, going therefore to determine respectively the elastic force of the FPS on the pier and the elastic force of the FPS on the abutment.

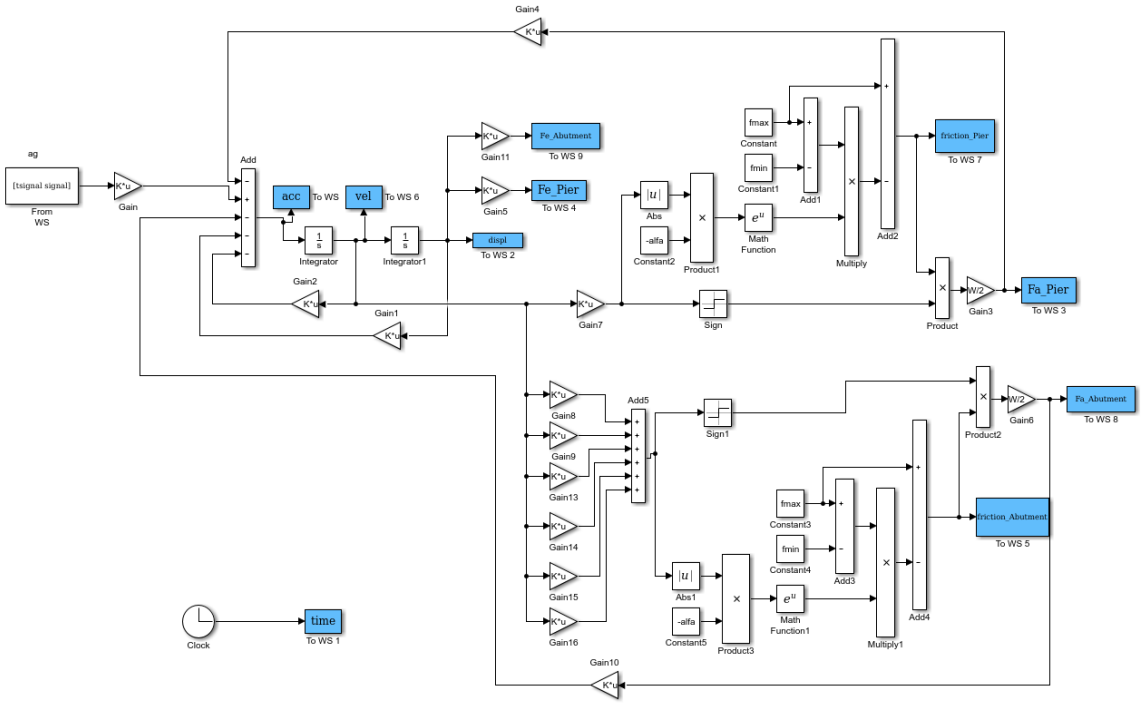

Figure 4.6: Model implemented in the MATLAB & Simulink® environment of the 6+1 DOF pier - abutment interaction.

4.3 Parametric study

In the present study, 172.800 non-linear dynamic simulations were launched in the MATLAB & Simulink® environment, obtaining as many different structural responses for the superstructure (deck) and the substructure (pier and abutment). To do this, several parameters were taken into consideration, both deterministic and random, and a Matlab code was created, set up with various "for" cascade cycles. The control parameters used have been selected among the various values reported in the literature and are reported in detail below.

4.3.1 Sliding friction coefficient as a random parameter

The experimental data developed by [19], [20], [21] on sheet type Teflon bearings, as described in Chapter 3, have pointed out that friction is a complex phenomenon, not complying with the Coulomb friction law (friction constant during sliding) and several mechanisms (such as sliding velocity, normal load, temperature effects, number of cycles) contribute to its variability and can modify its statistical values under dynamic conditions showing a very high uncertainty within the range considered.

Recalling the formula of friction, rewritten in terms of relative displacements:

$$\mu_d = f_{max} - (f_{max} - f_{min})e^{-\alpha|\dot{v}_d|} \tag{4.21}$$

in this thesis, it is chosen to model the friction coefficient at high speed, f_{max}, as a random variable with a function of Gaussian probability density (PDF), whose interval chosen for the characterization of this parameter is between 0.5% and 5.5% with an average value equal to 3% (*Figure 4.7*). Moreover, the friction coefficient at low velocities, f_{min}, is also a random variable, correlated in this study to f_{max} through the relation $f_{min} = f_{max}/3$, while for α is assumed a value of 30, based on regression of the experimental results [19], [20], [21].

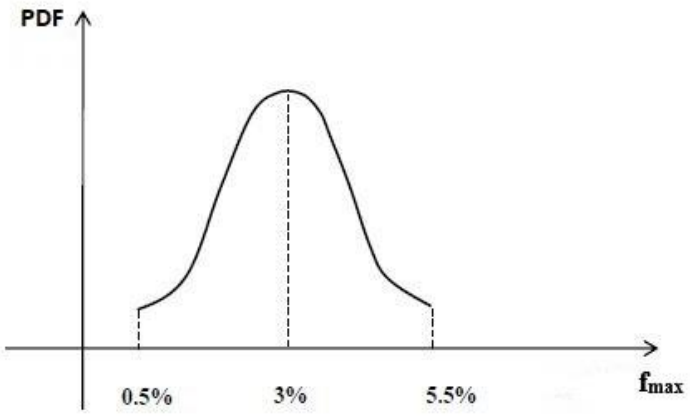

Figure 4.7: Gaussian probability density function of the f_{max} variable.

Starting from the probability density functions of the random variable, the Latin Hypercube Sampling (LHS) method, developed by Mckay et al. [14], widely employed in many literatures works [26], [27], has been used as a stratified sampling technique to generate the

input data samples of the structural models, by sampling 15 values from PDF and perform the non-linear dynamic analyses.

4.3.2 Deterministic structural parameters

They have been analysed 720 different types of bridges, obtained by the combination of the deterministic structural parameters (*Table 4.1*) with 15 random values of sliding friction coefficient, which characterize the bridge and the isolation level.

Table 4.1: Deterministic structural parameters values.

T_p [s]	T_d [s]	λ [-]
0.05	1	0.1
0.1	2	0.15
0.15	3	0.2
0.2	4	

It is noteworthy that, from the fundamental period of the pier T_p with top free condition, we can obtain the height of the pier, going to invert the following formula [24]:

$$T_p = \sqrt{\frac{\bar{m}_p h^4}{EI}} \cdot \frac{2\pi}{(1.875)^2} \tag{4.21}$$

where $\bar{m}_p$ is the mass per unit length, h is the height and EI is the flexural rigidity of the pier. Equation (4.21) is based on the fundamental period of a uniform cantilever beam under transverse vibrations.

4.3.3 Seismic parameters

An essential necessity for the scientific community is to define models as much as possible realistic of the seismic action to be used in the field design; considering the non-linear dynamic analyses as the only acceptable means to establish the reliability of the structures subject to seismic excitations, then the latter must necessarily be representative of

the site seismicity, appropriately justified on the basis of the seismogenic characteristics of the source, at the site conditions recording, at the magnitude, at the distance from the source and at the maximum horizontal acceleration expected at the site. In general, the limit states, as evidenced also by NTC08, can be verified using accelerograms, which can be recorded (or natural), synthetic (or simulated), or artificial, defined as follows:

- Recorded or natural accelerograms: are recordings of natural events readily available in the databases of recognized research institutions;
- Synthetic or simulated accelerograms: are generated through a modeling, carried out with both deterministic and stochastic methods, capable of simulating the effects of connected physical processes to the motion of the ground: genesis of the earthquake, wave propagation and surface response of the site under investigation. The evolution of this modeling over the years has been remarkable, even if their application is complex, as it requires the definition of a number elevated parameters for the characterization of ground seismic motion not always easy to determine.
- Artificial accelerograms, or sample functions (realizations) of a random process based for example on "Random Vibration Theory".

In this study, 30 natural ground motion records with only horizontal components, deriving from 19 different seismic events, have been taken in consideration (as indicated by NTC08). These ground motion records were taken from the banks given online websites: Pacific Earthquake Engineering Research Center (PEER, 2016) [28]; Italian Accelerometric Company (ITACA, 2016) [29]; Internet Site for European Strong Motion Data (ISESD, 2016) [30]. The characteristics of the selected ground motion records are reported in (*Table 4.2*), while the (*Figure 4.8*) shows the pseudo-acceleration elastic response spectra $S_{pa}(T)$ of the unscaled records versus the vibration period T. Their greatest source-to-site distance (R) is 98.2 km, their moment magnitude (M) varies in the range between 7.6 and 6.0, and their PGA, between 0.13 and 0.94 g.

Table 4.2: Selected ground motion records characteristics.

No.	Year	Earthquake name	Recording station name	$V_{S,30}$ [m/s]	Source [fault type]	M [–]	R [km]	PGA [g]
1	1994	Northridge	Beverly Hills – Mulhol	356	Thrust	6.7	13.3	0.52
2	1994	Northridge	Canyon Country – WLC	309	Thrust	6.7	26.5	0.48
3	1994	Northridge	LA – Hollywood Stor	316	Thrust	6.7	22.9	0.36
4	1999	Duzce, Turkey	Bolu	326	Strike-slip	7.1	41.3	0.82
5	1999	Hector Mine	Hector	685	Strike-slip	7.1	26.5	0.34
6	1979	Imperial Valley	Delta	275	Strike-slip	6.5	33.7	0.35
7	1979	Imperial Valley	El Centro Array #11	196	Strike-slip	6.5	29.4	0.38
8	1995	Kobe, Japan	Nishi-Akashi	609	Strike-slip	6.9	8.7	0.51
9	1995	Kobe, Japan	Shin-Osaka	256	Strike-slip	6.9	46.0	0.24
10	1999	Kocaeli, Turkey	Duzce	276	Strike-slip	7.5	98.2	0.36
11	1999	Kocaeli, Turkey	Arcelik	523	Strike-slip	7.5	53.7	0.22
12	1992	Landers	Yermo Fire Station	354	Strike-slip	7.3	86.0	0.24
13	1992	Landers	Coolwater	271	Strike-slip	7.3	82.1	0.42
14	1989	Loma Prieta	Capitola	289	Strike-slip	6.9	9.8	0.53
15	1989	Loma Prieta	Gilroy Array #3	350	Strike-slip	6.9	31.4	0.56
16	1990	Manjil, Iran	Abbar	724	Strike-slip	7.4	40.4	0.51
17	1987	Superstition Hills	El Centro Imp. Co.	192	Strike-slip	6.5	35.8	0.36
18	1987	Superstition Hills	Poe Road (temp)	208	Strike-slip	6.5	11.2	0.45
19	1987	Superstition Hills	Westmorland Fire St.	194	Strike-slip	6.5	15.1	0.21
20	1992	Cape Mendocino	Rio Dell Overpass	312	Thrust	7.0	22.7	0.55
21	1999	Chi-Chi, Taiwan	CHY101	259	Thrust	7.6	32	0.44
22	1999	Chi-Chi, Taiwan	TCU045	705	Thrust	7.6	77.5	0.51
23	1971	San Fernando	LA – Hollywood Stor	316	Thrust	6.6	39.5	0.21
24	1976	Friuli, Italy	Tolmezzo	425	Thrust	6.5	20.2	0.35
25	1980	Irpinia, Italy	Bisaccia	496	/	6.9	21.3	0.94
26	1979	Montenegro	ST64	1083	Thrust	6.9	21.0	0.18
27	1997	Umbria – Marche	ST238	n/a	Normal	6.0	21.5	0.19
28	2000	South Iceland	ST2487	n/a	Strike-slip	6.5	13	0.16
29	2000	South Iceland (a.s.)	ST2557	n/a	Strike-slip	6.4	15.0	0.13
30	2003	Bingol	ST539	806	Strike-slip	6.3	14.0	0.30

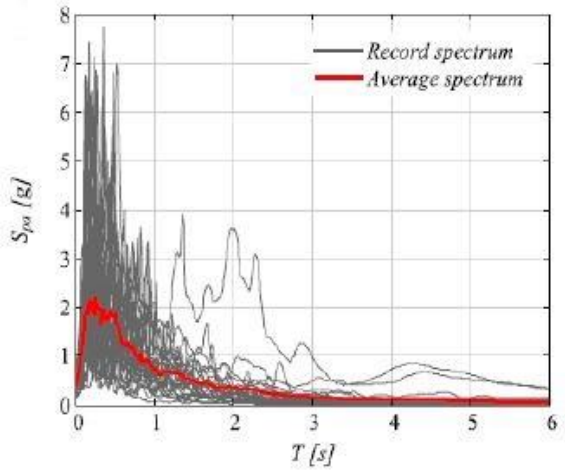

Figure 4.8: Pseudo-acceleration response spectrum for the unscaled records.

On the other hand, 8 values for the intensity measures (IM) have been assumed and a selected spectral parameter coinciding with $S_d(T_d)$ has been chosen as IM parameter (*Table 4.3*), regarding which to scale the 30 ground motion records.

Table 4.3:Selected intensity measures, $S_d(T_d)$

Intensity	1	2	3	4	5	6	7	8
$S_d(T_d)$ (m)	0,10	0,15	0,20	0,25	0,30	0,35	0,40	0,45

The IM parameters have been chosen respecting the following three properties:

1. ***Efficiency***: an IM is efficient if the variability of the structural response, expressed by the dispersion of the damage level for each assigned value of IM, is lower than a value considered acceptable. The choice of a more efficient IM compared to another allows to obtain a reduction in the number of analyses to be performed without losing in terms of accuracy of the estimate. This is one of the reasons why, generally, the PGA is not used as a parameter of seismic intensity IM, especially in the case of very flexible structures, preferring instead the spectral ordinate to the period of an elastic SDOF system, chosen as representative of the structure, even if studied with non-linear dynamic analyses, to obtain a lower dispersion on the response. Moreover, in structural analyses, IMs are not used at the source, but at the construction site, as they are more efficient than those that characterize the signal at great distances from the site.
2. ***Scaling robustness***: an IM is robust to scaling if the accelerogram scaled to that determined intensity measure not observed, produces the same effects in terms of structural response that would produce a not scaled accelerogram having "naturally" that determined intensity measure.
3. ***Sufficiency***: an IM is sufficient if, and only if, the information that IMs consider in relation to the structural response, does not increase if we add information about the magnitude, the distance of the earthquake or any other characteristics of the seismic signal that caused that intensity measure. The IM must be sufficient with respect to all the variables that appear in the integral of hazard: if, for example, we want to evaluate the

energy dissipated during a seismic event in a structure, we cannot consider in the analysis an intensity measure coinciding with the PGA or with the spectral ordinates, since such IMs do not take into account any information regarding the duration of the excitation (factor on which the dissipated energy strongly depends).

CHAPTER 5

5. SEISMIC RELIABILITY ANALYSIS OF ISOLATED BRIDGES WITH FPS

Bridges are key elements of transportation systems. Previous seismically induced damages to these structures, the significant cost of reconstruction and the need to bridges' immediate operation revealed the necessity of seismic vulnerability assessment of them according to performance-based earthquake engineering philosophy. Such methodology requires accurate prediction of seismic capacity of the bridges and seismic demand associated to them. To achieve this goal, a newly born analysis method, called Incremental Dynamic Analysis (IDA), has been proposed by Vamvatsikos and Cornell [31].

In the current study, IDA is applied to reach the relationship between the seismic capacity and the demand of the structure and evaluate the structural performance accurately. IDA curves provide appropriate result formats which may be used to estimate the annual average frequency of exceeding predefined damage states and develop fragility curves of the bridges. Moreover, they may be integrated with hazard curves in order to evaluate the seismic reliability of the structure.

5.1 Incremental dynamic analysis (IDA)

The first step in determining the seismic reliability of isolated bridges with FPS is the development of incremental dynamic analyses (IDA) [31]. The pier-abutment structural systems, with (5+1) degree of freedom (DOF), were analysed combining the deterministic structural parameters, T_p, T_d and λ, with each value of the statistical sample of the coefficient of friction, μ_d. Furthermore, the damping coefficients for the deck ξ_d (coinciding with the damping coefficient of the devices) and for the pier ξ_p, were assumed respectively equal to 0% and 5%. The damping coefficient ξ_d is considered equal to zero, consistently with other

works which assume that friction is the only source of damping in the isolators [35], [38]. Finally, considering the periods of the pier and the deck listed in (4.3.12), we obtain degree of isolation values ($\Pi_\omega = \omega_p/\omega_d$) between 5 (rigid superstructure) and 80 (flexible superstructure).

Therefore, non-linear dynamic analyses were performed by subjecting each structural model to 30 seismic records in MATLAB & Simulink® [32], scaled to eight intensity measure values (spectral displacement corresponding to the fundamental period of the structure) within the incremental dynamic analysis, through the following scale factor:

$$SF = \frac{IM_{target}}{IM} = \frac{S_{d,target}(T_d)}{S_d(T_d)} \tag{5.1}$$

In this way, we obtained 30 ground motion records having the same "shape" as the starting ones, but that in correspondence of the T_d period all return the same displacement $S_{d,target}$. This procedure is not strictly necessary but helps to ensure that the spectra of the individual ground motion records are like the reference spectrum, at least around the fundamental vibration period of the superstructure. This helps to reduce the variability of the seismic response of the structure from record to record, which means to be able to evaluate the behavior of the structure, conditioned to the value of the design spectrum at that period, with less uncertainty, with the same number of analyses [34]. Moreover, with this procedure, we obtain structural responses independent of the seismic hazard in terms of Magnitude (M) and Distance (R) [33], i.e. we have separated the uncertainties related to the intensity of seismic input from those relative to the characteristics of the records.

To evaluate the seismic damage, as well as by common design practice and as indicated in the literature, it was decided to use the time history of the relative displacements of the superstructure, in correspondence of the pier (u_d) and of the abutment ($u_{d,abut}$), and the time history of the absolute displacement of the pier (u_p), taken with their maximum values. In this way a cartesian plane was constructed, in which the values of the IM parameter (S_d) on the abscissa axis and the values of the EDP (Engineering Demand Parameter) on the ordinate axis have been reported, obtaining for each of the 8 values of the IM, 450 different values of the EDP, obtained by subjecting each of the 15 μ_d belonging to the statistical sample to 30 different ground motion records, scaled from time to time for a precise value of $S_{d,target}$.

For a fixed spectral intensity, we obtain a sample of data that can be thought to be extracted from a lognormal distribution. This assumption permits to estimate, with a limited

number of samples, the response at different percentile levels, which is very useful for system reliability assessment. It also permits to obtain a closed-form analytical estimate of the seismic risk [37]. The sample of data, consisting of structural responses, therefore represents the request for performance (in terms of displacement) of the superstructure and substructure, i.e. the Seismic Demand. The lognormal distribution can be adapted to each response parameter by estimating the sample geometric mean, GM(EDP), and the sample lognormal standard deviation, or dispersion, σ_{ln}(EDP). Knowing the sample lognormal mean and the dispersion it is possible to determine the values of the 50^{th}, 84^{th} and 16^{th} percentile of each lognormal distribution [35]. Therefore, the statistical parameters and each percentile are calculated from the results of 450 simulations (15 values of the coefficient of friction combined with the 30 seismic records) for each intensity measure level considered. The IDA results of the deck (at the pier and abutment) and of the pier are plotted in (*Figure 5.1-12*) versus the intensity measure; each figure contains several curves, corresponding to the different percentile and λ values.

The (*Figure 5.1-5.4*) show the IDA curves relative to the maximum deck displacement, $u_{d,max}$. For low T_p values the influence of λ is almost nothing, while for medium-high values the variability of this parameter causes slight deviations in the structural response, which tend to decrease with increasing T_d. The lognormal mean of the structural response decreases with the increase of T_d; this happens because resonance phenomena occur, since the values of the pendulum period are very low, which make the structural response result greater for low values of the deck period. On the other hand, the dispersion remains approximately constant.

The (*Figure 5.5-5.8*) show the IDA curves relative to the maximum deck (abutment) displacement, $u_{d,abut,max}$, which reflect a very similar trend to the previous ones.

Finally, the (*Figure 5.9-5.12*) show the IDA curves relative to the maximum pier displacement, $u_{p,max}$. In this case, the structural response decreases with increasing T_d and λ, and there is a higher variability when the latter parameter changes, which decreases with increasing T_d and T_p, i.e. with increasing structural flexibility. As for the dispersion, instead, it tends to increase with increasing of the deck flexibility.

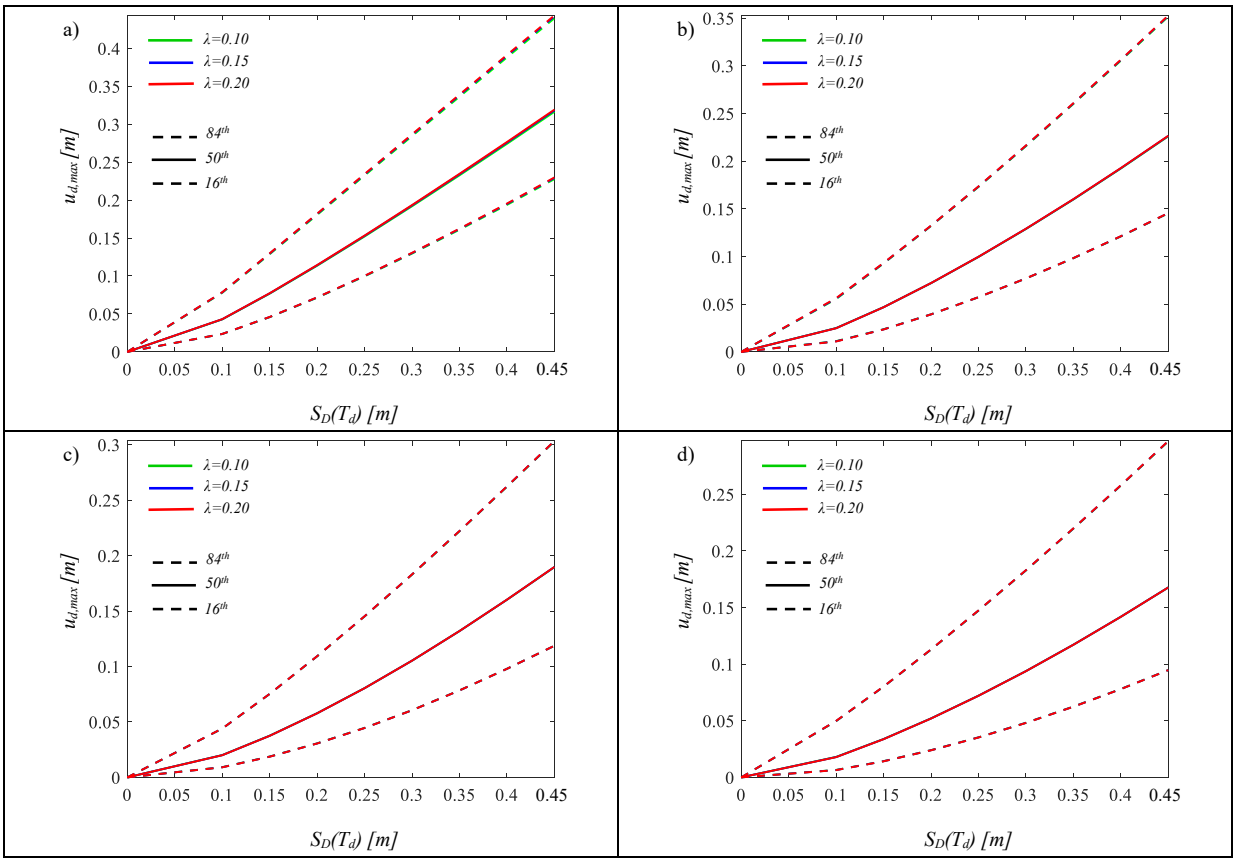

Figure 5.1:IDA curves of the deck for T_p=0.05 and T_d=1s (a), T_d=2s (b), T_d=3s (c), T_d=4s (d).

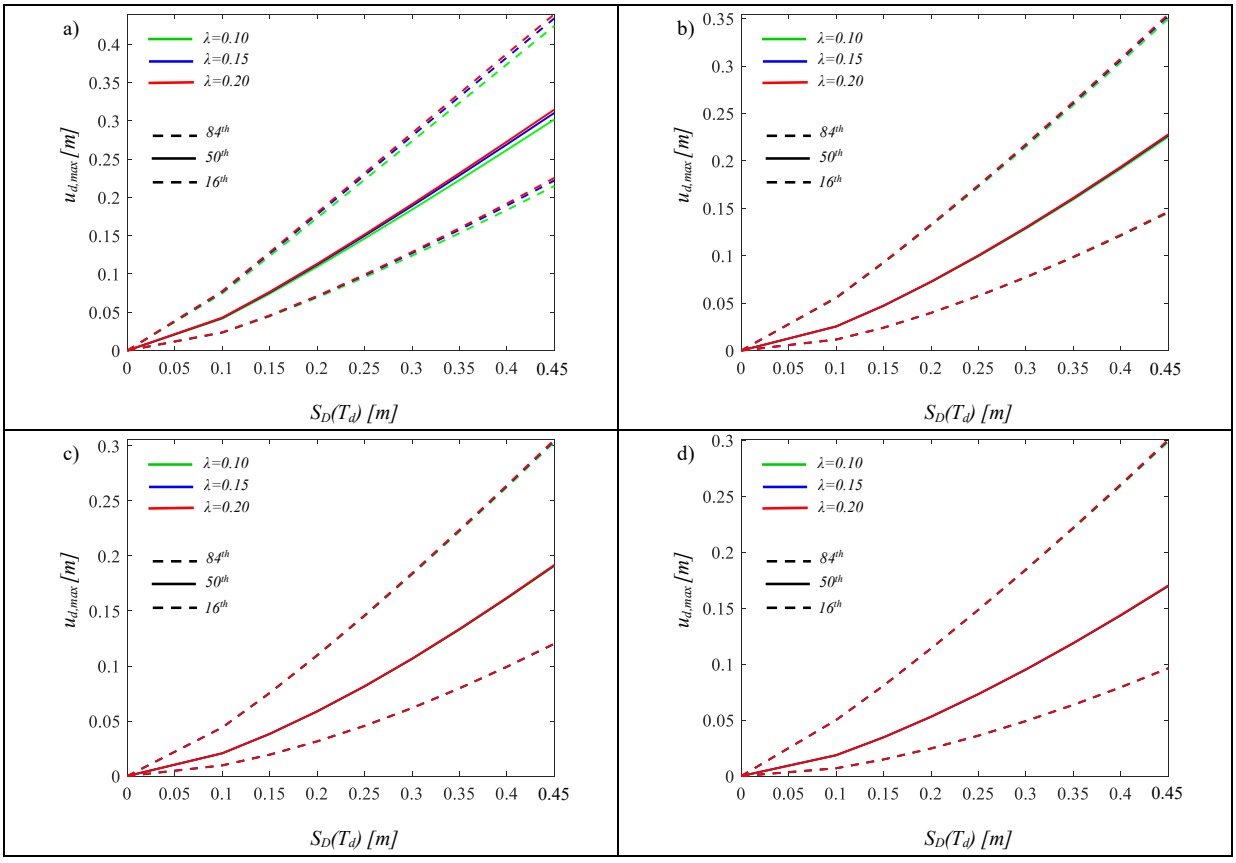

Figure 5.2: IDA curves of the deck for T_p=0.10 and T_d=1s (a), T_d=2s (b), T_d=3s (c), T_d=4s (d).

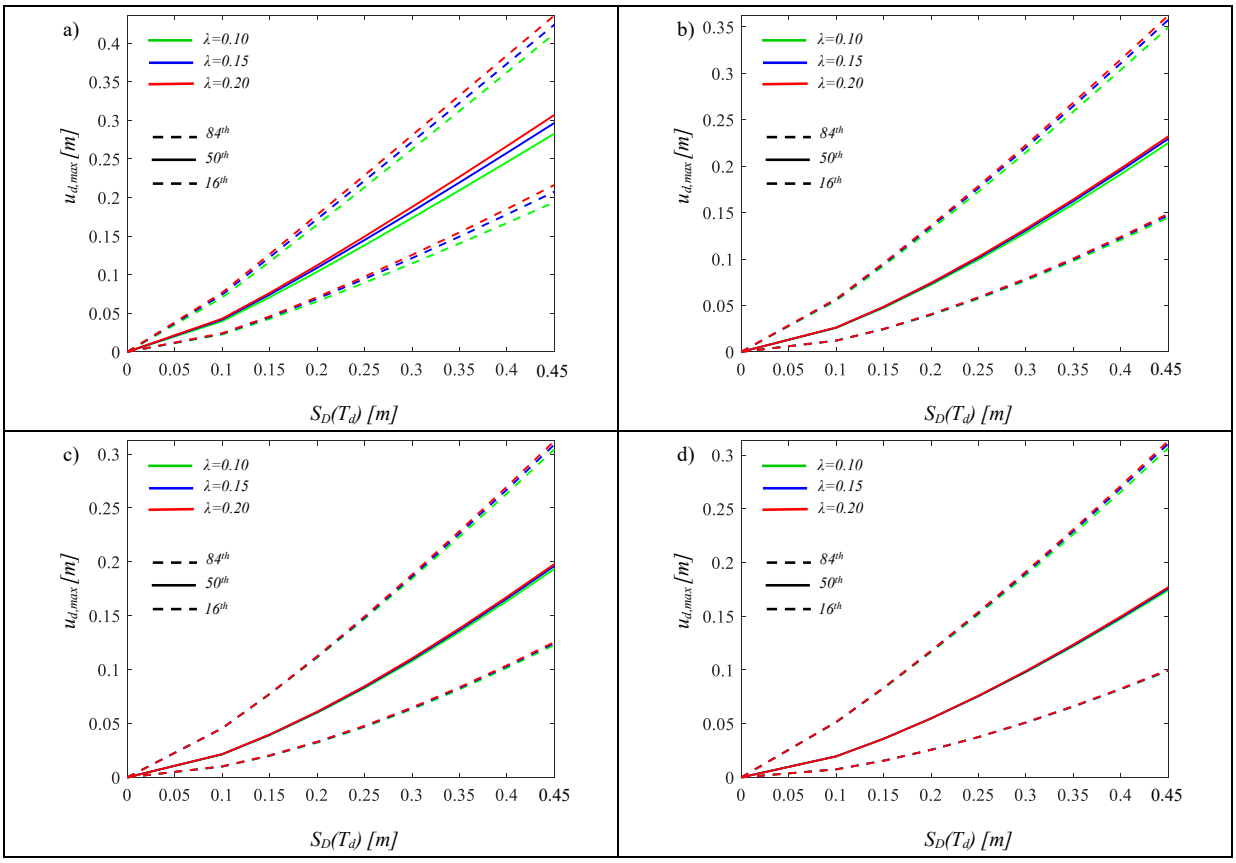

Figure 5.3: IDA curves of the deck for T_p=0.15 and T_d=1s (a), T_d=2s (b), T_d=3s (c), T_d=4s (d).

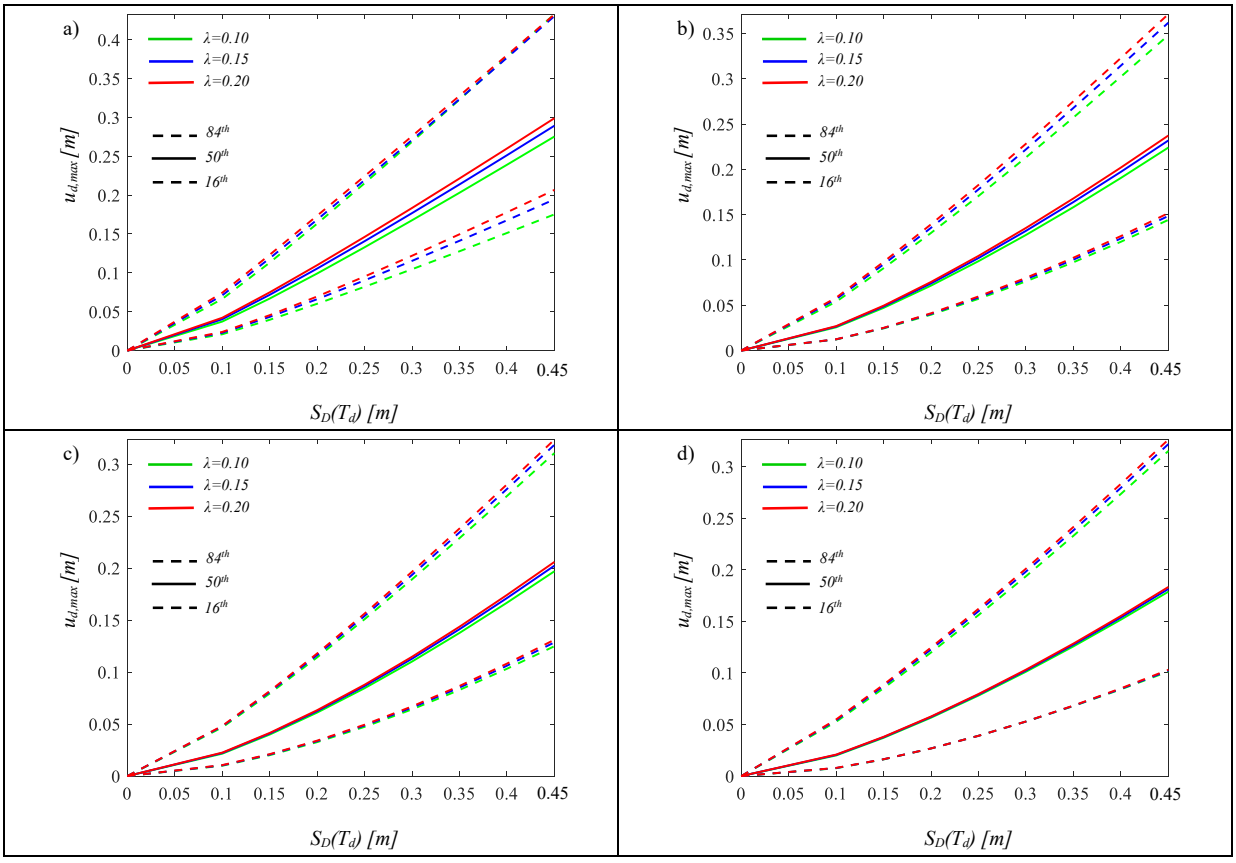

Figure 5.4: IDA curves of the deck for T_p=0.20 and T_d=1s (a), T_d=2s (b), T_d=3s (c), T_d=4s (d).

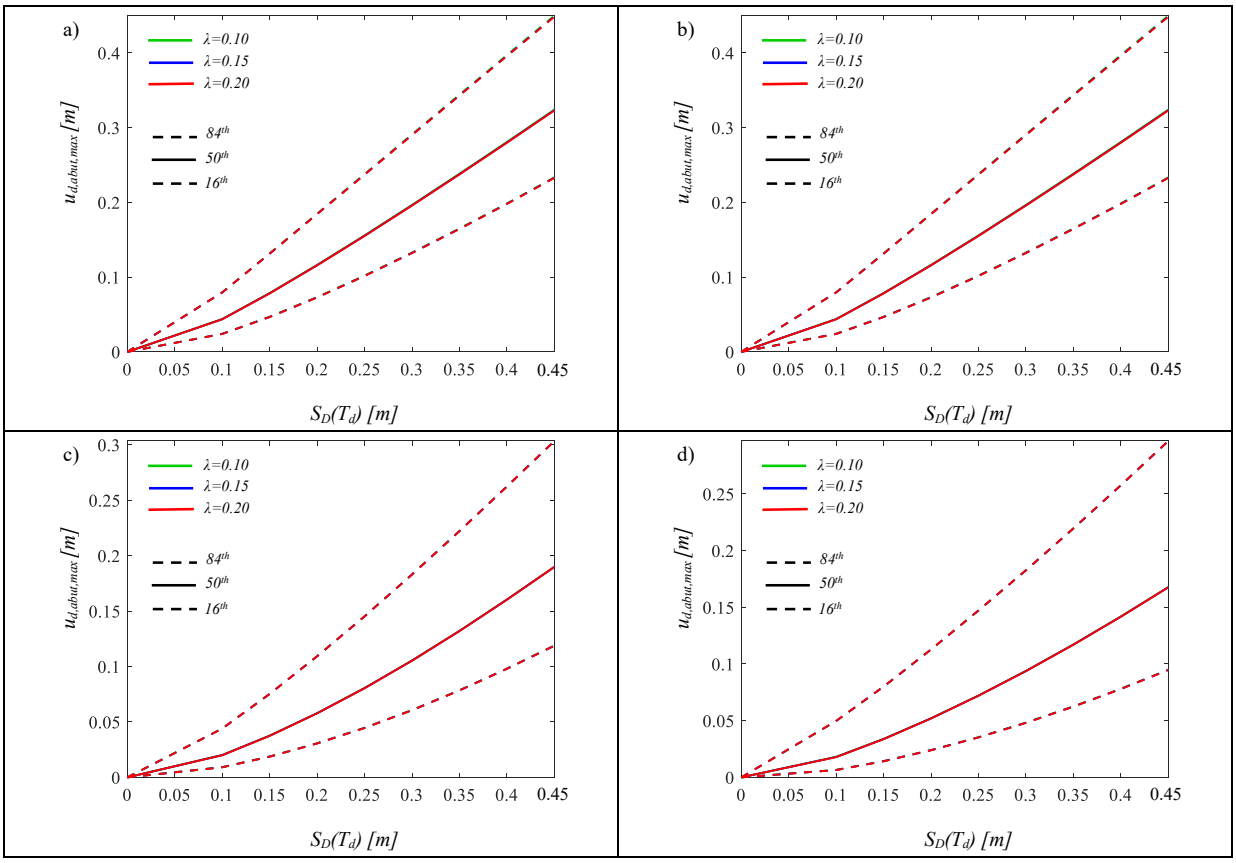

Figure 5.5: IDA curves of the deck (abutment) for T_p=0.05 and T_d=1s (a), T_d=2s (b), T_d=3s (c), T_d=4s (d).

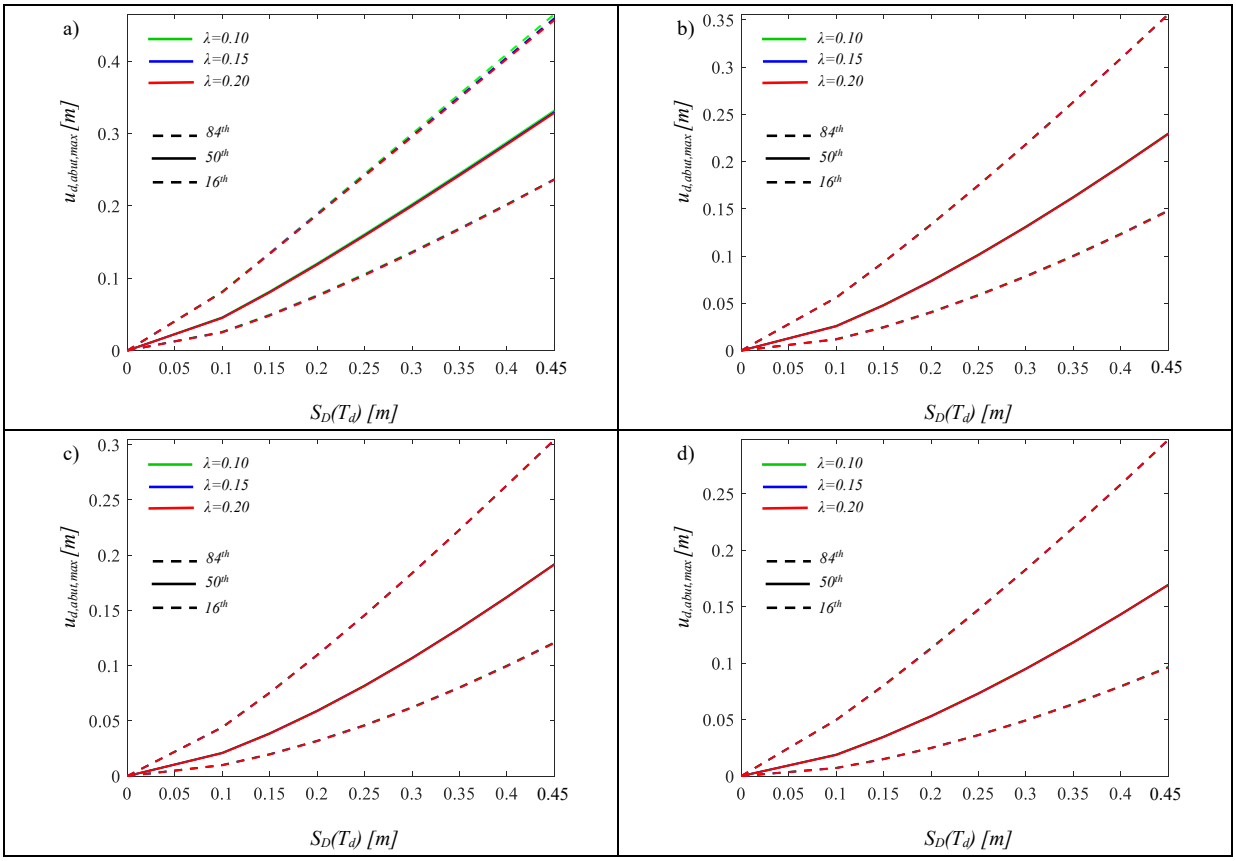

Figure 5.6: IDA curves of the deck (abutment) for T_p=0.10 and T_d=1s (a), T_d=2s (b), T_d=3s (c), T_d=4s (d).

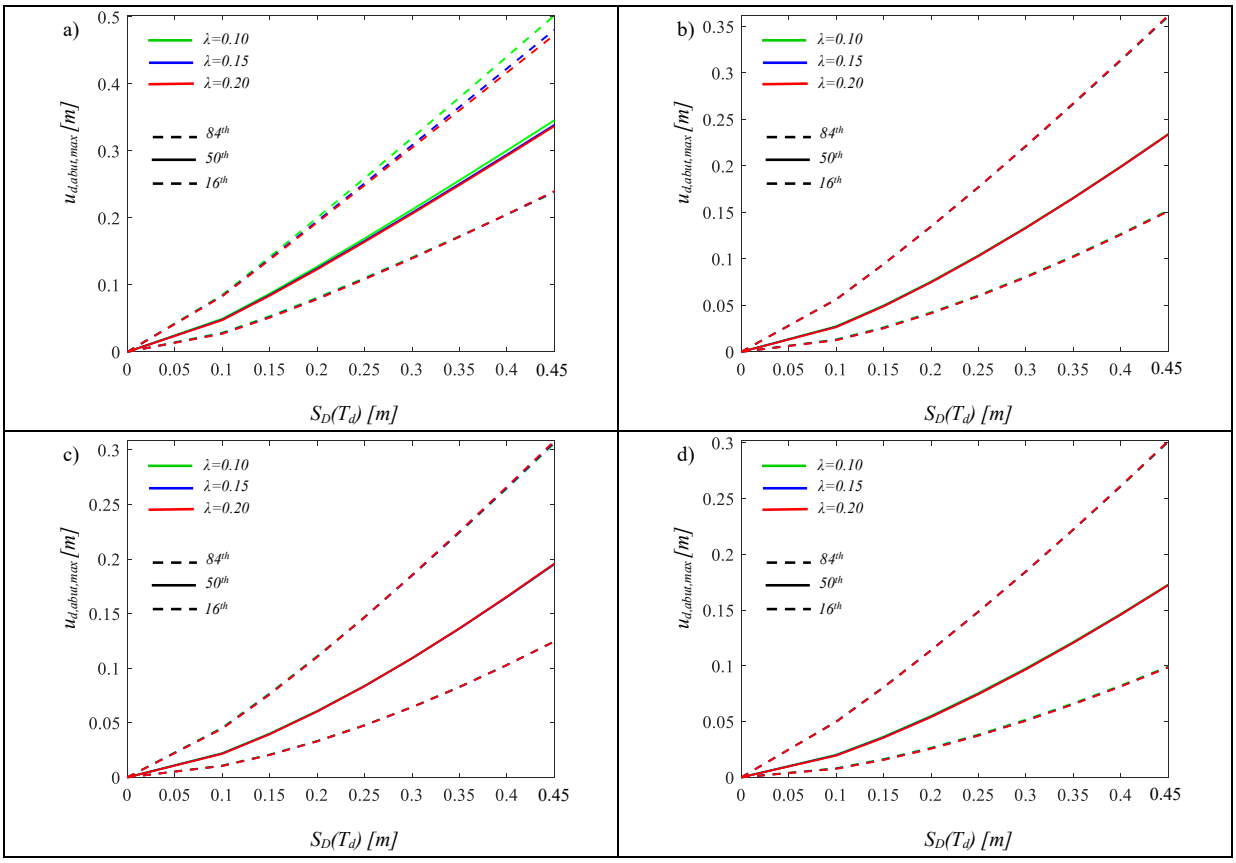

Figure 5.7: IDA curves of the deck (abutment) for T_p=0.15 and T_d=1s (a), T_d=2s (b), T_d=3s (c), T_d=4s (d).

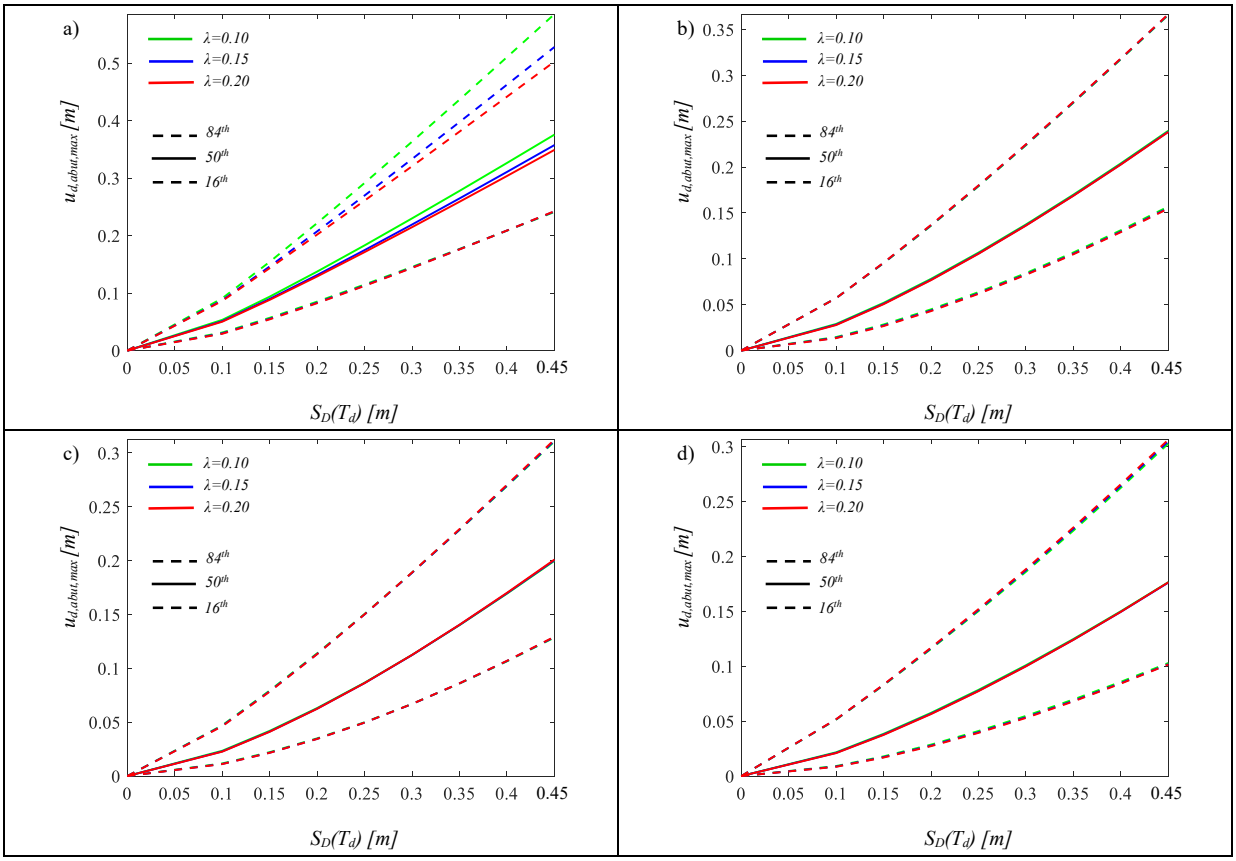

Figure 5.8: IDA curves of the deck (abutment) for T_p=0.20 and T_d=1s (a), T_d=2s (b), T_d=3s (c), T_d=4s (d).

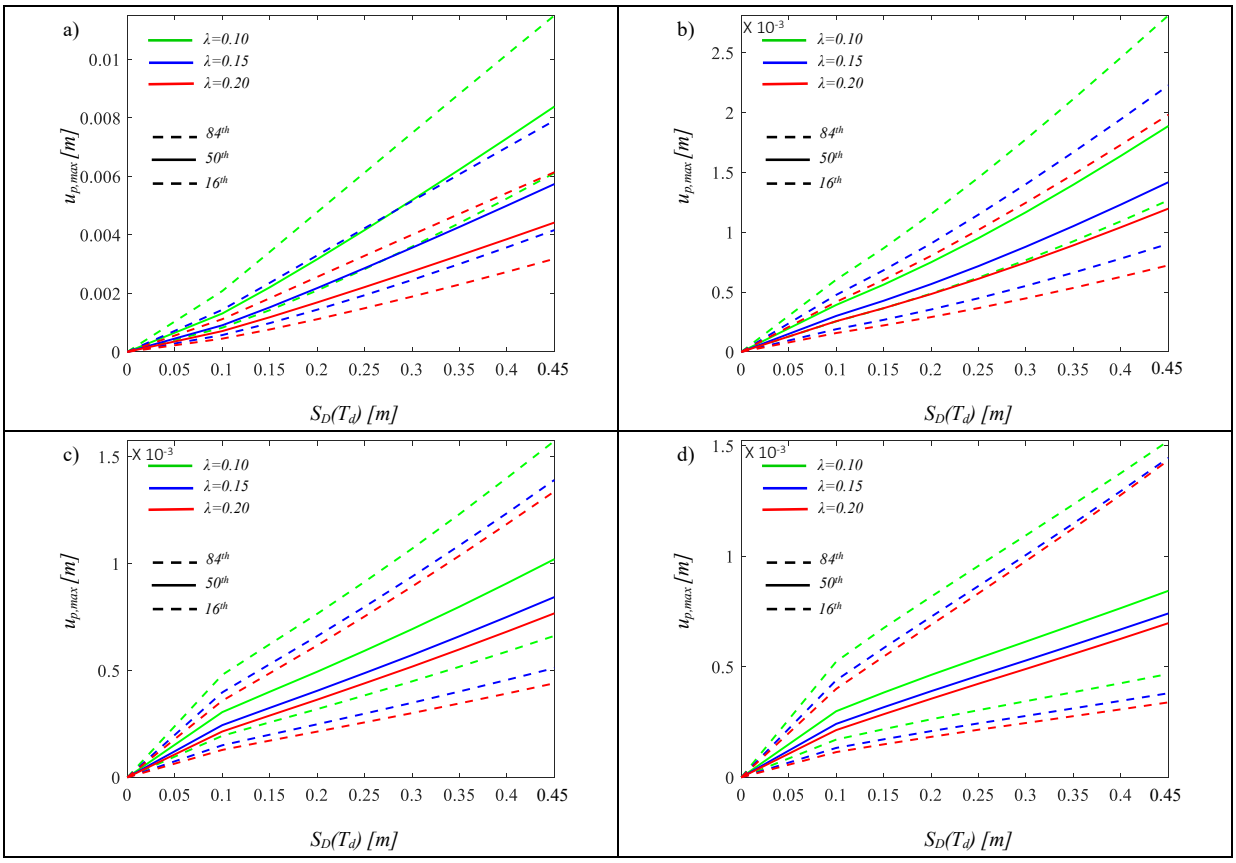

Figure 5.9: IDA curves of the pier for T_p=0.05 and T_d=1s (a), T_d=2s (b), T_d=3s (c), T_d=4s (d).

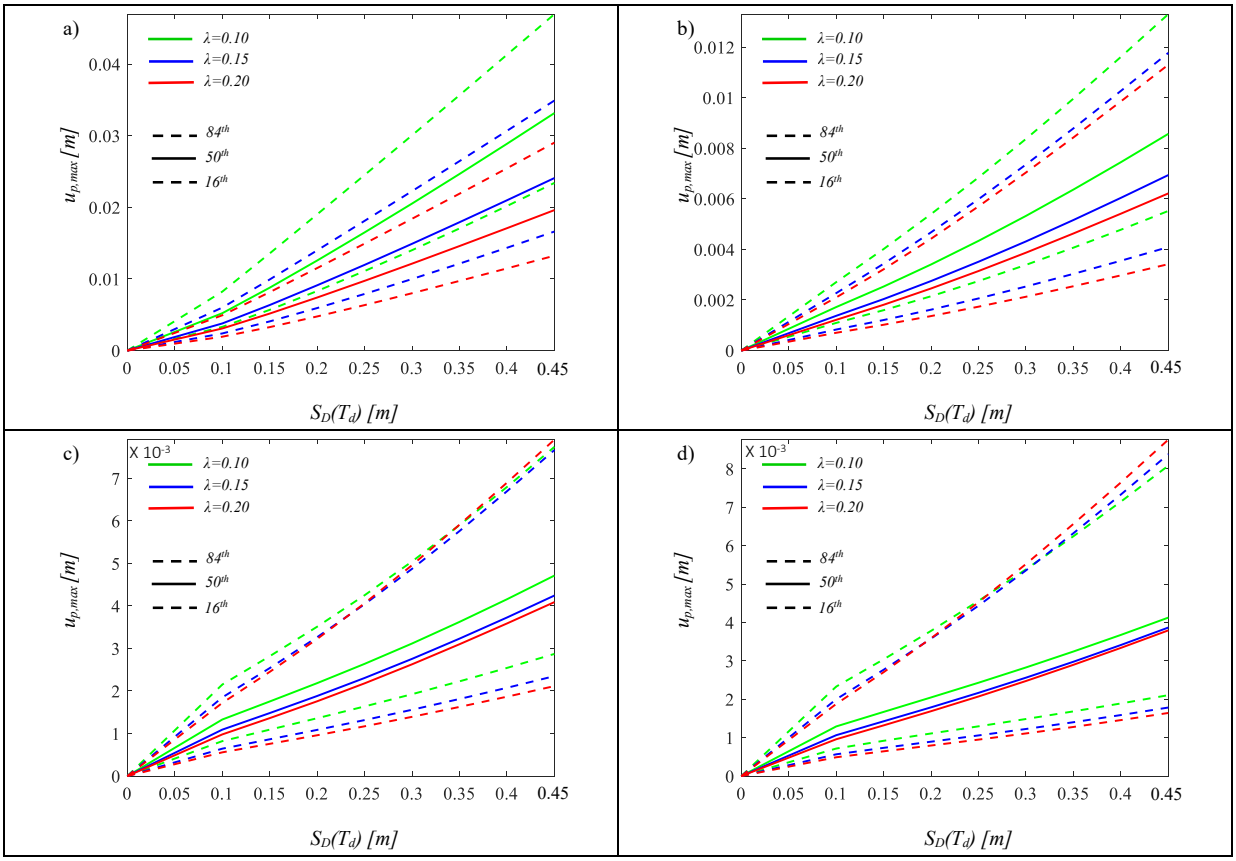

Figure 5.10: IDA curves of the pier for T_p=0.10 and T_d=1s (a), T_d=2s (b), T_d=3s (c), T_d=4s (d).

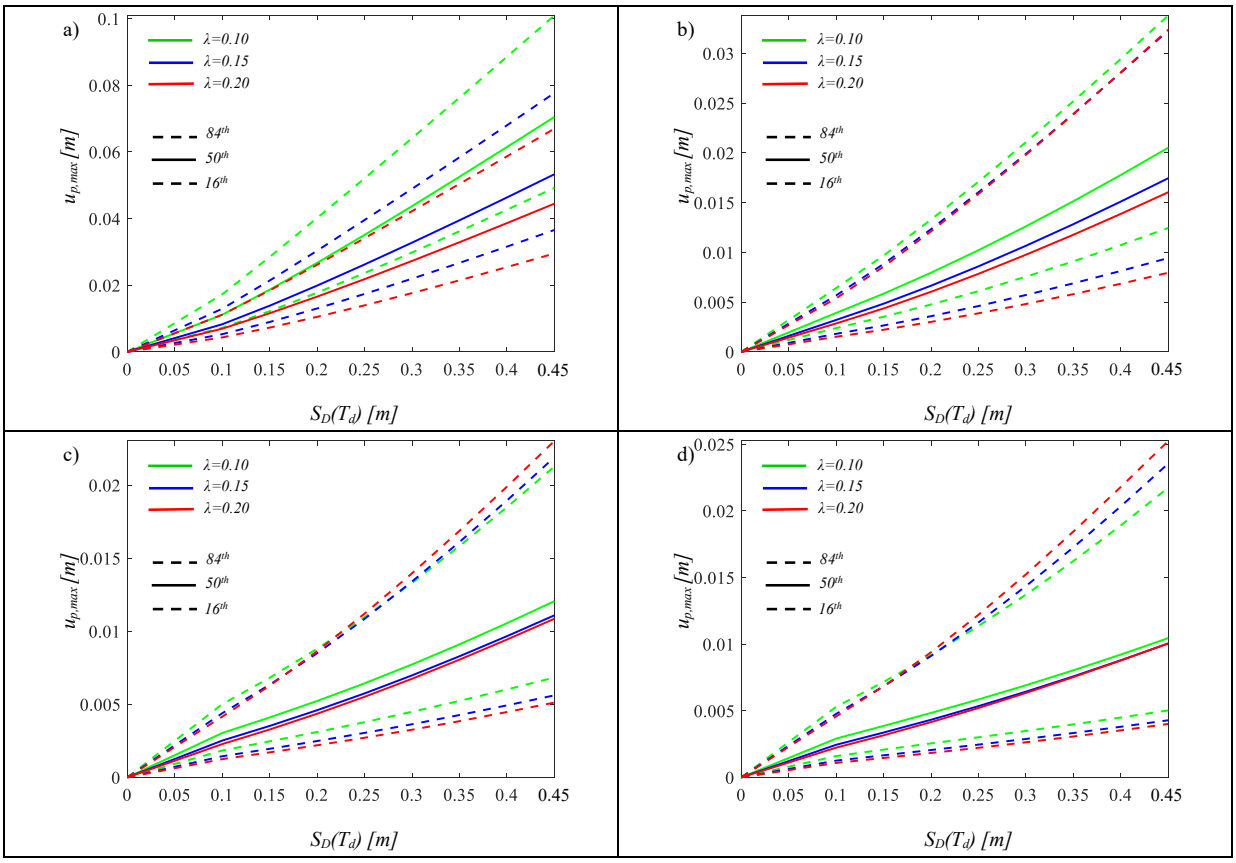

Figure 5.11: IDA curves of the pier for T_p=0.15 and T_d=1s (a), T_d=2s (b), T_d=3s (c), T_d=4s (d).

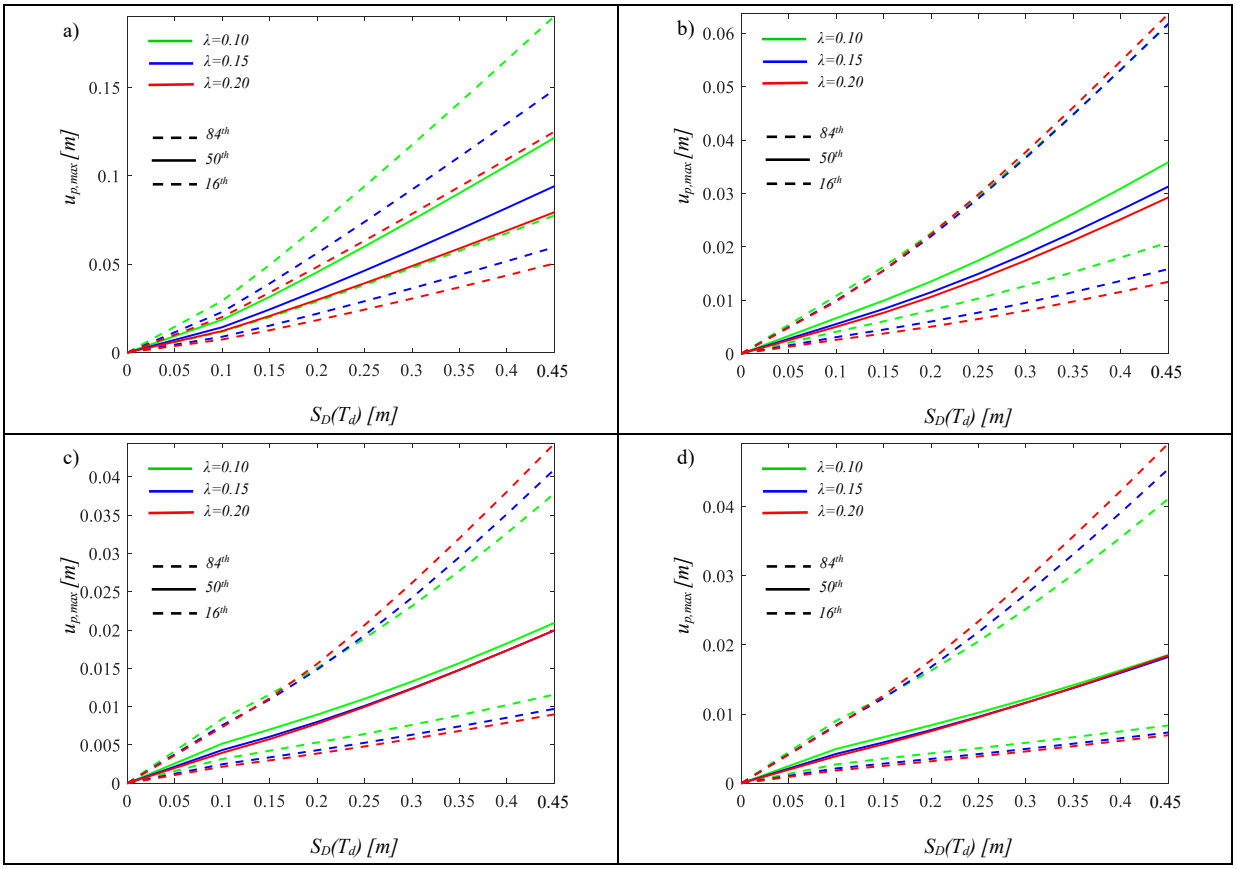

Figure 5.12: IDA curves of the pier, for T_p=0.20 and T_d=1s (a), T_d=2s (b), T_d=3s (c), T_d=4s (d).

5.2 Seismic fragility analysis

Once the non-linear dynamic analyses have been performed, the second step for the evaluation of seismic reliability of seismically isolated bridges with FPS devices, is the evaluation of the seismic fragility of the structure. The seismic fragility can be defined as the probabilities P_f exceeding different limit states at each level of the intensity measure (IM). For this reason, the limit state thresholds need to be defined.

The Limit States related to the isolation system have been defined, in terms of not exceeding of nine different values of the in-plan radius, r, of the FPS devices $u_{d,max}$ = r[m] and $u_{d\_abut,max}$ = r[m] (*Table 5.1*).

Table 5.1: Radius in plan values of FPS related to the different limit states.

Limit State	1	2	3	4	5	6	7	8	9
r[m]	0,10	0,15	0,20	0,25	0,30	0,35	0,40	0,45	0,50

While, about the substructure (pier), Pier Drift Index (PDI) have been defined as Performance Objectives, starting from the 4 Performance Limit States. As can be seen in the tables below, the International Standard (FEMA 274) [6] requires performance for the isolated bridges (PDI_{IB}) equal to 1/3 of the performance relative to the non-isolated bridge, PDI, (*Table 5.2*):

Table 5.2: Performance Limit States for isolated bridges (Fema 274).

Limit State		**PDI**	**PDI_{IB}**
LS1	Fully Operational	PDI=0,7%	PDI_{IB}=0,23%
LS2	Operational	PDI=1,5%	PDI_{IB}=0,5%
LS3	Life Safety	PDI=2,5%	PDI_{IB}=0,83%
LS4	Near collapse	PDI=5%	PDI_{IB}=1,67%

In this thesis, all the above-mentioned Limit States, related to both substructure and superstructure, are assumed to be deterministic.

Once the Limit States have been defined, we can proceed with the calculation of the Probability of failure (P_f) of the EDP value, associated to each Limit State, which is represented by the complement to 1 of the value of the Cumulative Distribution Function $F_{EDP|IM=im^*}$ of not exceeding the prefixed limit value, and represents a point in the fragility curve relative to that given Limit State. Therefore, the probability of failure, P_f, for an intensity measure level, $IM = im^*$, related to the isolation level and the substructure, can be defined, respectively, as:

$$P_f(im) = P\left[DM \geq LS_{d,i} | IM = im^*\right] \tag{5.2}$$

$$P_f(im) = P\left[DM \geq LS_{p,i} | IM = im^*\right] \tag{5.3}$$

where DM is the Damage Measure, that corresponds to the radius in plan for the isolation system, to the Pier Drift Index for the substructure.

Considering a level of intensity $IM = im^{**} > im^*$, the probability distribution $f_{EDP|IM=im^{**}}$ is shifted to right respect to $f_{EDP|IM=im^*}$, and at the same Limit State remains associated with it a greater Probability of failure and a new point in the Fragility plane [S_d-P_f]; continuing this process for all the $IM \equiv S_d$ intensity levels chosen for the analyses and for all the Limit States considered, the tracing of the fragility curve is completed. The points that identify the fragility curves for each Limit State were then approximated by a lognormal distribution, through the following procedure:

- For each Limit State, the standard normal variable u_r was calculated associated with the i^{th} point of the fragility curve;
- On the lognormal plane, in which the logarithm of the seismic intensity in the abscissas and the variable u_r in the ordinates are reported, the linear regression curve is determined, which identifies the fragility curve corresponding to the considered Limit State. From this regression the form parameters of the probability law are obtained. In fact, the regression equation is of the type:

  $$u_r = a \cdot \ln(S_d) + b \tag{5.4}$$

  Considering that the lognormal distribution of x is equivalent to a Gaussian distribution of variable y=ln(x) of parameters λ_y and σ_y, representative respectively of mean and standard deviation of y, introducing:

  $$u_r = \frac{y - \lambda_y}{\sigma_y} \tag{5.5}$$

we can obtain:

$$\sigma_y = \frac{1}{a} \tag{5.6}$$

$$\lambda_y = -\frac{b}{a} \tag{5.7}$$

- With the parameters found, the probability of failure may be calculated:

$$P_f = 1 - \Phi\left[\frac{\ln(\lambda_y | LS_i)}{\sigma_y}\right] \tag{5.8}$$

where Φ is the Cumulative Distribution Function operator.

5.2.1 Seismic fragility curves

The (*Figure 5.13-5.24*) show the fragility curves of each structural model (therefore with the variation of the dynamic characteristics T_p and T_d) referring to the isolation level (deck, at the pier and abutment) and the substructure (pier), for each State Limit and each value of the λ. Generally, the seismic fragility decreases for increasing the limit state thresholds. Moreover, it can be seen how these curves reflect the same trend of the IDA curves; fragility (vulnerability) decreases as the fundamental period of vibration, T_d, increases.

In the fragility curves of isolation system at the pier (*Figure 5.13-16*) and abutment (*Figure 5.17-20*), the influence of λ is almost nothing for low values of T_p, while for medium-high values of this latter the variability of λ causes slight deviations in the structural response, which tend to decrease with increasing T_d.

On the other hand, in the fragility curves of the pier (*Figure 5.21-24*) there is a higher variability with the variation of λ , and the pier results less fragile (vulnerable) when this parameter increase. Therefore, for low T_p values and medium-high T_d values, we can see how the probability of failure assume negligible values, due to the high rigidity that characterizes the substructure and the low seismic demand of the superstructure.

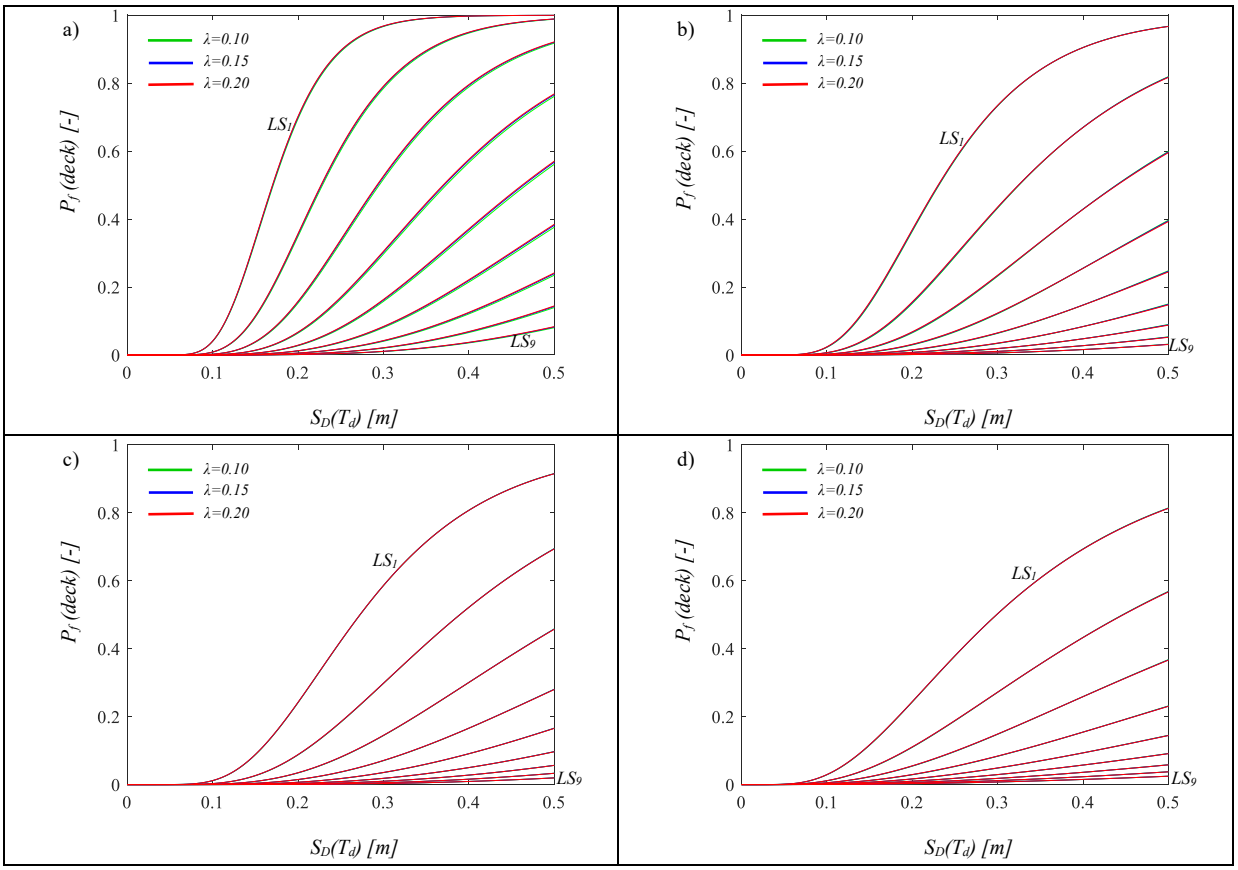

Figure 5.13: Fragility curves of the deck for T_p=0.05 and T_d=1 s (a), T_d=2s (b), T_d=3s (c), T_d=4s (d).

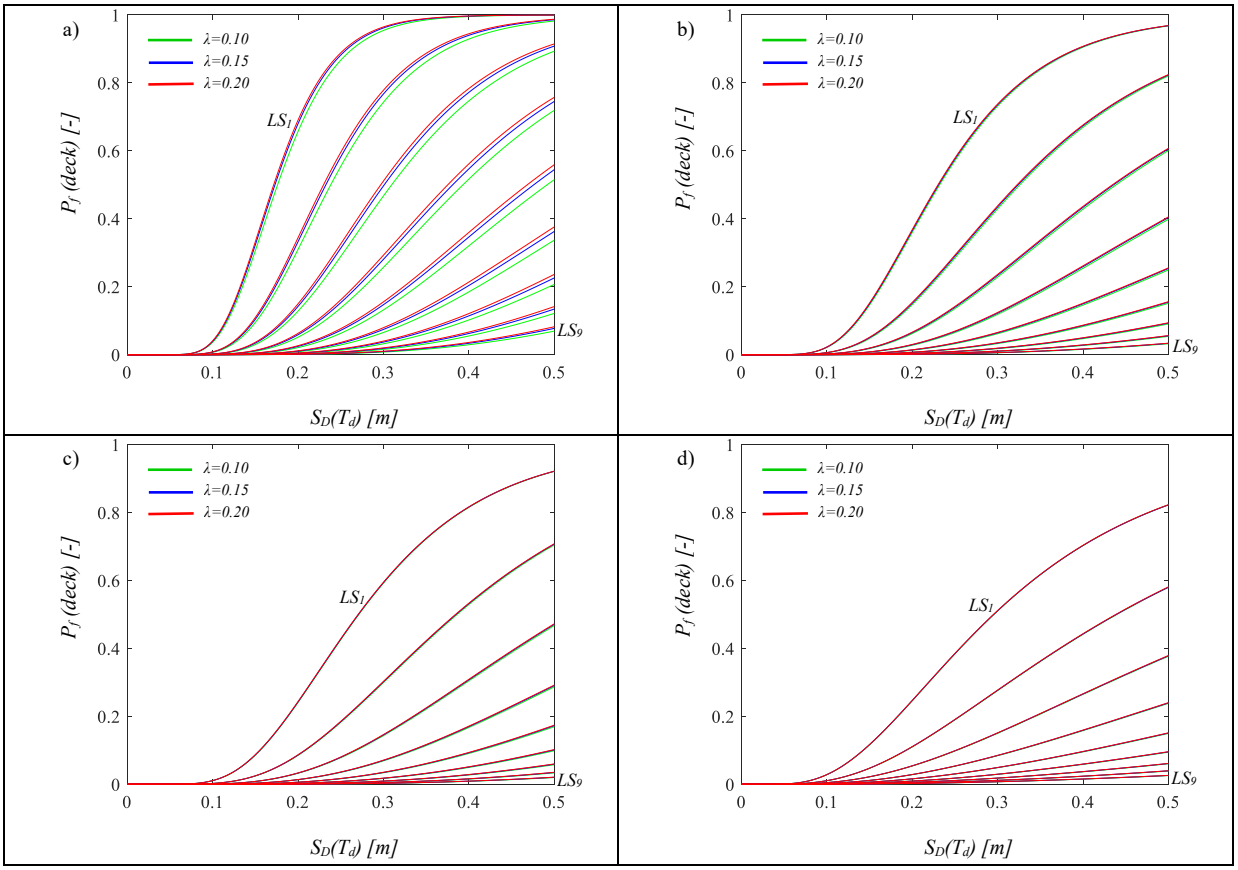

Figure 5.14: Fragility curves of the deck for T_p=0.10 and T_d=1s (a), T_d=2s (b), T_d=3s (c), T_d=4s (d).

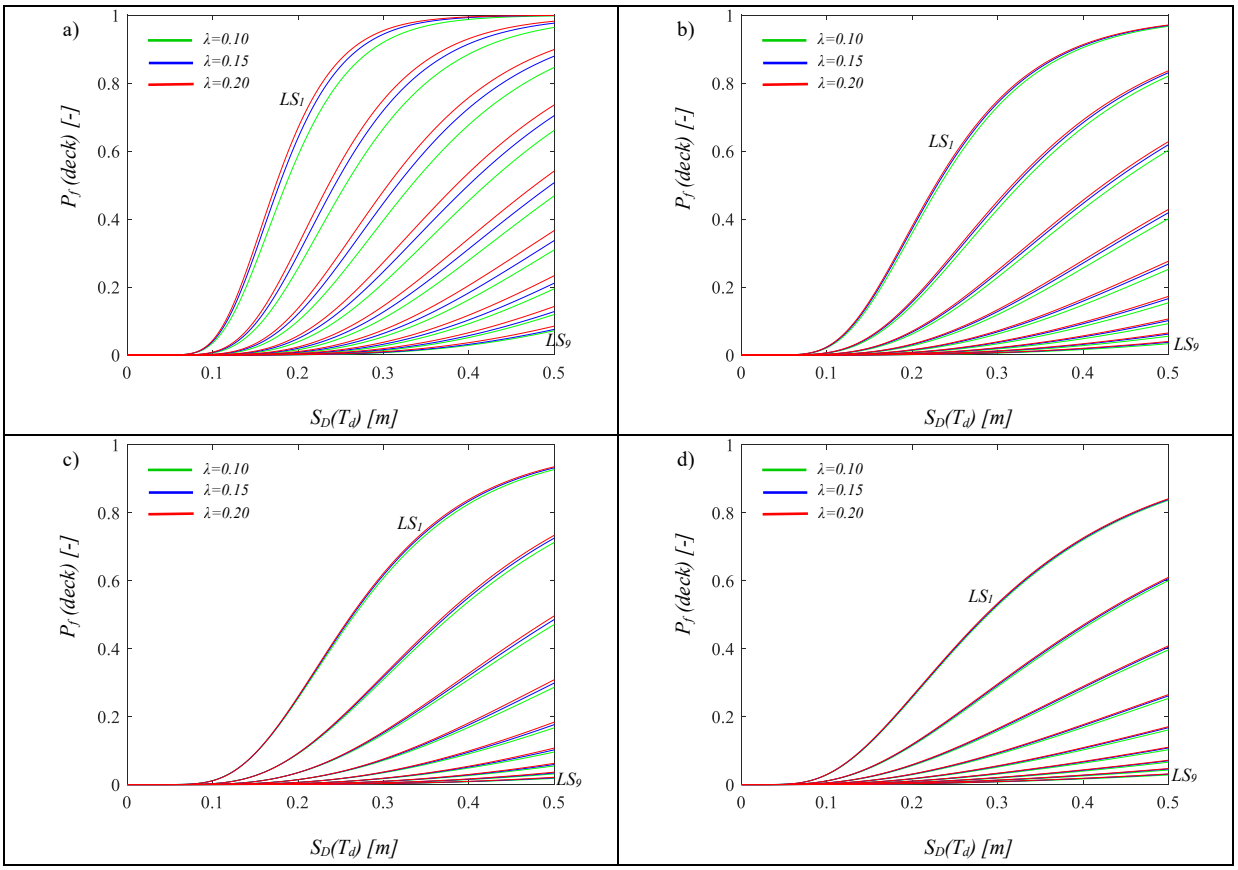

Figure 5.15: Fragility curves of the deck for T_p=0.15 and T_d=1s (a), T_d=2s (b), T_d=3s (c), T_d=4s (d).

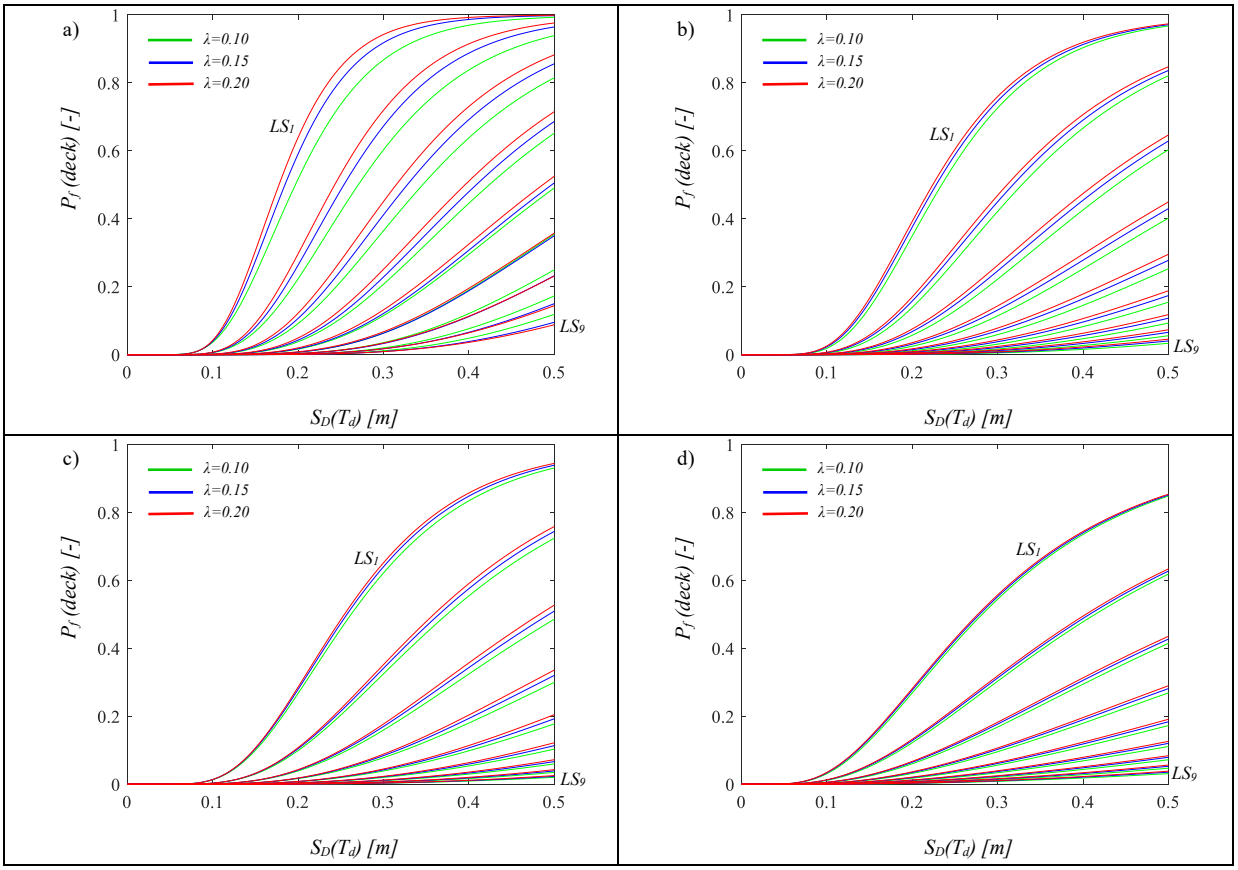

Figure 5.16: Fragility curves of the deck for T_p=0.20 and T_d=1s (a), T_d=2s (b), T_d=3s (c), T_d=4s (d).

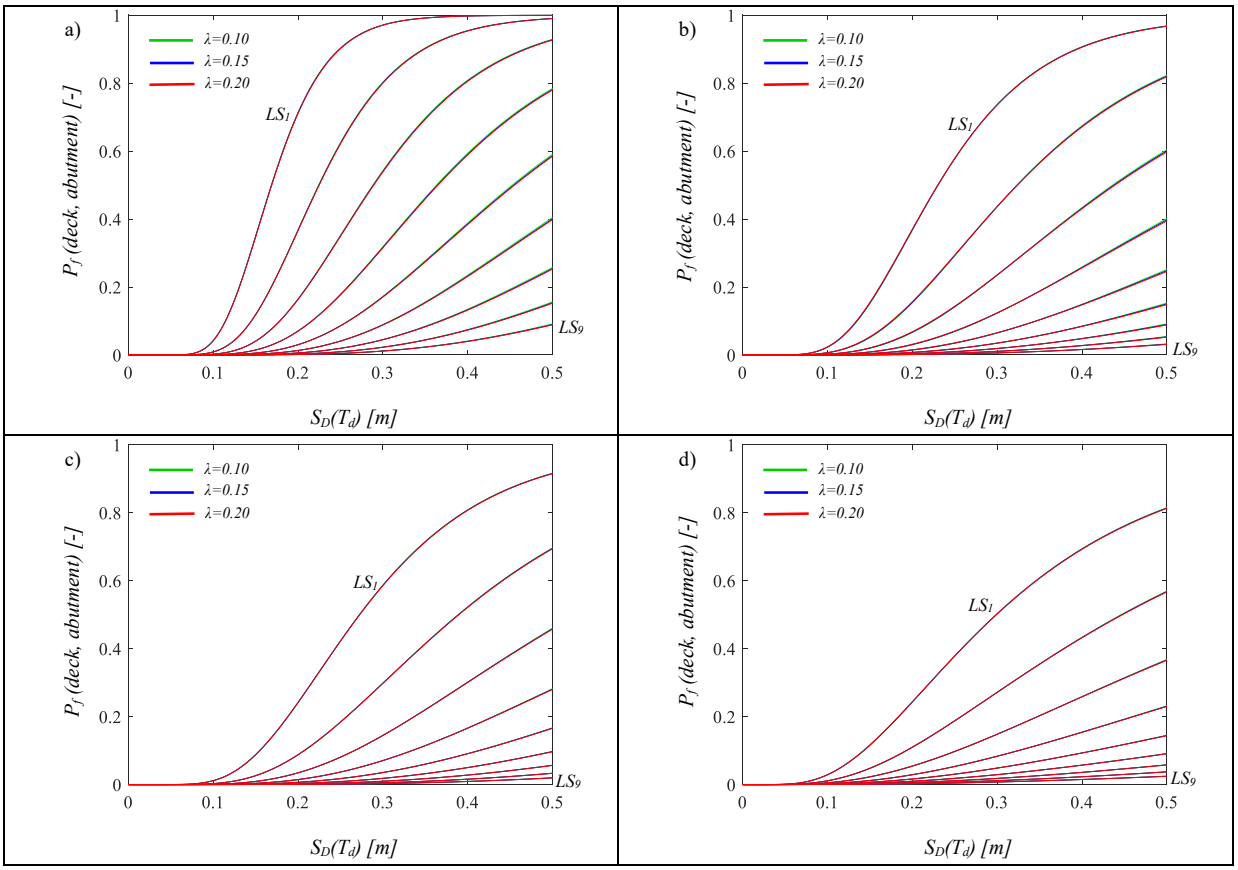

Figure 5.17: Fragility curves of the deck(abut.) for T_p=0.05 and T_d=1s (a), T_d=2s (b), T_d=3s (c), T_d=4s (d).

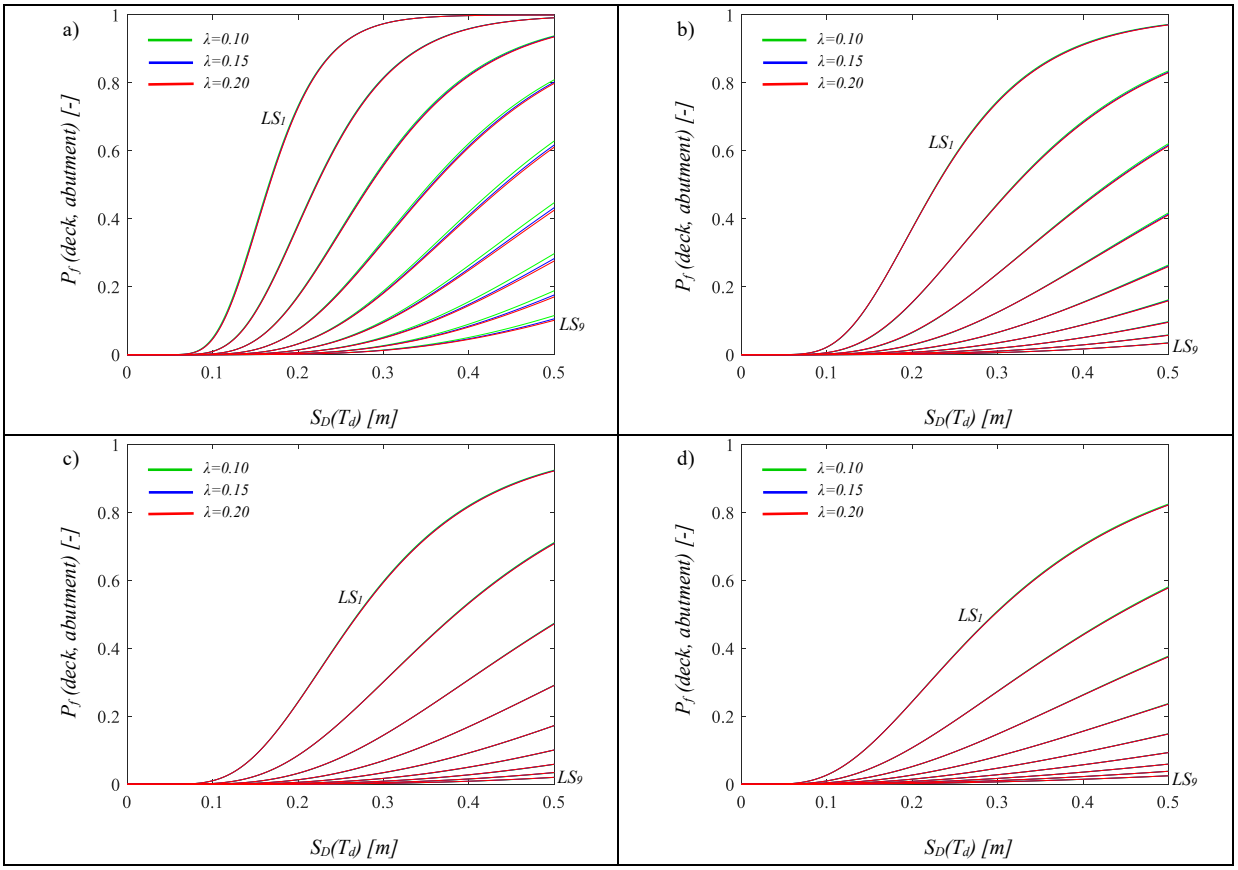

Figure 5.18: Fragility curves of the deck (abut.) for T_p=0.10 and T_d=1s (a), T_d=2s (b), T_d=3s (c), T_d=4s (d).

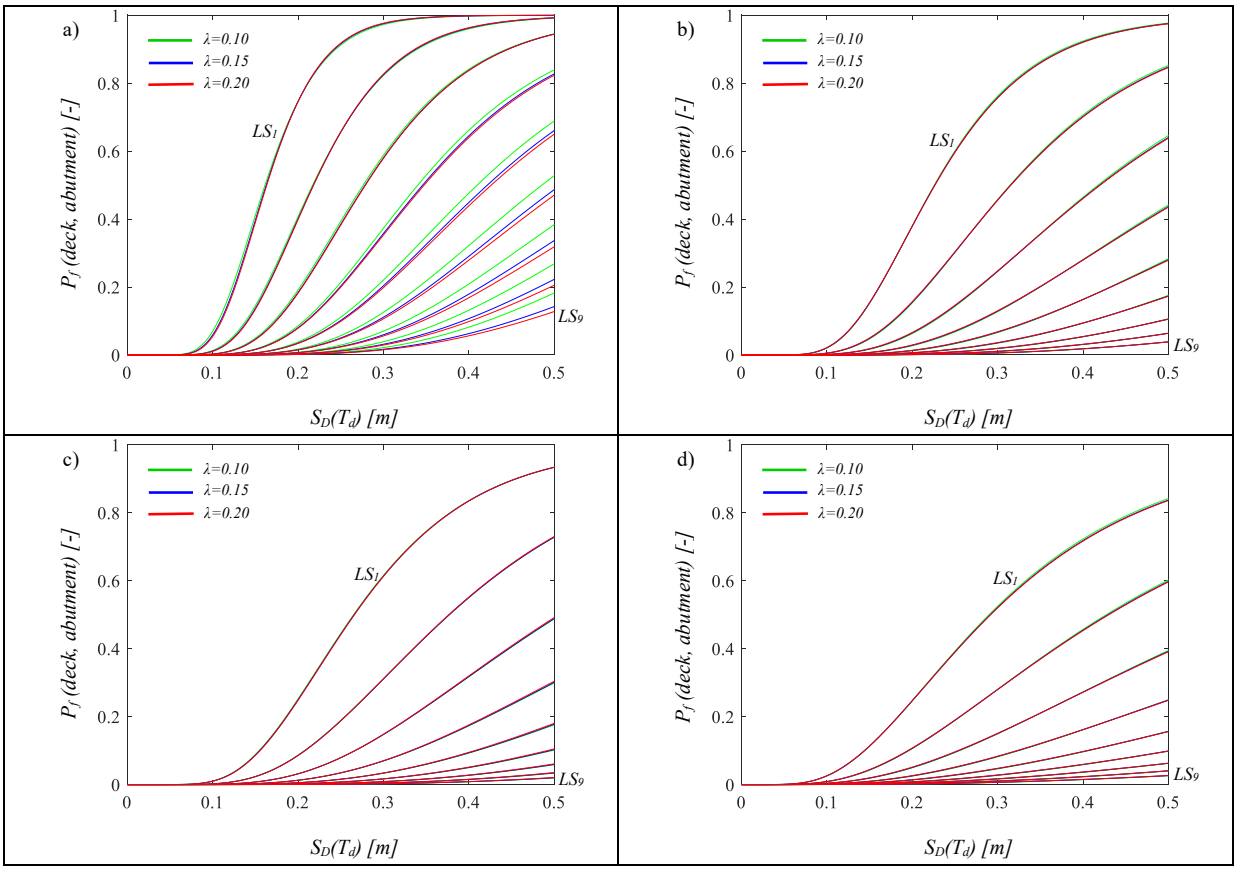

Figure 5.19: Fragility curves of the deck (abut.) for T_p=0.15 and T_d=1s (a), T_d=2s (b), T_d=3s (c), T_d=4s (d).

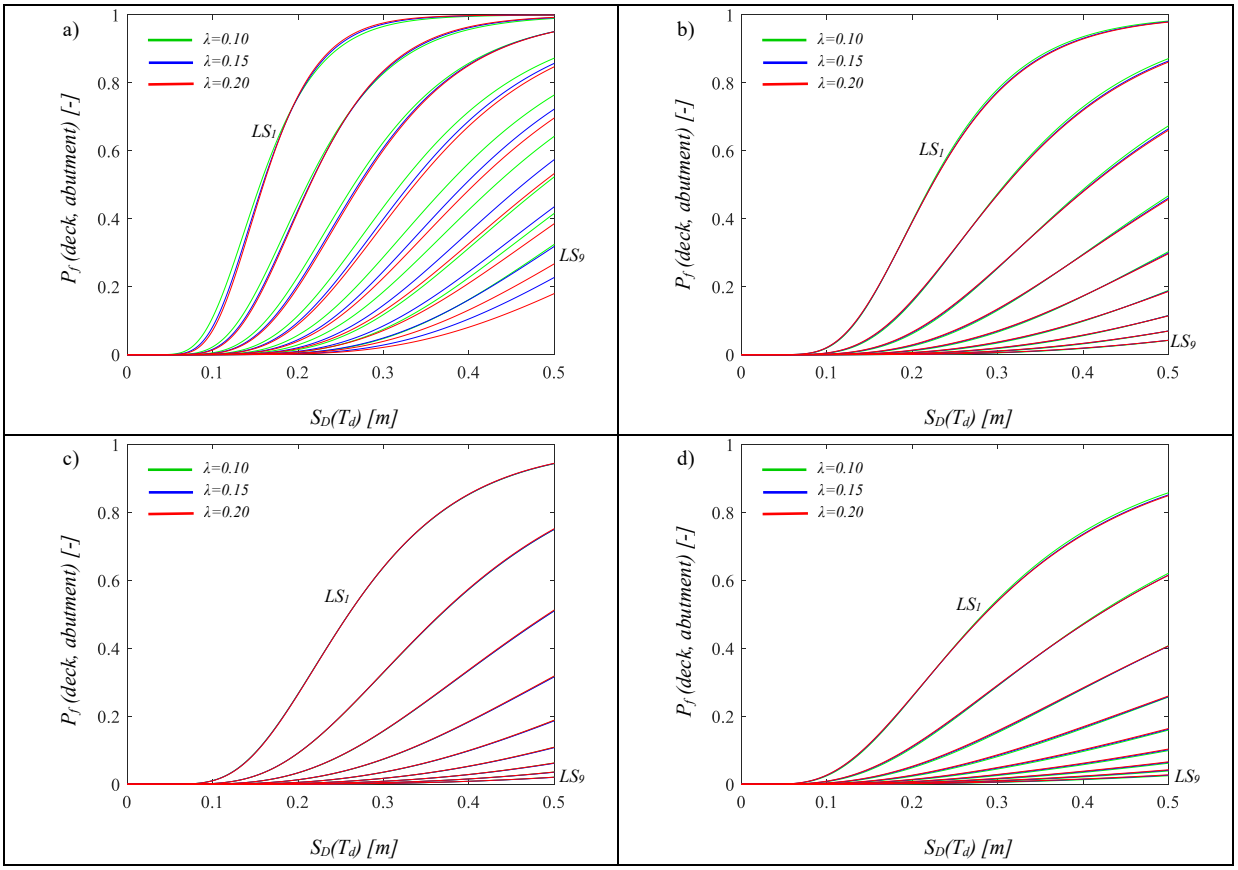

Figure 5.20: Fragility curves of the deck (abut.) for T_p=0.20 and T_d=1s (a), T_d=2s (b), T_d=3s (c), T_d=4s (d).

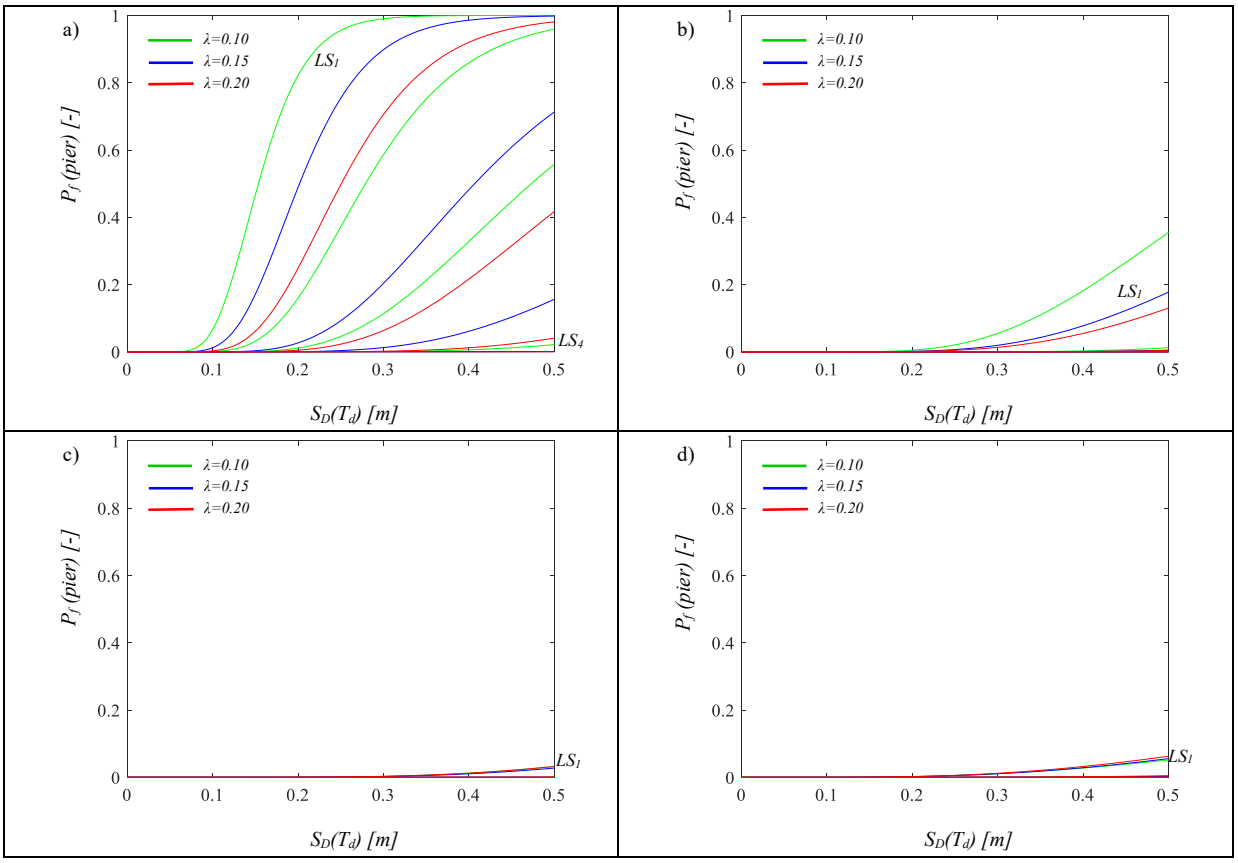

Figure 5.21: Fragility curves of the pier for T_p=0.05 and T_d=1s (a), T_d=2s (b), T_d=3s (c), T_d=4s (d).

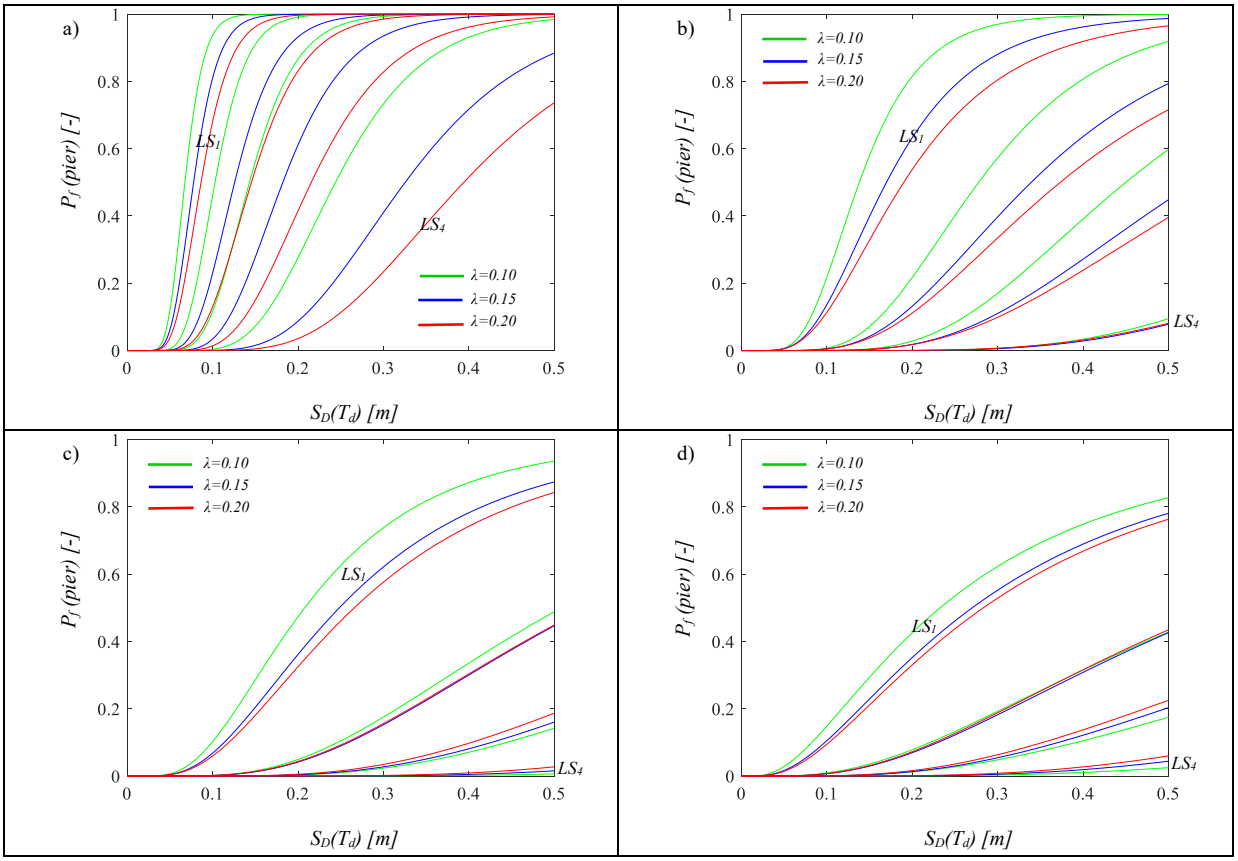

Figure 5.22: Fragility curves of the pier, for T_p=0.10 and T_d=1s (a), T_d=2s (b), T_d=3s (c), T_d=4s (d).

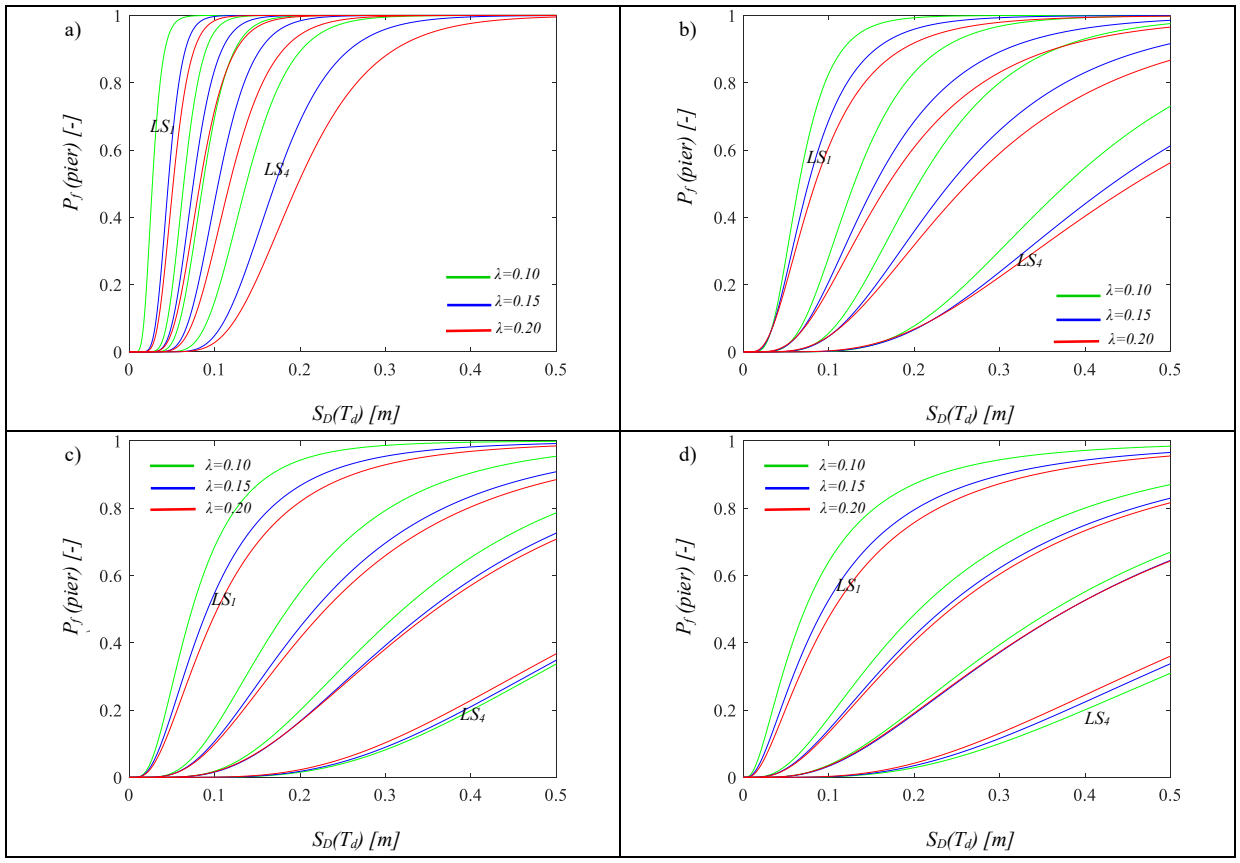

Figure 5.23: Fragility curves of the pier for T_p=0.15 and T_d=1s (a), T_d=2s (b), T_d=3s (c), T_d=4s (d).

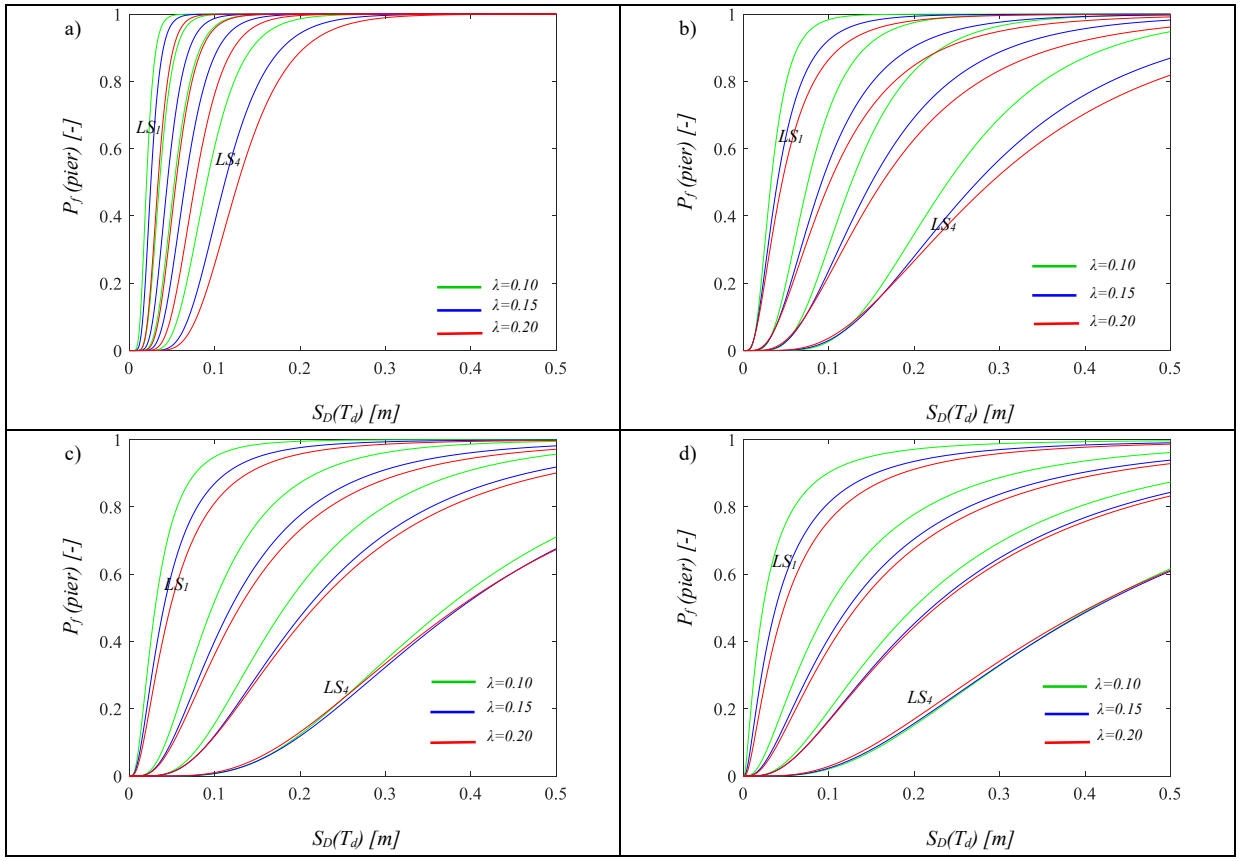

Figure 5.24: Fragility curves of the pier for T_p=0.20 and T_d=1s (a), T_d=2s (b), T_d=3s (c), T_d=4s (d).

5.3 Site seismic hazard

The seismic hazard curve of a site $\lambda_s(s)$, provides the annual mean frequency of exceeding of the s value by a quantity representative of the local seismic intensity S. The seismic intensity can be expressed in terms of PGA or a spectral ordinate corresponding to the fundamental period of the structure subject of study.

In the present thesis work, the site considered for the evaluation of the local seismic hazard is the L'Aquila city (Italy), with geographic coordinates 42°38'49''N 13°42'25''E, ID:26306, and the seismic intensity will be expressed in terms of spectral displacement S_d.

Through the "INPV DPC-INGV-S1" Project of the INGV [36], which considers as a representative parameter of the local seismic intensity the PGA, it was possible to detect nine values of the latter, respectively at 16th, 50th and 84th percentile. To each value of PGA is associated the Probability of exceeding (P_{VR}) in 50 years and an annual mean frequency of exceeding (λ_s) (*Table 5.3*), therefore nine Periods of Return, T_R, since the following relation is valid:

$$\lambda_s(s_i) = \frac{1}{T_{R,i}} \qquad \text{with} \quad i = 1, ..., 9 \tag{5.9}$$

where s_i is the value of the S intensity at the ith T_R: $s_i = S(T_{R,i})$

Table 5.3: L'Aquila: PGA values at 50th, 16th and 84th percentiles, in function of the nine return periods considered by INGV.

P_{VR} [-]	**T_R [years]**	**λ_s [years^{-1}]**	**PGA (16th) [g]**	**PGA (50th) [g]**	**PGA (84th) [g]**
2%	2475	0.0004	0.4098	0.4522	0.5227
5%	975	0.0010	0.3031	0.3341	0.3674
10%	475	0.0021	0.2378	0.2608	0.2844
22%	201	0.0050	0.1736	0.1906	0.2038
30%	140	0.0071	0.1510	0.1640	0.1754
39%	101	0.0099	0.1309	0.1424	0.1535
50%	72	0.0139	0.1111	0.1226	0.1318
63%	50	0.0199	0.0919	0.1041	0.1115
81%	30	0.0332	0.0680	0.0789	0.0871

The hazard curves, in terms of PGA for each percentile, are represented in (*Figure 5.25*).

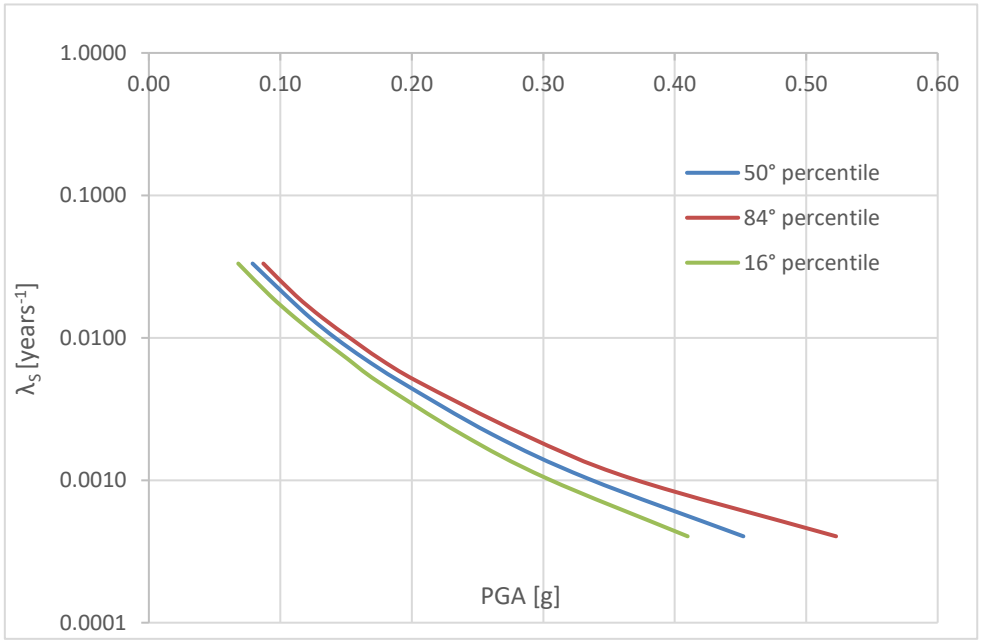

Figure 5.25: Seismic hazard curve in terms of PGA for L'Aquila site (Italy).

In addition, the parameters F_0 and T_c^* are also provided by the "INPV DPC-INGV-S1" Project, which are a function of the Return Period, T_R, only and do not vary with the percentile used for the PGA. In this way, starting from the hazard curves in terms of PGA it was possible to calculate the elastic response spectrum in terms of displacement of the horizontal component of the seismic excitation, at the 50th percentile, for the 4 fundamental periods of the isolated superstructure (T_d = 1,2,3,4 s) and the mean hazard curves $\bar{\lambda}_s$ (defined in 9 points) were also calculated, which are obtained by multiplying the median curve λ_s by an amplification factor:

$$\bar{\lambda}_s(s) = \lambda_s(s) exp\left(\frac{1}{2}\beta_H^2\right) \tag{5.10}$$

The parameter β_H is evaluated with the following expression:

$$\beta_H = \frac{ln(S_{84\%}) - ln(S_{16\%})}{2} \tag{5.11}$$

and it allows to estimate the epistemic uncertainty on the hazard. $S_{84\%}$ and $S_{16\%}$ represent the spectral displacements evaluated at 84th and 16th percentile respectively.

At this point, a quadratic function has been adapted in the logarithmic space ln($\bar{\lambda}_s(s)$)-ln(S), of the type:

$$ln\left(\bar{\lambda}_s(s)\right) = k_1(ln(S)^2) + k_2(ln(S)) + k_3 \tag{5.12}$$

and therefore, the relation in the linear space is determined:

$$\bar{\lambda}_s(s) = exp \cdot (k_1\,(ln(S))^2 + k_2\,ln(S) + k_3) \tag{5.13}$$

Obtaining the hazard curves (*Figure 5.26*) for the 4 structural periods above.

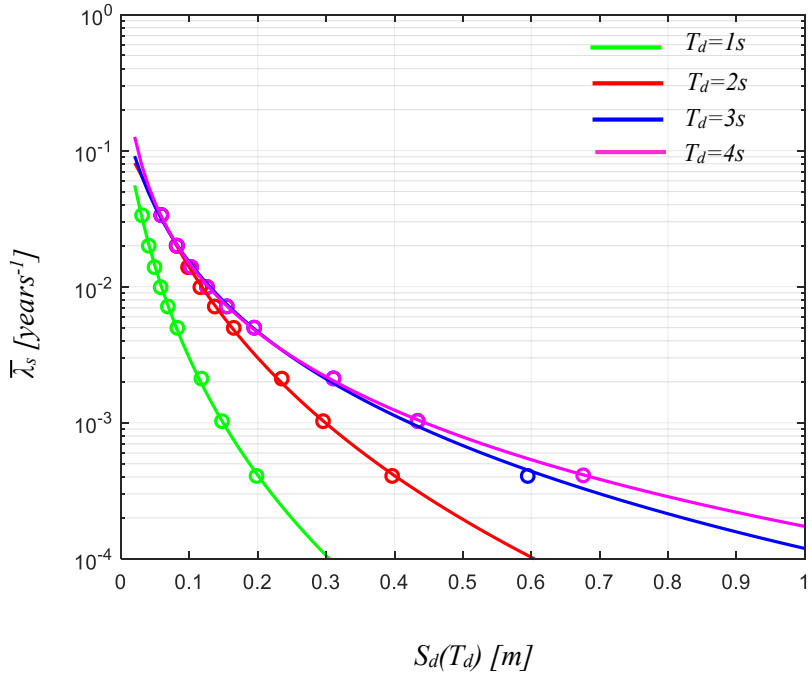

Figure 5.26: Seismic hazard curve in terms of S_d for the four structural periods (T_d), for the site of L'Aquila.

5.4 Seismic reliability analysis

According to the Pacific Earthquake Engineering Research (PEER) Center modular approach, and with the aim to assess the seismic reliability of both the isolation level and the substructure, the mean annual rates exceeding the corresponding limit states, λ_{LS}, have to be evaluated through the integration between the fragility curves and the seismic hazard curve, expressed in terms of the same IM, related to the reference site:

$$\lambda_{LS} = \int P_f(s) \cdot \left|\frac{d\bar{\lambda}_s(s)}{d(s)}\right| d(s) \quad (5.14)$$

Which can be approximated, using the Law of Total Probability, with the following sum:

$$\lambda_{LS} \cong \sum_{i=1}^{n} P_f(s_i) \cdot |\lambda_i| \quad (5.15)$$

In which the sum is extended to a number n of points such as to make the estimate stable.

Next, the mean annual rates of both the superstructure and substructure, λ_{LS}, have to be transformed into probabilities of exceedance within the time frame of interest (e.g., 50 years) by using a Poisson distribution [8] (*Table 5.4*)

$$P_f(50years) = 1 - e^{-\lambda_{LS} \cdot 50years} \quad (5.16)$$

Table 5.4: PDI for isolated bridges, related to the different LSs and with reference to the acceptable P_f^*.

Limit State		**Pier drift index (PDI)**	**Acceptable Probability of failure (P_f^*)**
LS1	Fully Operational	0.23 %	$5 \cdot 10^{-1}$
LS2	Operational	0.5 %	$1.6 \cdot 10^{-1}$
LS3	Life Safety	0.83 %	$2.2 \cdot 10^{-2}$
LS4	Near collapse	1.67 %	$1.5 \cdot 10^{-3}$

Thus, obtaining the Reliability curves valid for the superstructure and the substructure, which show the probabilities of excess of each Limit State over a period of 50 years.

5.4.1 Reliability curves of the Pier

The following (*Figure 5.27*) show the reliability curves valid for the substructure. These curves were derived in the Limit States Pier - Probability of failure LS_i plane by fixing the vibration period of the deck (T_d) and varying the pier period (T_p) and the mass ratio (λ).

From the results it can be noticed that the last limit state (Life Safety) is not respected; this is because the limit states taken into consideration for the pier are very stringent and performing (equal to 1/3 of the standard ones). More flexible piers, therefore with medium-high T_p values, may exceed the limit state due also to the randomness of the friction

coefficient. On the other hand, an increase in the vibration period of the FPS devices leads to an increase in seismic demand in the pier.

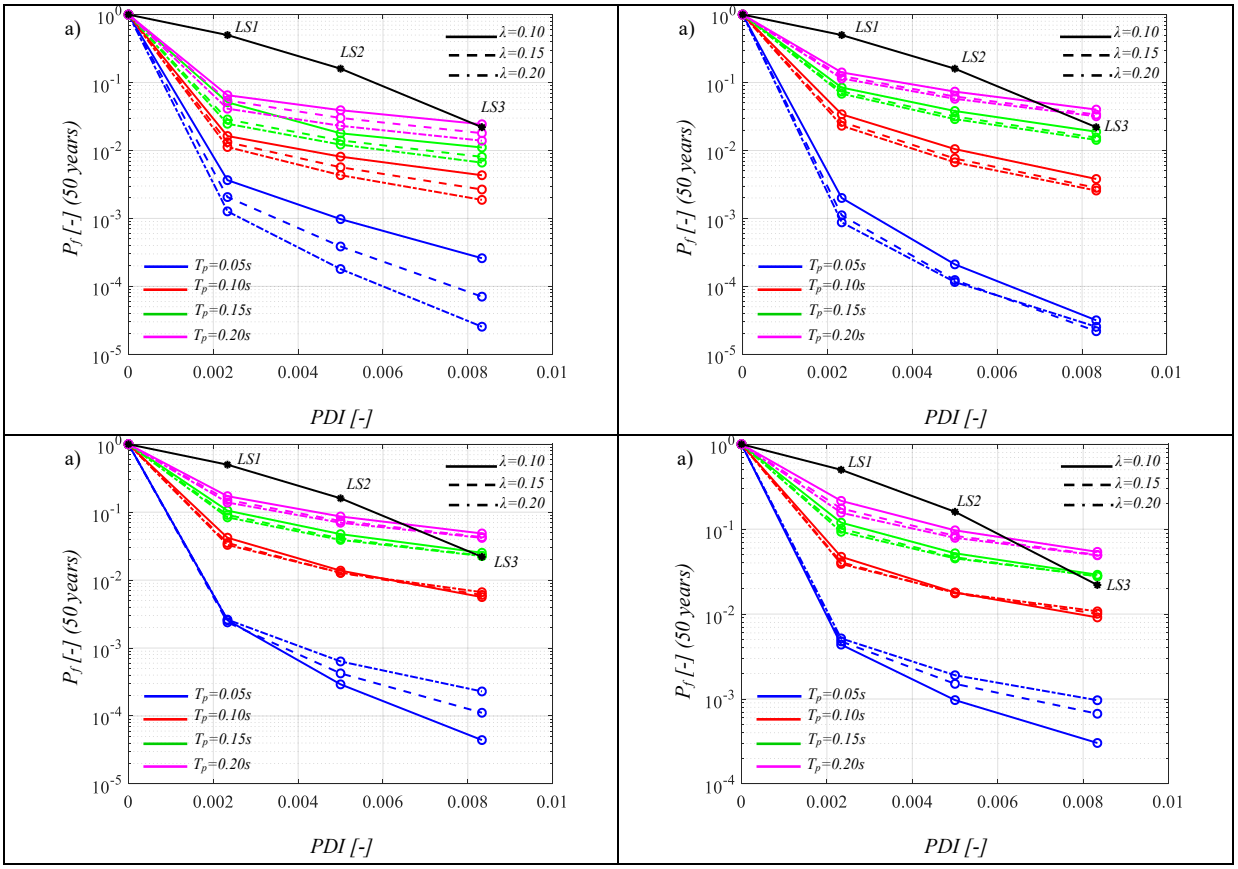

Figure 5.27: Reliability curves of the pier for Td =1s (a), Td =2s (b), Td =3s (c), Td =4s (d).

5.4.2 Reliability curves of the Deck

The following figures show the reliability curves valid for the isolation level, pier side *(Figure 5.28*) and abutment side (*Figure 5.29*). These curves were derived in the Limit States Isolation Level - Probability of failure LS_i plane by fixing the vibration period of the deck, T_d, and varying the pier period, T_p, and the mass ratio, λ.

The reliability analysis results revealed that the isolating system is seismically less reliable as its fundamental period, T_d, (and thus the curvature radius of the FP isolators) increases, since higher and higher failure probabilities correspond to the same limit state.

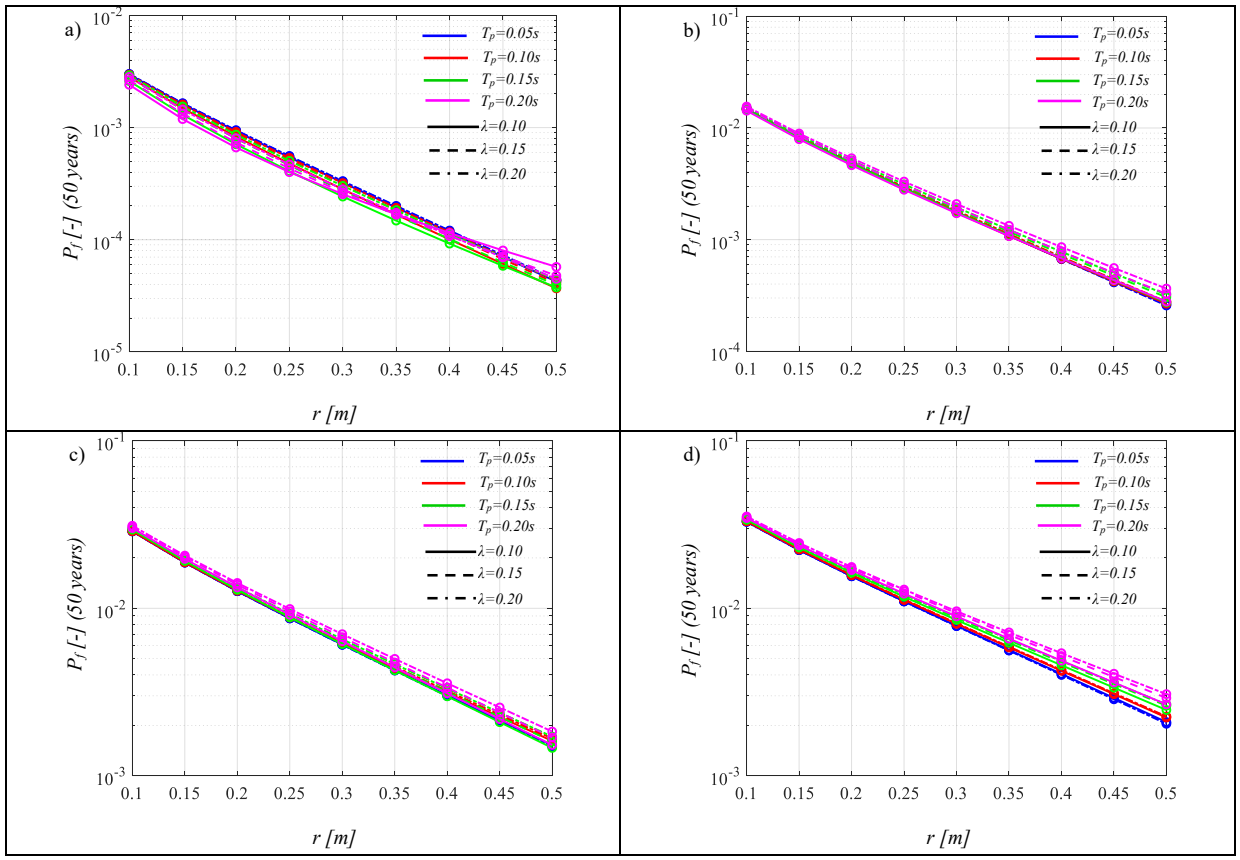

Figure 5.28: Reliability curves of the deck for Td =1s (a), Td =2s (b), Td =3s (c), Td =4s (d).

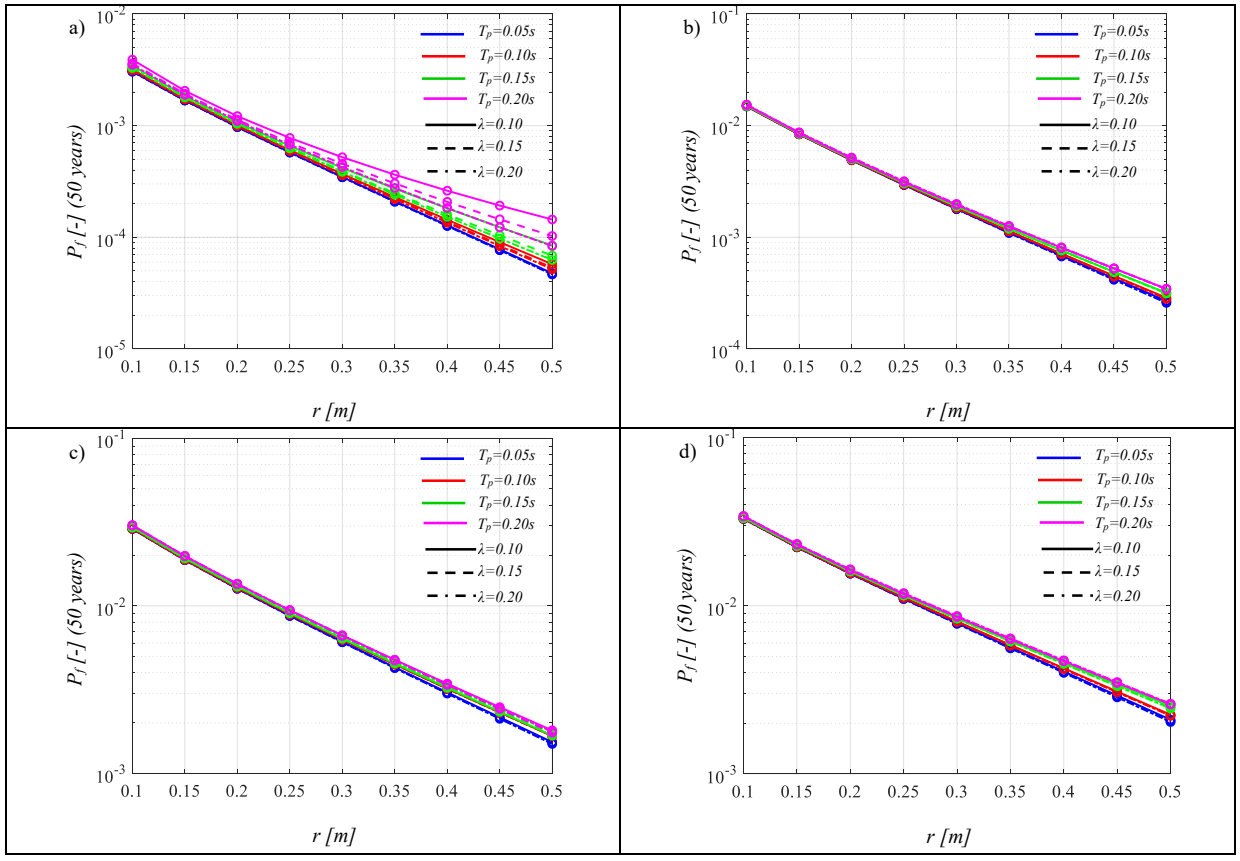

Figure 5.29: Reliability curves of the deck (abutment) for Td =1s (a), Td =2s (b), Td =3s (c), Td =4s (d).

5.4.3 Seismic Reliability-Based Design (SRBD) abacuses

The reliability curves obtained for the isolation level were then processed in a semilogarithmic plane and interpolated with a linear regression law. In this way we obtained regression lines (with an average coefficient of determination equal to R-square = 0.998 which demonstrates the goodness of the way in which the observed results are replicated by the model), which represent the seismic reliability-based design (SRBD) abacuses, that can be used for the preliminary design of the dimensions in plan (i.e., radius in plan, r, of the concave surface) of the friction pendulum devices, depending on structural properties in an area with a seismic hazard similar to that considered, in order to respect the expected reliability level.

Following are represented the linear regressions of the reliability curves, valid for the isolation level, pier side (*Figure 5.30*), and abutment side (*Figure 5.31*), for the 4 periods of the deck, T_d, used. From the results we can see how the demand for isolation is higher for medium-high values of T_d; in particular, the exceeding of the probability $P_f = 1.5 \cdot 10^{-3}$ (relative to the limit state of collapse) is reached through a radius in plant, r, ranging from 0.15m (for low T_d values) to 0.60 for (for high T_d values), depending on the values of structural properties. In the design phase, it is therefore convenient to adopt T_d values not too high.

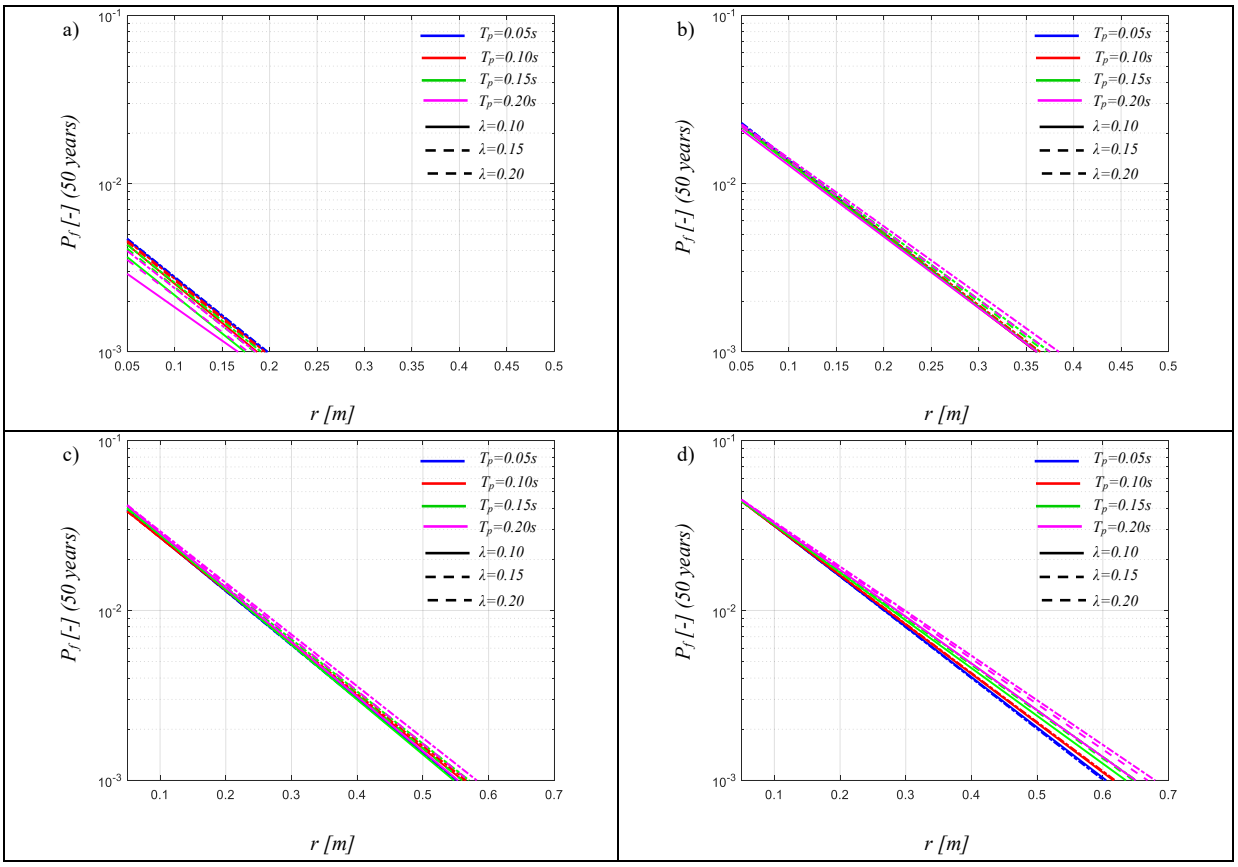

Figure 5.30: FPS Design Abacuses of the deck for Td =1s (a), Td =2s (b), Td =3s (c), Td =4s (d).

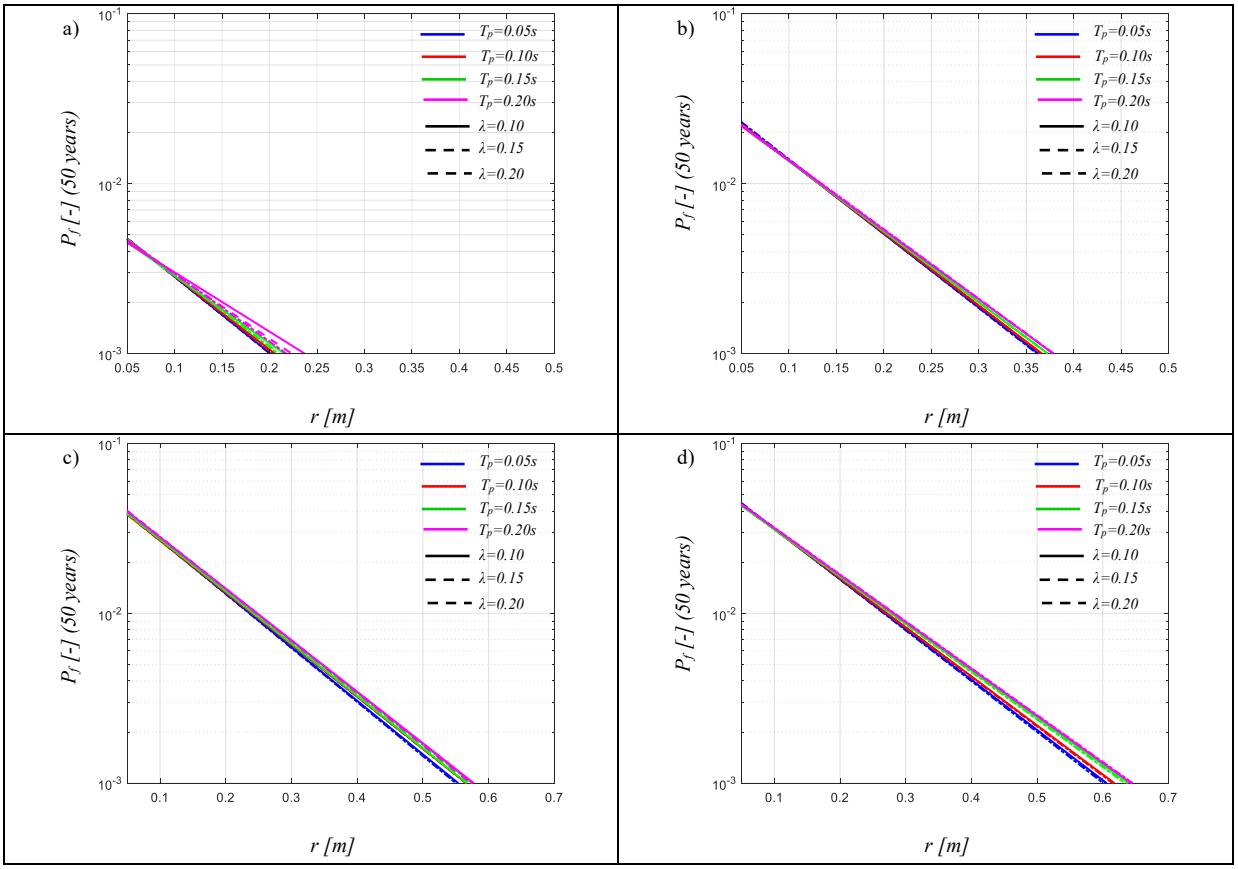

Figure 5.31: FPS Design Abacuses of the deck (abutment) for Td =1s (a), Td =2s (b), Td =3s (c), Td =4s (d).

CHAPTER 6

6. CONCLUSIONS

The seismic reliability of a (5+1) degree-of-freedom bridge model, isolated by single concave sliding bearings has been assessed. The evaluation was made through the execution of 172,800 nonlinear dynamic parametric analyses, considering 30 natural seismic records, scaled to eight intensity measures (IM), and considering the dynamic friction coefficient of the Friction Pendulum devices as a random parameter. The parametric analysis has been carried out by varying both these variables and the main dynamic characteristics of the system, i.e. the vibration periods of the pier, T_p, and of the isolating system T_d, and the ratio between the pier and deck masses, i.e., mass ratio, λ.

The structural model has been simulated through an algorithm implemented in the MATLAB&Simulink® computing software and the analyses have been implemented considering a fixed-step integration. The estimates of the response statistics obtained for each parameter combination reflected the effect of the variability of the characteristics of the selected records at different intensity levels and they have been used for deriving fragility curves and for seismic risk analyses.

Actually, after selecting a reference site, town of L'Aquila (Italy), relevant limit state functions have been derived, according to National and International regulations, in order to assess the fragility, i.e. the vulnerability, of the system, by calculating the conditional probability of failure of the different limit states considered, given a specific intensity of the seismic action.

In particular, an Incremental Dynamic Analysis (IDA) has been firstly performed to reach the relationship between the seismic demand and the capacity of the structure and evaluate the structural performance accurately.

The IDA curves related to the superstructure and the pier show that the seismic demand decreases with the increase of the period of the superstructure; this happens because resonance phenomena occur, since the values of the pendulum period are very low, which make the structural response result greater for low values of the deck period. The influence of

the mass ratio, λ, in the IDA curves concerning the superstructure, is almost nothing for low values of the pier period, while for medium-high values the variability of this parameter causes slight deviations in the structural response, which tend to decrease with increasing T_d. Regarding the structural response of the pier, instead, there is a higher variability when the mass ratio changes, which decreases with increasing T_d and T_p, i.e. with increasing structural flexibility.

The structural responses obtained with the non-linear dynamic analyses were then treated in a reliability key, thus arriving at the derivation of the vulnerability and reliability curves. In fact, IDA curves provided appropriate result formats which allowed estimating the annual average frequency of exceeding predefined damage states and developing fragility curves of the bridge.

The fragility curves, referred both to the isolating system and the substructure, have been plotted in function of each limit state and for each dynamic characteristic of the bridge, i.e. the superstructure and substructure vibration periods and the mass ratio.

Specifically, the vulnerability analyses are substantially in agreement with the results that had already provided the nonlinear dynamic analyses. Fragility (vulnerability) decreases as the fundamental period of vibration, T_d, increases; for low T_p values and medium-high T_d values, we can see how the probability of failure assume negligible values, due to the high rigidity that characterizes the substructure and the low seismic demand of the superstructure.

Successively, the site's hazard curves have been developed in terms of spectral pseudo-displacement, that is, the average number of events exceeding a definite value of the spectral pseudo-displacement.

Once the annual average frequency of exceeding a specific limit state has been calculated, through a convolution process between the system fragility and the seismic hazard of the site, the probability of failure, in a time interval of fifty years, has been evaluated. Hence, they have been obtained the reliability curves related to the isolation level and to the substructure.

The reliability curves of the substructure show that the last limit state (Life Safety) is not respected; this is because the limit states taken into consideration for the pier are very stringent and performing (equal to 1/3 of the standard ones). More flexible piers, therefore with medium-high T_p values, may exceed the limit state due also to the randomness of the friction coefficient. Furthermore, an increase in the vibration period of the superstructure (then an increase in the vibration period of the FPS devices) leads to an increase in seismic

demand in the pier. From the reliability analysis results it can be noted that isolating system and substructure are seismically less reliable as the fundamental period, T_d, increases, since higher and higher failure probabilities correspond to the same limit state.

It is interesting to observe how the reliability of the isolation system decreases with the increase of the curvature radius of the isolator, in a manner exactly contrary to what is seen in the analysis of the vulnerability, and this happens for any period of the pier and mass ratio considered. This circumstance is because an increase in the radius of curvature causes a translation, of the isolated structure, on areas of the displacements spectrum with higher periods and consequently with higher ordinates. This causes an increase in the local seismic hazard (at the same annual exceeding frequencies, higher spectral displacements correspond) that in the convolution with the vulnerability results to have a greater weight than the latter (which, instead, decreases with the increase of the radius of curvature).

Finally, the reliability curves of the isolating system have been interpolated by a linear regression to obtain, in function of the fixed dynamic characteristics of the substructure and the isolator, the friction pendulum design abacuses. These are based on the in-plan radius values to be provided for the FP design, so that the probability of failure lies in a range whose order of magnitude may be considered acceptable.

References

[1] Bertero RD, Bertero VV. Performance-based seismic engineering: the need for a reliable conceptual comprehensive approach. Earthquake Engineering and Structural Dynamics 2002; 31:627e52.

[2] SEAOC Vision 2000 Committee. Performance-based seismic engineering. Report prepared by structural engineers association of California. 1995. Sacramento, CA.

[3] NTC08. Norme tecniche per le costruzioni. Gazzetta Ufficiale del 04.02.08, DM 14.01.08, Ministero delle Infrastrutture.

[4] T.H. Wen, C.H. Loh (2005) "Establishing the relationship between damage measure, seismic hazard, structural ductility and period for pbsd", Journal of the Chinese Institute of Vol. 28, No. 4, pp. 617-626 (2005).

[5] Aoki Y., Ohashi Y., Fujitani H., Saito T.,Kanda J., Emoto T., Kohno M., (2000): "Target seismic performance levels in structural design for buildings", 12WCEE.

[6] (FEMA-274). NEHRP Commentary on the guidelines for the seismic rehabilitation of buildings. Washington, DC; 1997.

[7] Cornell CA. Hazard, Ground Motions and Probabilistic assessment for PBSD. In: Performance based seismic design concepts and implementation. PEER report 2004/05. Pacific Earthquake Engineering Research Center, University of California Berkeley; 2004 p. 39–52.

[8] Cornell CA. Engineering seismic risk analysis. Bull Seismol Soc Am 1968; 58(5):1583–606.

[9] http://esse1-gis.mi.ingv.it/

[10] https://emidius.mi.ingv.it/GNDT2/

[11] Rossetto T, Elnashai AS. Derivation of vulnerability functions for European-type RC structures based on observational data. Engineering Structures 2003; 25:1241–1263.

[12] Di Pasquale G, Orsini G, Romeo RW. New developments in seismic risk assessment in Italy. Bulletin of Earthquake Engineering 2005; 3:101–128.

[13] Dolce M, Kappos A, Masi A, Penelis G, Vona M. Vulnerability assessment and earthquake damage scenarios of the building stock of Potenza (Southern Italy) using Italian and Greek methodologies. Engineering Structures 2006; 28:357–371.

[14] Mckay MD, Conover WJ, Beckman RJ. A comparison of three methods for selecting values of input variables in the analysis from a computer code. Technometrics 1979; 21:239–45.

[15] Palazzo B. (1991). "Seismic behavior of base isolated buildings", International meeting on earthquake protection of buildings.

[16] Palazzo B. (1995). "Metodologie di controllo di sistemi sismicamente isolati". Università degli studi di Salerno.

[17] Kelly James M., "Theory and Practice of Seismic-Isolation Design", Earthquake Engineering Research Center University of California at Berkeley, 1996.

[18] Naeim F, Kelly JM. Design of seismic isolated structures: from theory to practice. John Wiley & Sons, Inc.; 1999.

[19] Mokha A, Constantinou MC, Reinhorn AM. Teflon bearings in base isolation. I: Testing. J Struct Eng 1990; 116(2):438–54.

[20] Constantinou MC, Mokha A, Reinhorn AM. Teflon bearings in base isolation. II: Modeling. J Struct Eng 1990; 116(2):455–74.

[21] Constantinou MC, Whittaker AS, Kalpakidis Y, Fenz DM, Warn GP. Performance of seismic isolation hardware under service and seismic loading. Technical report MCEER-07-0012; 2007.

[22] Zayas VA, Low SS, Mahin SA. The FPS earthquake resisting system Report No. CB/EERC-87/01. Berkeley, California: Earthquake Engineering Research Center, University of California; 1987.

[23] Zayas VA, Low SS, Mahin SA. A simple pendulum technique for achieving seismic isolation. Earthq Spectra 1990; 6:317–33.

[24] Jangid, R. (2008). Stochastic Response of Bridges Seismically Isolated by Friction Pendulum System. Journal of Bridge Engineering.

[25] Elia Efraim, Boris Blostotsky (2012), "Design of bridge seismic protection system and selection of its parameters using capabilities of Simulink®", 14th International Conference on Computing in Civil and Building Engineering.

[26] Dolsek M. Incremental dynamic analysis with consideration of modeling uncertainties. Earthq Eng Struct Dynam 2009; 38:805–25.

[27] Vorˇechovsky´ M, Novák D. Correlation control in small-sample Monte Carlo type simulations I: a simulated annealing approach. Probab Eng Mech 2009; 24(3):452–62.

[28] http://peer.berkeley.edu/

[29] http://itaca.mi.ingv.it/

[30] http://www.isesd.hi.is/ESD_Local/frameset.htm

[31] Vamvatsikos D, Cornell CA. Incremental dynamic analysis. Earthq Eng Struct Dyn 2002;31(3):491e514.

[32] Math Works Inc. MATLAB-high performance numeric computation and visualization software. 1997. User's Guide, Natick: MA, USA.

[33] Iervolino I., Cornell C.A. (2004). "Sulla Selezione degli Accelerogrammi nella Analisi Non Lineare delle Strutture", atti XI Convegno Nazionale "L'Ingegneria Sismica in Italia", Genova.

[34] Iervolino I., Cornell C.A. (2005). "Record selection for nonlinear seismic analysis of structures", Earthquake Spectra, Vol. 21, No. 3, pp. 685-713.

[35] Castaldo P, Tubaldi E. Influence of FPS bearing properties on the seismic performance of base-isolated structures. Earthq Eng Struct Dyn 2015;44(15): 2817e36.

[36] Meletti C., Montaldo V., 2007. Stime di pericolosità sismica per diverse probabilità di superamento in 50 anni: valori di ag. Progetto DPC-INGV S1, Deliverable D2, http://esse1.mi.ingv.it/d2.html

[37] Castaldo, P., Palazzo, B., & Della Vecchia, P. (2015). Seismic Reliability of Base-isolated Structures with Friction Pendulum Bearings. Engineering Structures, pp. 80-93.

[38] Ryan KL, Chopra AK. Estimation of seismic demands on isolators based on nonlinear analysis. J Struct Eng 2004;130(3):392e402.